CHALMERS
UNIVERSITY OF TECHNOLOGY

Transport through Magnetic Molecules with Spin-Vibron Interaction

Thesis for the degree of Erasmus Mundus Master of Science
in Nanoscience and Nanotechnology

AHMED KENAWY

Promoter: Prof. Janine Splettstößer and Maciej Misiorny, Ph.D
Co-promoter: Prof. Chris van Haesendonck

KU LEUVEN

Department of Microtechnology and Nanoscience
Applied Quantum Physics Laboratory
CHALMERS UNIVERSITY OF TECHNOLOGY
Göteborg, Sweden 2016

Funded by the
Erasmus+ Programme
of the European Union

Thesis for the degree of erasmus mundus
master of science in nanoscience and nanotechnology

Transport through magnetic molecules with spin-vibron interaction

AHMED KENAWY

Department of Microtechnology and Nanoscience
Applied Quantum Physics Laboratory
Chalmers University of Technology
Göteborg, Sweden 2016

Transport through magnetic molecules with spin-vibron interaction
AHMED KENAWY

Thesis for the degree of Erasmus Mundus Master of Science
in Nanoscience and Nanotechnology

Promoter: Prof. Janine Splettstößer and Maciej Misiorny, Ph.D
Co-promoter: Prof. Chris van Haesendonck
External referee: Prof. Tomas Löfwander

Applied Quantum Physics Laboratory
Department of Microtechnology and Nanoscience
Chalmers University of Technology
SE-412 96 Göteborg
Sweden

Cover
Differential conductance of a vibrating magnetic molecule inserted in a three-terminal junction.

Printed by Chalmers Reproservice
Göteborg, Sweden 2016

Transport through magnetic molecules with spin-vibron interaction
Thesis for the degree of Erasmus Mundus Master of Science in Nanoscience and Nanotechnology

AHMED KENAWY

Department of Microtechnology and Nanoscience
Applied Quantum Physics Laboratory
Chalmers University of Technology

Abstract

Electronic transport through single-molecule devices is a powerful spectroscopic tool to probe various degrees of freedom at the nanoscopic level. Among these degrees of freedom, molecular vibrations are of particular relevance since they can result in drastic effects such as transport blockade. While the effect of the interaction between the molecular charge and vibrations on transport through a single magnetic molecule has already been characterized, additional research, especially from the theoretical perspective, is still required to examine the vibrations' coupling to the molecular spin and its impact on the magnetic anisotropy. For this reason, the aim of this thesis is to provide and scrutinize a theoretical model for transport through a single magnetic molecule that takes into account the threefold interplay between charge, spin and molecular vibrations. For a quantum mechanical treatment, the real-time diagrammatic technique is employed to study transport in the sequential tunneling regime. However, exploiting Bloch-like equations, it is proven that coherent superpositions do not influence transport for a molecule embedded between *nonmagnetic* electrodes. Consequently, using classical rate equations with Fermi golden rule is sufficient to capture the full picture. Based on this approach, it is shown that the coupling of the molecular vibrations modulates the magnetic anisotropy of a molecule along both the uniaxial and transverse directions, which results in various implications on transport properties, most notably transport blockade. This demonstrates yet another possibility to modify the magnetic properties of molecules by controlling the vibrational excitations. For instance, the anisotropy barrier can be enhanced to potentially improve the stability of a magnetic molecule as a nanoscopic memory element.

Keywords: molecular transport, single-molecule electronics, molecular spintronics, magnetic anisotropy, molecular vibrations, spin-vibron coupling, quantum coherences.

Acknowledgements

It is my pleasure to acknowledge the efforts of the many people who made the completion of this thesis possible. First and foremost, I would like to thank my promoter Janine Splettstößer for giving me the opportunity to work on this exciting project. Her guidance, insights and constructive feedback were not only essential to the success of this project, but also to helping me become a better researcher.

I would also like to express my sincerest gratitude to my daily supervisor Maciej Misiorny for his continuous support throughout the entire duration of the project. I profited enormously from his willingness to share his scientific knowledge as well as practical and technological skills. I must also acknowledge his extensive efforts in helping me improve this text.

Secondly, I would also like to thank Chris van Haesendonck for agreeing to be my co-promoter and for his insightful discussions about experimental studies related to my theoretical work. Furthermore, I want to thank everyone with whom I had an enlightening conversation, especially those working at the applied quantum physics lab in Chalmers University of Technology.

Last, but not least, I must extend my profound gratitude to my parents, Nashwa Radwan and Mohamed Kenawy, and my sister Maha for being supportive and caring for the two-year duration of this M.Sc. program. I would like to thank my travel and study companion, and also my dear friend, Ghada Badawy. Moreover, I am grateful for the encouragement of all my friends, most notably Mohamed Ehab and Abdelwhab Saeed.

Ahmed Kenawy, Göteborg, 2016

Contents

1

Introduction

The thesis at hand presents a theoretical study of transport through single molecules. In particular, the issue under scrutiny is *the effect of the threefold coupling between spin, charge and molecular vibrations on the transport properties of magnetic molecules.* Studying molecular transport lies at the heart of contemporary research, either with the purpose of achieving functional molecular devices or to gain better understanding of the various quantum mechanical phenomena accessible at the single-molecule level. Accordingly, the following introduction aims to motivate and frame the scientific context of this study. The introduction is organized as follows. Section 1.1 explains the recent interest in molecular electronics, whereas in Sec. 1.2 the concept of single-molecule junctions is introduced together with a brief summary of the recent studies in literature. The properties of bare magnetic molecules under consideration in this thesis are discussed in Sec. 1.3. Finally, in Sec. 1.4, the main research problem addressed in the present work is defined along with an overview of the following chapters.

1.1 Molecular electronics

The microfabrication industry and its leading invention, the *field-effect transistor* (FET), are of crucial importance to today's information technologies. The scalability of this industry has sustained its exponential growth over decades, maintaining Moore's law. However, increasing challenges with further scaling down of conventional silicon integrated circuits (ICs) sparked interest in other novel scaling routes, one of which is *molecular electronics* [1, 2]. Molecules are an attractive alternative to silicon-based technologies since their size ranges from 1 to 100 nm, which enables achieving nanoscale structures in the same length scale of cutting-edge miniaturized ICs [3]. Moreover, molecular electronics represents a paradigm shift from top-down lithography to bottom-up approach, where well-controlled nano-structures can be self-assembled from basic building blocks to create functional devices [4]. Self-assembly allows for associating function with structure; hence, it provides molecules with tailor-made electronic, magnetic and light-interacting properties [5]. As a result, molecules could cover a wide-range of applications, ranging from logic and memory to light-harvesting devices [6].

1.2 Single-molecule junctions

Recent interest in molecules as functional devices can also be attributed to the rapid technological advances that permit the isolation and manipulation of individual molecules [7]. Figure 1.1 illustrates a schematic of the basic building block of molecular electronics research, namely a *single-molecule junction*, where a molecule is embedded between two electrodes, a source and a drain,

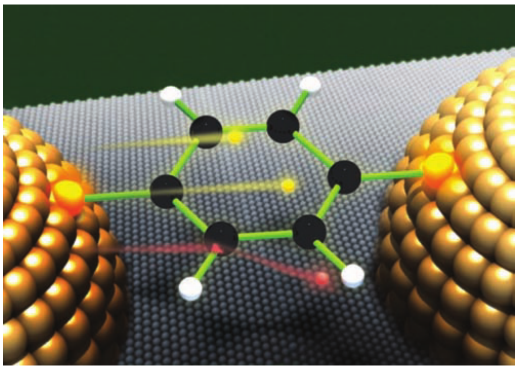

Figure 1.1: Single-molecule junction. Illustration of a benzene molecule trapped between two metallic electrodes on top of a substrate acting as a gate. Such single-molecule junctions are the basic building block of contemporary research on molecular electronics. Image taken from Ref. [7]

on top of a metallic gate. Over the past years, immense progress has been made to fabricate nanogaps with trapped single molecules. The most widely adopted techniques are summarized in Fig. 1.2 with the fabrication details described in the caption. Employing these techniques, various electronic circuitries have been demonstrated including switches [8–12], transistors [13–15] and memories [16, 17].

Interestingly, studying charge transport through molecular junctions turned out to be a powerful spectroscopic tool for investigating various degrees of freedom at the level of individual molecules [21]. By analyzing the conductance of a molecule at low temperature[1], one can obtain information about its energy spectrum, in addition to, the different excitations that take place within the molecule. Among these excitations, magnetic and vibrational ones are of particular interest in the present work, as discussed in Sec. 1.3. The question, then, arises: how to model a molecule suspended in a molecular junction between two electrodes? For a bare molecule, the energy spectrum can be approximated by discrete levels. Moreover, before embedding the molecule into a junction, it can only exist in a fixed charge state, i.e., it contains a certain number of electrons. Upon attachment to the electrodes, the charge state of the molecule can change because electrons can now tunnel between the molecule and the electrodes through barriers that form at the molecule-electrode interface. Due to these electron tunneling processes, the energy levels of the molecule become broadened, which is characterized by the tunnel-coupling parameter Γ. If the level-broadening is considerably smaller than the level-spacing Δ and the thermal energy of electrons $k_{\mathrm{B}}T$, i.e., $\Gamma \ll k_{\mathrm{B}}T$ and Δ, one can assume that the discrete energy spectrum of the molecule is still valid even after coupling to the electrodes. This condition is referred to as the *weak coupling regime* and is assumed throughout the present work. It should be noted that the weak and also the intermediate[2] coupling regimes are the relevant ones to study single molecules in electronic transport measurements since the energy spectrum and, hence, the properties of the molecule are not drastically altered due to coupling to the electrodes.

Unlike bare molecules, the electrodes are typically modeled as a continuous energy spectrum with *Fermi-Dirac statistics*, as depicted in the electrochemical diagrams in Fig. 1.3(a), where the

---

[1] The temperature should be sufficiently low to allow for resolving quantization effects either due to the discrete energy spectrum of a molecule or due to other excitations.

[2] The intermediate coupling is defined as the regime in-between the strong ($\Gamma \gg k_{\mathrm{B}}T$, Δ) and the weak ($\Gamma \ll k_{\mathrm{B}}T$, Δ) coupling regimes. This regime is particularly important to study higher-order tunneling processes, in contrast to weak coupling where only first-order transport is relevant [22].

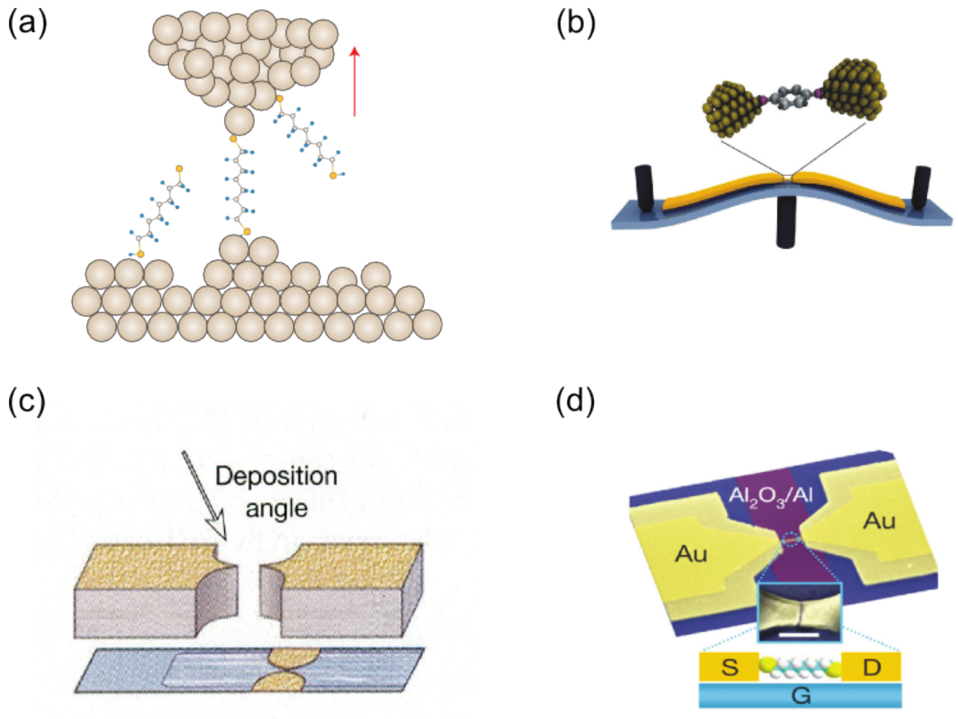

Figure 1.2: Experimental techniques used to create nanogaps for measuring single-molecule conductance. **(a)** Conductance measurement using *scanning tunneling microscopy* (STM). The technique works as follows: First a functionalized substrate is approached by a conducting tip. Next, the tip is retracted slowly, until there is only one molecule attached to it and, then, measurement takes place. The resultant configuration is a two-terminal setup which sets a limit on the capability of the technique. Image taken from Ref. [18]. **(b)** *Mechanically-controlled break junction* (MCBJ). A push rod is used to mechanically break a metallic wire on a flexible substrate. By optimizing the flexibility of the substrate and precise control of the push rod, nanogaps are obtained in which molecules can be placed. Image taken from Ref. [8]. **(c)** Fabrication of *nanogaps using a lithographic top-down approach.* By using a shadow mask and carefully tuning the angle of evaporation, metal electrodes can be deposited with nanogaps in between. Image taken from Refs. [15, 19]. **(d)** *Electromigrated molecular junction.* By passing a high density current through a metallic wire, the momentum transfer of the energetic electrons can lead to displacement of the wire atoms; hence, creating a nanogap. Image taken from Ref. [20].

dotted line represents the chemical potential of the source μ_s and the drain μ_d. In this example, the molecule can exist in two charge states differing by one electron, referred to as the neutral state N and the charged state $N+1$, as indicated by two energy levels in Fig. 1.3(a). In the absence of a bias voltage, no charge transport takes place due to the equilibrium of the chemical potential between the source and the drain. In this case, only the energy levels below the chemical potential of the electrodes are filled, whereas the energy levels above are empty. For the electrochemical diagram illustrated on the left-hand side of Fig. 1.3(a), the level with the energy $\mu(N)$ is filled, which corresponds to a molecule in the neutral state N. Upon applying a bias voltage V, the chemical potential gradient $\mu_\text{s} - \mu_\text{d}$ between the source and the drain can enable electrons to tunnel through the molecule. However, if the bias energy is less than the energy required to add an electron to the molecule, there is a *blockade* of transport and the molecule exists only

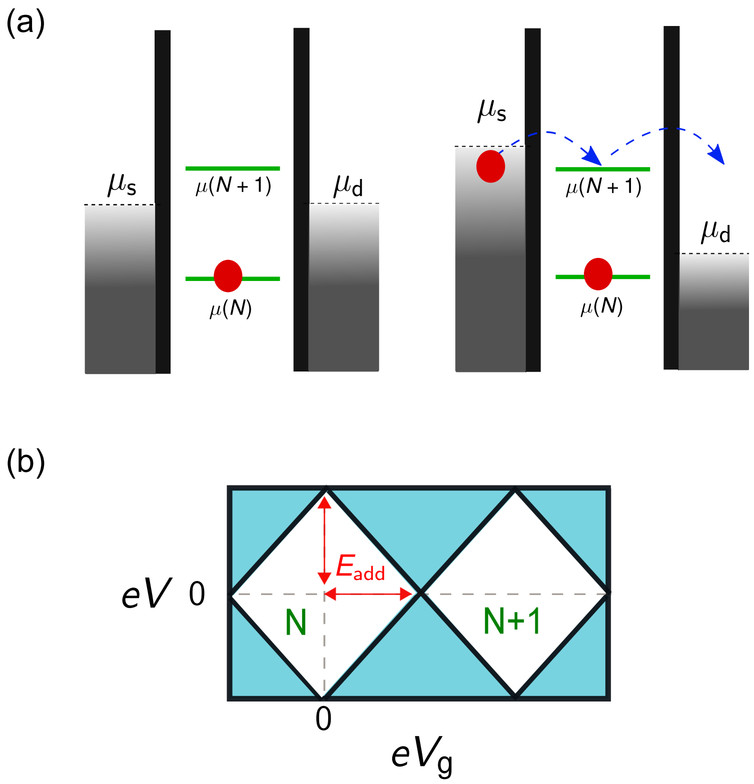

Figure 1.3: Transport through a molecular junction. **(a)** Electrochemical diagrams showing *blockade* (*left*) and *sequential tunneling* (*right*). **(b)** Schematic illustration of a typical differential conductance map as a function of the bias voltage V and gate voltage V_g. The white diamonds are the regions where the molecule exist in one charge state only, either the neutral state N or the charged state $N+1$, due to transport blockade. The red arrow represents the *addition* energy with respect to the gate and bias voltages, which refers to the energy required to add one electron to the molecule to alter its charge state. Colored regions represent the sequential tunneling regime where the molecule changes its state as electrons *sequentially* tunnel from the source to the drian via the molecule.

in the neutral state N. As the bias voltage increases, the energy level $\mu(N+1)$ enters the bias window and the blockade is lifted as depicted on the right side of Fig. 1.3(a). Consequently, electrons sequentially tunnel from the source to the drain one by one via the molecule; hence the name *sequential tunneling regime*. In this regime, the molecule alternates between the two charge states, N and $N+1$, as electrons tunnel through. These two regimes are typically observed in differential conductance $\partial I/\partial V$ plots, where I and V are the charge current through and voltage across the junction, respectively. Figure. 1.3(b) shows a schematic differential conductance map, also known as *stability diagram*, where the white diamonds represent the blockade regions with stable charge states N and $N+1$. On the other hand, the sequential tunneling regime with alternating charge states is represented by the colored diamonds. It should be remarked that these stability diagrams are acquired based on three-terminal conductance measurement. Accordingly, for a two-terminal setup such as scanning tunnel microscopy (STM), one-dimensional differential conductance plots are used instead, i.e., dI/dV versus bias voltage V. For the sake of completeness, both types of plots are typically shown when discussing results in the following chapters.

So far, only transitions that involve the charge of the molecule have been considered. However, as already mentioned, molecules exhibit additional degrees of freedom, most importantly magnetic ones which are the focus of this thesis. Consequently, the following section introduces the origin of magnetic excitations in magnetic molecules and presents a similar example where transitions occur between the different magnetic states of the molecule.

1.3 Magnetic molecules

The goal of the present thesis is to study the impact of the interaction between spin and molecular vibration on transport properties of magnetic molecules. For this reason, the focus here is on magnetic molecules that possess a large spin, i.e., a spin greater than that of an electron ($S > 1/2$). Importantly, such molecules typically exhibit a magnetic anisotropy, that is, an energetic preference to orient spin along a specific direction [23]. The magnetic properties of these particular molecules can be appropriately captured by the giant-spin Hamiltonian [23, 24]

$$\hat{\mathcal{H}}_{\text{mol}} = -D\big(\hat{S}_z\big)^2 + E\Big[\big(\hat{S}_x\big)^2 - \big(\hat{S}_y\big)^2\Big], \tag{1.1}$$

which means that the molecule is represented by an effective giant spin $\boldsymbol{S}$. The first term in Eq. (1.1) characterizes the *uniaxial magnetic anisotropy* of the molecule, conventionally chosen along the z-direction, with the uniaxial anisotropy constant D. The second term describes the *transverse magnetic anisotropy* with the transverse anisotropy constant $|E| \leq |D|/3$ [23]. Even in the absence of magnetic field and transverse magnetic anisotropy ($E = 0$), the uniaxial anisotropy of the molecules lifts the degeneracy of the magnetic ground state and, hence, the spin states of the molecule are split into $2S + 1$ states.[3] It should be emphasized that although the focus of this thesis is on magnetic molecules, the giant-spin Hamiltonian is also applicable to other magnetic systems, such as magnetic adatoms and clusters [25–27].

Furthermore, based on the sign of the uniaxial anisotropy constant D, one can distinguish two distinctive classes of the magnetic molecules under consideration. First, for $D > 0$ the spin moment prefers to point along the easy axis (z-direction), resulting in a parabolic energy spectrum as shown in Fig. 1.4 where the states of a molecule, in the absence of transverse magnetic anisotropy, are represented in terms of the spin projections along the z-axis, i.e., the states are characterized by the magnetic quantum number M. In particular, the magnetic ground state consists of two degenerate molecular states, one corresponding to the spin moment pointing in the positive z-direction and the other pointing in the opposite direction, as marked by blue arrows in Fig. 1.4. Later in this thesis, this behavior will be referred to as the *easy-axis* type of magnetic anisotropy. A well-known example of this particular class are single-molecule magnets (SMM), a special group of magnetic molecules exhibiting a strong uniaxial magnetic anisotropy at low temperature, which results in a bistable magnetic states, either parallel or antiparallel to the easy-axis [23]. Importantly, to reverse its spin-orientation from one of these metastable states to the other one, the molecule has to overcome the parabolic potential barrier by changing its magnetization step-by-step via the consecutive spin states. The magnetization reversal of the molecule from the negative to the positive z-direction, or vice versa, can be seen as flipping a bit from state 0 to 1. For this reason, SMMs are being investigated as a prospective nanoscopic spintronic device capable of storing and processing quantum information [28]. However, so far only few experimental demonstrations of SMMs memory exist in literature [29], since the magnetic bistability is only present at low temperature. As for

---

[3] This can be readily understood by making an analogy to electrons. An electron has a spin $S = 1/2$ and, hence, it can be in $2S + 1$ states from $-S$ to S, that is the spin-up $|\uparrow\rangle$ and spin-down $|\downarrow\rangle$ states.

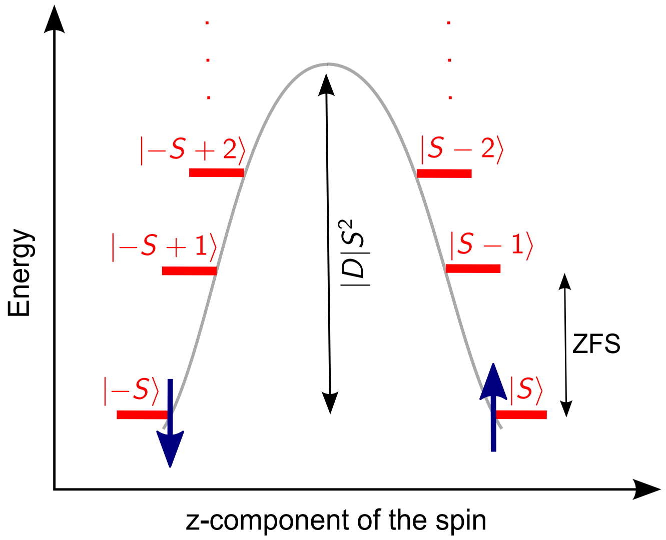

Figure 1.4: Energy spectrum of a magnetic molecule with the *easy-axis* type of magnetic anisotropy. The uniaxial magnetic anisotropy splits the ground state of the molecule into $2S+1$ states, where S is the total spin of the molecule. An energy barrier given by $D(S)^2$, separates the two metastable ground states (blue arrows). To flip its spin-orientation, the molecule goes through the consecutive spin states to climb over the potential barrier. The energy difference between the ground and first excited states is usually referred to as *zero-field splitting* (ZFS)

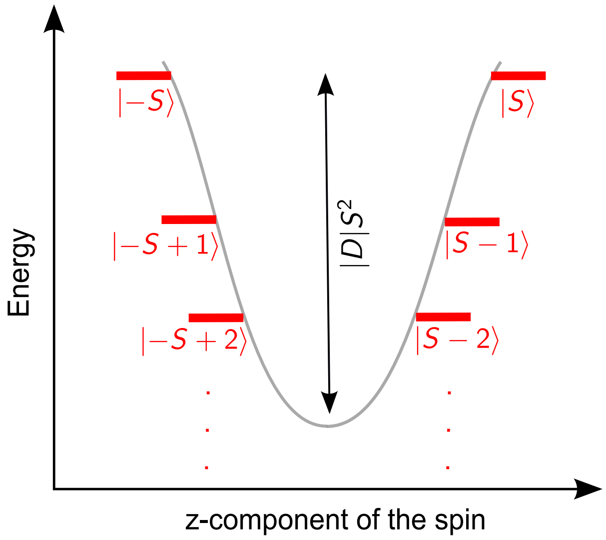

Figure 1.5: Energy spectrum of a magnetic molecule with the *easy-plane* type of magnetic anisotropy. The anisotropy of the molecules splits the spin states into $2S+1$ with S as the total molecular spin. In contrast to Fig. 1.4, the spin moments prefer to orient along the plane perpendicular to the easy-axis (z-axis). Thus, the states with the largest magnetic quantum number, i.e., S_z spin projections, are the least stable.

magnetic structures where the uniaxial anisotropy constant is negative ($D < 0$), the spin moments prefer to align along the plane perpendicular to the easy-axis (z-axis). Consequently, in terms of S_z spin projections, the ground state consists of states with the lowest magnetic quantum numbers, as schematically depicted in Fig. 1.5. This class is later called as the *easy-plane* magnetic anisotropy

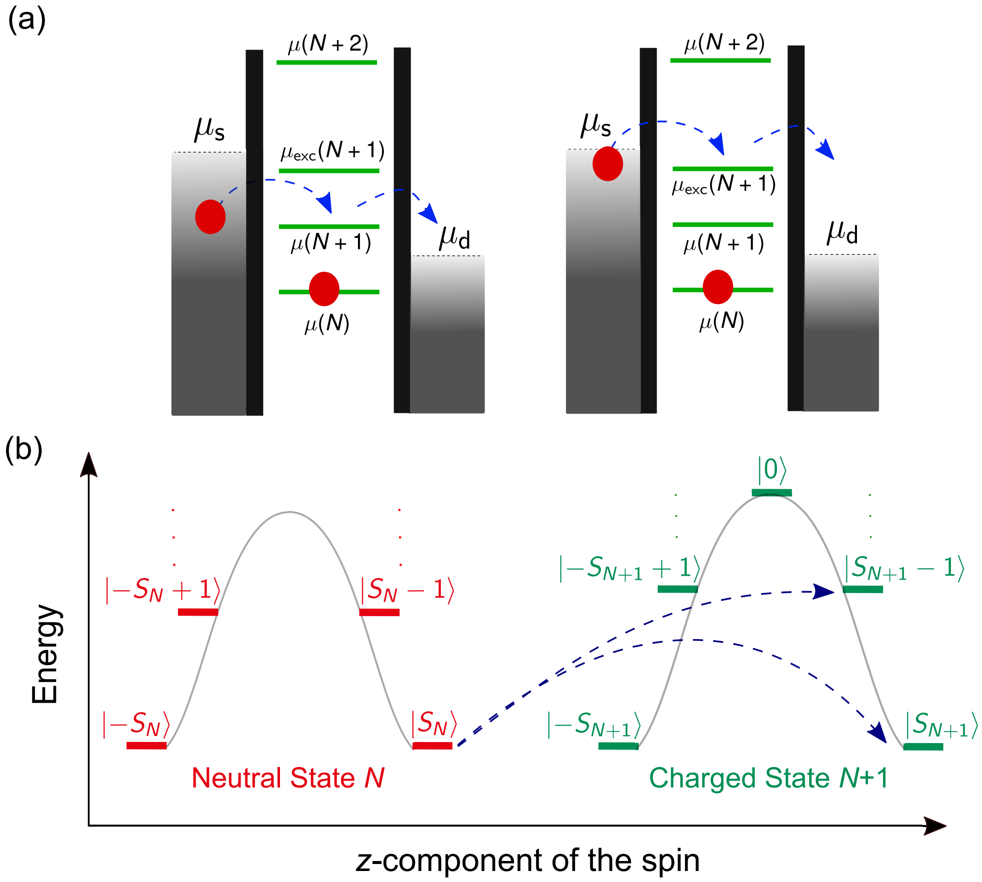

Figure 1.6: Schematic diagrams of ground and excited state transitions in a generic magnetic molecule. **(a)** Electrochemical diagram showing two transition possibilities, either involving the ground states (*left*) or the excited states (*right*). **(b)** Double-well potential for a magnetic molecule in the neutral N (*left*) and charged $N+1$ (*right*) states where two transitions are indicated. The first occurs from the ground states of the neutral molecule to the charged ground state, while the second occurs via an excited charged molecular state, that is $|N+1, S_{N+1}-1\rangle$. Since transitions between molecular states occur due to the tunneling of an electron either with a spin up or spin down, the absolute difference in magnetic quantum number between the two possible final states must be one. In addition, due to conservation of spin momentum, only transitions where the magnetic quantum number changes by 1/2 is allowed. For instance, a transition from the state $|S_N\rangle$ to $|-S_{N+1}\rangle$ is forbidden since $|-S_{N+1}-S_N| > 1/2$. The role that spin conservation plays as a selection rule for allowed transitions is further discussed in Sec. 2.3.

case. Examples of systems belonging to this particular class can be found in Ref. [27]. In the discussion about the coupling between spin and molecular vibrations in Chap. 3, an example of each class is presented to illustrate how the molecular vibrations impact their electronic transport properties.

Now, similarly to the previous section, it is of interest to model transport through a magnetic molecule placed in a junction. Consequently, an illustrative example is briefly discussed to demonstrate how the magnetic spin states affect the transport characteristics. In this example, the effect of transverse magnetic anisotropy is neglected, i.e., $E = 0$. Unlike nonmagnetic ones, each charge state of a magnetic molecule is no longer represented by a single level, but rather by $2S_n + 1$

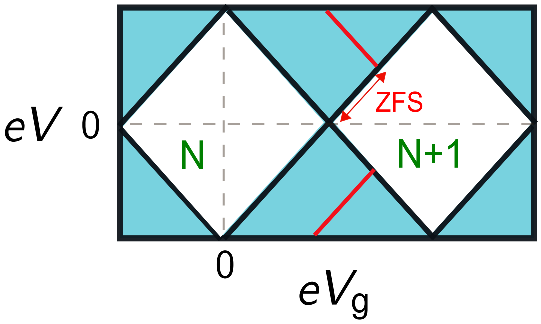

Figure 1.7: Stability diagram. Differential conductance plot, $\partial I/\partial V$, as a function of gate V_g and bias V voltage showing, in comparison to Fig. 1.3(b), an additional red line that reflects the transition to the excited state of the charged molecule. The additional energy required corresponds to the difference between the ground and first excited spin states of the charged molecule, namely the zero-field splitting.

spin states, where S_n is the spin of the molecule at the charge state n. Thus, each molecular state is now characterized by two quantum numbers $|n, M_n\rangle$ where M_n is the S_z projection of the spin-state of the molecule in the charge state n. For instance, for the molecule under discussion, a half-integer spin S_N is assumed for the *neutral* state and, in turn, the *charged* state possesses an integer spin S_{N+1}. As already explained, no charge transfer takes place at zero bias due to the equilibrium of chemical potential between the source μ_s and the drain μ_d. Upon applying bias V, the difference in chemical potential $\mu_\mathrm{s} - \mu_\mathrm{d}$ allows an electron to tunnel from the source to the drain, via the molecule. Figure 1.6(a) depicts two possibilities for such a tunneling event. The first possibility, shown on the left side of Fig. 1.6(a), occurs when an electron tunnels to the molecule causing it to alter its charge state from the neutral state N to the charged state $N+1$ via a ground-state to ground-state transition. In other words, a transition from the neutral molecular state $|N, S_N\rangle$ to the state $|N+1, S_{N+1}\rangle$ occurs. Alternatively, the molecule could make a transition from the neutral N to the charged state $N+1$ via an excited spin state, as illustrated on the right side of Fig. 1.6(a). This represents a transition from the neutral molecular state $|N, S_N\rangle$ to the state $|N+1, S_{N+1}-1\rangle$.[4] An example of these two transitions is indicated on the energy spectrum of the neutral and charged molecules by blue arrows and typically observed in stability diagrams, as shown in Fig. 1.7. The energy required to achieve this transition is the difference between the ground and first excited spin states of the charged molecule, namely the *zero-field splitting*, which is denoted by ZFS on the stability diagram. It is worth mentioning that electron transport measurements described here could also be used to determine the magnetic anisotropy of single magnetic molecule embedded in a junction, which cannot be measured by other experimental tools since they are applicable to an ensemble of molecules rather than individual ones. Using such spectroscopic tool, the uniaxial and transverse anisotropy constants of the Fe$_4$ SMM have been experimentally obtained in [30] and [31], respectively.

In the previous example, the effect of the transverse anisotropy was disregarded and, hence, the S_z spin projection was a good quantum number to characterize the molecular spin states. However, if $E \neq 0$ one can see that the second term of Eq. (1.1) breaks the rotational symmetry around

---

[4] It should be noted that there exists two similar transitions from the other ground state of the neutral molecule, namely from the molecular state $|N, -S_N\rangle$ to the two states $|N+1, -S_{N+1}\rangle$ and $|N+1, -S_{N+1}+1\rangle$, where it can also be seen that the absolute difference between the magnetic quantum number of the two possible final states is one.

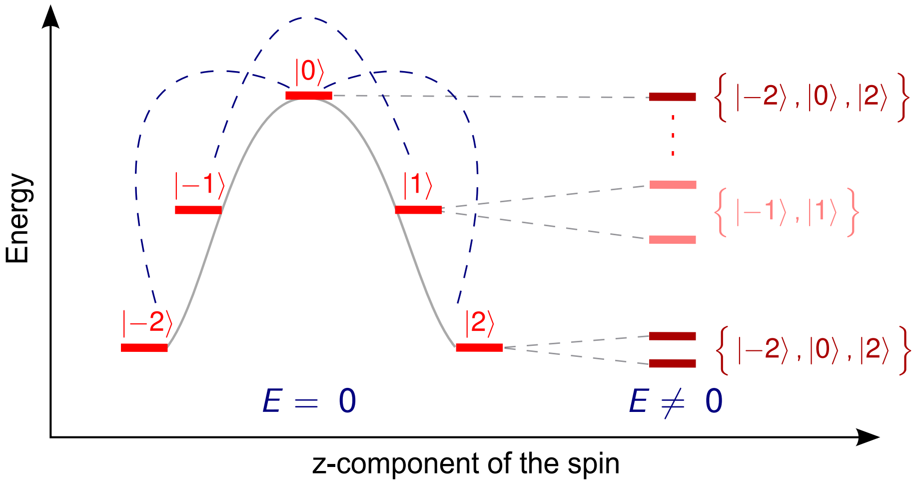

Figure 1.8: Energy spectrum of a magnetic molecule with spin $S = 2$ in the presence of transverse magnetic anisotropy. The transverse magnetic anisotropy breaks the rotational symmertry around the z-axis and, hence, splits the molecular states into two uncoupled sets consisting of an admixture of the pure S_z projections, as shown on the schematic energy spectrum by the two distinctive degrees of the color red. By reformulating the operators $\hat{S}_x$ and $\hat{S}_y$ in Eq. (1.1) in terms of the ladder operators, we can see that the transverse magnetic anisotropy only mixes every other state as indicated by the blue dashed lines. Accordingly, the two uncoupled sets, from which the new states are composed, become $\{ |-2\rangle, |0\rangle, |2\rangle \}$ and $\{ |-1\rangle, |1\rangle \}$.

the z-axis leading to mixing of S_z states. Since $\hat{S}_x = (1/2)[\hat{S}_+ + \hat{S}_-]$ and $\hat{S}_y = (1/2\imath)[\hat{S}_+ - \hat{S}_-]$, the second term in Eq. (1.1) can be rewritten as $(E/2)\left[\left(\hat{S}_+\right)^2 + \left(\hat{S}_-\right)^2\right]$, where $\hat{S}_+$ and $\hat{S}_-$ are the spin raising and lowering operator, respectively [23]. In particular, one finds that the transverse anisotropy couples every other state. For example, for a magnetic molecule with $S = 2$, the raising and lowering operators couple the states with the S_z projection equal to -2, 0 and 2, as shown in Fig. 1.8. The implication of the coupling between the S_z projections is an additional relaxation mechanism, namely *quantum tunneling of magnetization* (QTM) [23, 32–34]. As previously discussed, transitions between the neighboring spin-states are required to overcome the anisotropy barrier. Here one can see that an additional pathway arises due to the transverse anisotropy because mixing of the spin-states allows for transitions across the barrier. This effect gives rise to steps in magnetization relaxation curves, which are a typical signature of SMMs.

1.3.1 Molecular vibrations

An additional degree of freedom of key relevance to the thesis at hand are *molecular vibrations*. Molecules embedded in single-molecule junctions vibrate with discrete frequencies, which are a characteristic fingerprint of these molecules [35]. Importantly, these vibrations can couple to the charge and the spin of the tunneling electrons, so that when an electron tunnels via the molecule, it can excite vibrations by causing a transition from a vibrational ground state to an excite one [35]. The interaction between electronic charge and vibrations has been experimentally studied in single-molecule junctions based on carbon derivatives, specifically carbon nanotubes and fullerenes, [36–41], and also in other single molecules [42–45]. It was shown that charge-vibron[5] coupling drastically impacts the transport properties of individual molecules. For instance, in the case of strong

---

[5] Vibrons are quantized energy quanta associated with molecular vibrations.

coupling, a transport blockade can occur at low bias, which is referred to as Franck Condon blockade [46].

Recently, this coupling has also been observed in the context of magnetic molecules such as for the Fe_4 SMM where the signature of Franck Condon low bias blockade was detected [47]. The aforementioned experimental studies prove the significant influence of molecular vibrations on the transport characteristics of single molecules, in general, and magnetic molecules, in particular. Interestingly, molecular vibrations can couple not only to the *charge*, but also to the *spin* of magnetic molecules, which is referred to as the spin-vibron coupling. This interaction has been experimentally demonstrated by Ganzhorn *et al.* [48] by coupling a SMM to the mechanical oscillations of a suspended carbon nanotube. Although, the charge-vibron coupling in the context of magnetic molecules has been theoretically studied for the first time by McCaskey *et al.* [35], one aspect that still requires a closer investigation is the additional coupling mechanism between spin and vibrations. For this reason, the goal of this thesis is to investigate the impact of the interplay between charge, spin and molecular vibrations on the transport properties of a single-magnetic molecule.

1.4 Aim and outline

Given the significance of electronic transport through single-molecule devices, either from the perspective of fundamental research as a spectroscopic tool or from an application point of view, it is evident that proper understanding of the interplay between the various degrees of freedoms involved at the level of individual molecules is required. Consequently, the purpose of the thesis at hand is to theoretically characterize the *effect of the threefold coupling between charge, molecular vibrations and spin on transport properties of magnetic molecules.* The analysis starts by reviewing the basics of transport through a single magnetic molecule, in the absence of molecular vibrations, using the so-called *real time diagrammatic technique* and *Fermi golden rule. We rigorously demonstrate that using the latter approach is sufficient owing to the vanishing contributions of quantum coherences between the molecular spin states in the case of nonmagnetic electrodes.* Thus, using Fermi golden rule formalism with stationary rate equations, the effect of charge-vibron coupling is briefly reviewed. Finally, the main contribution of this thesis, spin-vibron interaction, is addressed. It is shown that *coupling between spin and molecular vibrations induces an additional magnetic anisotropy component in both the uniaxial and transverse directions.*

The present work is organized as follows: Chapter 2 briefly introduces the model used to describe transport through a magnetic molecule inserted in a symmetric, as well as, asymmetric molecular junction, in addition to effect of charge-vibron coupling. The interaction between spin and molecular vibrations and its effect on magnetic anisotropy are discussed in Chap. 3. In Chap. 4, the role of quantum coherences in transport through a magnetic molecule is explored with the help of the real-time diagrammatic technique.

2

Theoretical background and model

The purpose of this chapter is to lay the theoretical framework of the present thesis by providing a description of transport through a single magnetic molecule. To beging with, Sec. 2.1 introduces the model used to describe a magnetic molecule embedded in a single-molecule junction in the weak coupling regime, whereas in Sec. 2.2 and Sec. 2.3 the formalism allowing for characterization of transport through a single magnetic molecule in the sequential tunneling regime is discussed. Using this formalism, two examples of transport through a magnetic molecule are given in Sec. 2.4. Finally, in Sec. 2.5, the interaction between electronic charge and molecular vibrations is incorporated into the model along with an example demonstrating its effect on transport properties.

2.1 Model of a magnetic molecule captured in a junction

In the introductory chapter, the properties of bare magnetic molecules were discussed and it was shown that the spin states of the molecule impact its transport properties. In this chapter, the aim is to analyze the transport in more detail by presenting a model for a single magnetic molecule weakly tunnel-coupled to two electrodes, a source and a drain, as demonstrated in the schematic diagram in Fig. 2.1. It should be emphasized that the discussion here refers to the *weak coupling regime* which is one of the relevant regimes to study the properties of individual molecules because the molecular level structure is preserved even after contacting the electrodes (*cf.* Sec. 1.2). In general, a molecule coupled to non-interacting leads (electrodes) can be described by the general model Hamiltonian [49, 50]

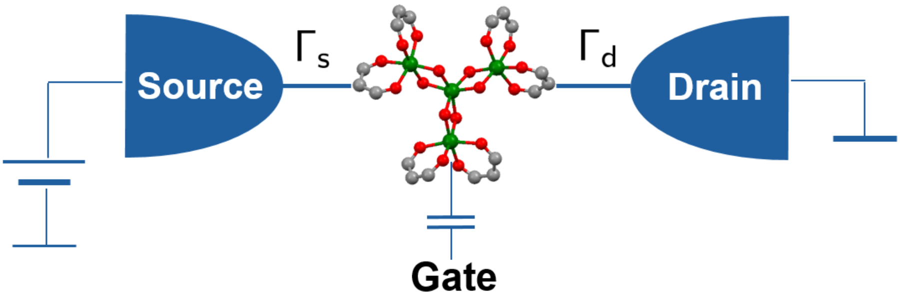

Figure 2.1: Single-molecule junction. A schematic illustration of a three-terminal junction with an embedded magnetic molecule. The junction is comprised of two electrodes, a source and a drain, weakly-coupled to the molecules such that electrons can tunnel from the source to the drain via the molecule. In addition, the molecule is capacitively coupled to the gate electrode which can be used to alter the charge state of the molecule.

$$\hat{\mathcal{H}} = \hat{\mathcal{H}}_{\text{mol}} + \hat{\mathcal{H}}_{\text{leads}} + \hat{\mathcal{H}}_{\text{tun}}. \tag{2.1}$$

Here, the molecular Hamiltonian $\hat{\mathcal{H}}_{\text{mol}}$ describes an individual magnetic molecule in a superposition of charge states n. Since the charging energy of individual molecules is usually high, the molecule is assumed to exist in only two charge states, referred to as the *neutral* state $n = N$ and the *charged* state $n = N + 1$ [49]. The molecular Hamiltonian $\hat{\mathcal{H}}_{\text{mol}}$ reads

$$\hat{\mathcal{H}}_{\text{mol}} = \sum_{n} \hat{\mathcal{H}}_{\text{spin},n} + (\varepsilon - eV_{\text{g}}) \sum_{l\sigma} \hat{d}_{l\sigma}^{\dagger} \hat{d}_{l\sigma}. \tag{2.2}$$

with

$$\hat{\mathcal{H}}_{\text{spin},n} = -D_n \big(\hat{S}_n^z\big)^2 + E_n \Big[\big(\hat{S}_n^x\big)^2 - \big(\hat{S}_n^y\big)^2\Big]. \tag{2.3}$$

As mentioned in Chap. 1, Eq. (2.3) is referred to as the *giant-spin Hamiltonian* [23, 24]. That is, the molecule can be represented by an effective charge-dependent spin $\boldsymbol{S}_n$. Specifically, the first term characterizes the uniaxial magnetic anisotropy of the molecule, conventionally chosen along the z-direction, with the charge state dependent *uniaxial anisotropy constant* D_n and the spin projection operator along the z-direction $\hat{S}_n^z$. Whereas, the second term describes the magnetic anisotropy along x and y directions, with the *transverse anisotropy constant* $|E_n| \leq |D_n|/3$ [23]. Moreover, the last term in the molecular Hamiltonian (2.2) accounts for a capacitively coupled gate V_{g} that allows for switching the molecule between the two accessible charge states by shifting the energy level ε of the charged state $N + 1$. The operators $\hat{d}_{l\sigma}^{\dagger}$ and $\hat{d}_{l\sigma}$ stand for the creation and annihilation of electrons in the molecular orbital l, respectively.

The second Hamiltonian $\hat{\mathcal{H}}_{\text{leads}}$ describes the left and right leads and it takes the following form

$$\hat{\mathcal{H}}_{\text{leads}} = \sum_{qk\sigma} \varepsilon_{k\sigma}^{q} \hat{a}_{k\sigma}^{q\dagger} \hat{a}_{k\sigma}^{q}, \tag{2.4}$$

where the leads are labeled by an index q to differentiate the left ($q = \text{L}$) and right ($q = \text{R}$) ones, and $\hat{a}_{k\sigma}^{q\dagger}$ ($\hat{a}_{k\sigma}^{q}$) is the creation (annihilation) operator of an electron with orbital quantum number k and spin σ in the lead with index q. The leads represent an infinite non-interacting reservoirs of electrons and, hence, they remain in equilibrium even if we remove or add few electrons. The electronic distribution in the leads is described by the *Fermi-Dirac* statistics as follows

$$f_q(\varepsilon) = \frac{1}{1 + \exp\left[\dfrac{(\varepsilon - \mu_q)}{k_{\text{B}}T}\right]}, \tag{2.5}$$

where $k_{\text{B}}T$ is the thermal energy, with Boltzmann constant k_{B}. The chemical potential of the electrodes is defined as $\mu_{\text{L(R)}} = \mu_0 \pm eV/2$ for a symmetrically applied bias voltage V, i.e., $V/2$ to the left and $-V/2$ to the right electrode. The equilibrium chemical potential of the electrodes is denoted here by μ_0. It should be noted that the convention used here is that the electronic charge $e < 0$.

Finally, the tunneling of electrons between the leads and the molecule is captured by the Hamiltonian

$$\hat{\mathcal{H}}_{\text{tun}} = \sum_{qlk\sigma} \Big\{ t_{l\sigma}^{q} \hat{d}_{l\sigma}^{\dagger} \hat{a}_{k\sigma}^{q} + \text{h.c.} \Big\}, \tag{2.6}$$

where the first term corresponds to the tunneling of an electron with spin σ and momentum k from an electrode with index q to the molecule, whereas its Hermitian conjugate in the second term represents a tunneling process in the opposite direction. The matrix element $t^q_{l\sigma}$ characterizes the coupling between the molecule and the electrodes and will later appear as part of the expression for the tunnel-coupling strength Γ. It is worth mentioning here that the electrode index, appearing in the tunneling matrix element $t^q_{l\sigma}$, implies that the coupling of the molecule to the left and right electrodes can be asymmetric as discussed in Sec. 2.4.3.

In the absence of transverse anisotropy $E = 0$, the states of the molecule can be characterized by two quantum numbers $|S_n, M_n\rangle$ where n is the charge of the molecule and S_n and M_n are the total and S_z projection of the spin-state of a molecule in charge state n, respectively. However, if $E \neq 0$ one can see that the second term of Eq. (2.3) breaks the rotational symmetry around the z-axis which mixes the S_z projections of the spin-states. Since $\hat{S}^z_n$ is Hermitian and, hence, its eigenstates form a complete set, the spin-states of the molecule can still be represented in the presence of transverse magnetic anisotropy as linear combinations of S_z projections. Thus, an arbitrary molecular state $|\chi_n\rangle$ in the charge state n can be represented as

$$|\chi_n\rangle = \sum_{M_n} C_{M_n} |S_n, M_n\rangle \,. \tag{2.7}$$

where C_{M_n} are the linear expansion coefficients.

2.2 Description of transport through a magnetic molecule

In the previous section, we discussed a general model for a single-molecule junction where electrons can tunnel from the source to the drain via the molecule. Now, our aim is to determine the total charge current through the molecule resulting from the tunneling of electrons. One way is to keep track of the transitions between the molecular states since these transitions correspond to electron tunneling processes. For instance, a transition from an arbitrary neutral molecular state $|\chi_N\rangle$ to a charged one $|\chi_{N+1}\rangle$ corresponds to the tunneling of an electron from the electrodes to the molecule. Importantly, in order to characterize the contribution of an arbitrary transition between molecular states to the current, it is required to know the *rate* at which this transition occurs, in addition to, the *occupation* of the initial molecular state for such transition. Consequently, the question now arises: how to obtain the occupation of the molecular states, or more generally, how to determine the quantum state of a magnetic molecule embedded in a junction between two electrodes?

Essentially, the state of a quantum system can be fully described with the help of the density matrix ρ

$$\rho = \sum_{\alpha} \mathcal{P}_\alpha |\alpha\rangle \langle\alpha| \,. \tag{2.8}$$

In particular, the diagonal elements of the density matrix describe the occupations (*probabilities*) of the states $|\alpha\rangle$ that the quantum system can be in, whereas the off-diagonal elements represents the coherent superpositions between these states (*coherences*). For our quantum system consisting of a molecule and two leads, our goal is to keep track of the *molecular* states. Accordingly, we can obtain a *reduced* density matrix for the molecule ρ^{red} by taking a trace over the degrees of freedom in the leads [50]. Thus, the sought probabilities of the molecular states $|\chi_n\rangle$ can be found on the diagonal part of the reduced density matrix of the molecule. However, it should be remembered that, since the transverse magnetic anisotropy leads to mixing of the pure S_z states of the molecule, it is legitimate to assume that the evolution of the off-diagonal elements is non-trivial and can have an impact on the total current through the molecule. Thus, it is indispensable to calculate the current using a method that captures the dynamics of the diagonal, as well as, the off-diagonal elements of the reduced density matrix.

Nevertheless, in literature, the coherent superpositions are usually assumed to be negligible and the classical rate equations with *Fermi golden rule* are typically used [30, 31, 35]. In other words, only the diagonal elements (probabilities) of the reduced density matrix are used to characterize transport through magnetic molecules. By contrast, in this thesis, before resorting to Fermi golden rule, we decided to verify the assumption that the off-diagonal elements can be ignored. Consequently, in Chap. 4, the *real-time diagrammatic technique* is employed for an exact treatment of the reduced density matrix to investigate *the role of quantum coherences on transport through individual magnetic molecules.* We prove that coherences can be ignored in the case of a molecule captured between *nonmagnetic* electrodes. Accordingly, the real-time diagrammatic technique collapses into the classical rate equations and Fermi golden rule, which is used in the present work throughout Chap. 2 and 3. However, in the case of *ferromagnetic* electrodes, coherent superposition between molecular states can, in fact, impact the transport properties as discussed in Sec. 4.3.1.

2.3 Sequential transport: master equation and Fermi golden rule

The purpose of this section is to explain the method used to calculate the tunneling current through a magnetic molecule, taking into consideration only the diagonal elements of the reduced density matrix. In order to describe the sequential transport through a magnetic molecule in the weak coupling limit, the transition rates between the molecular states $|\chi_n\rangle$ are calculated in the leading-order of the tunnel-coupling strength Γ using Fermi golden rule. Using these rates, a master equation can be constructed to obtain the occupational probabilities $\mathcal{P}_{\chi_n}$ of the molecular states [49]. The observables of the system, such as current and conductance, can be derived with the knowledge of transition rates and probabilities, as explained below.

To beging with, the probabilities of the molecular spin-states $\mathcal{P}_{\chi_n}$can be obtained from the stationary state master equation

$$\frac{\mathrm{d}\mathcal{P}_{\chi_n}}{\mathrm{d}t} = 0 = \sum_{q} \sum_{\chi_{n'},n'} \Big\{ W^{q}_{\chi_n,\chi_{n'}} \mathcal{P}_{\chi_{n'}} - W^{q}_{\chi_{n'},\chi_n} \mathcal{P}_{\chi_n} \Big\}, \tag{2.9}$$

where $W^{q}_{\chi_{n'},\chi_n}$ is the transition rate from a state $|\chi_n\rangle$ to a state $|\chi_{n'}\rangle$ due to the tunneling of an electron to or from an electrode q. Equation (2.9) describes the time evolution of the occupancy of an arbitrary molecular state $|\chi_n\rangle$ based on the transition rates between this state and other molecular states to which such transitions are allowed. Knowing the probabilities and transition rates, the charge current flowing into an electrode q can be calculated by

$$I_q = e \sum_{n,\chi_n} \sum_{n',\chi_{n'}} (n' - n) W^{q}_{\chi_{n'},\chi_n} \mathcal{P}_{\chi_n} \,. \tag{2.10}$$

Accordingly, the total charge current flowing through the molecule is given by

$$I = (I_{\mathrm{R}} - I_{\mathrm{L}})/2. \tag{2.11}$$

It can be seen from Eq. (2.9) and (2.10) that calculating the transition rates between the molecular states is a prerequisite for obtaining the probabilities and, hence, the current through the molecule. For this reason, the remaining part of this section is devoted to calculating these transition rates using Fermi golden rule, which is defined as [49]

$$\mathcal{W}^{|i\rangle}_{|f\rangle} = \frac{2\pi}{\hbar}\left| \langle f| \hat{\mathcal{H}}_{\text{tun}} |i\rangle \right|^2 \delta(E_f - E_i). \tag{2.12}$$

Equation (2.12) defines the transition rate from an initial state $|i\rangle$ with an energy E_i to a final state $|f\rangle$ with an energy E_f which occurs due to a perturbation, in this case a single electron tunneling process. Since the tunneling of a single electron involves transitions between molecular states corresponding to different charge states, the transition rate between two arbitrary molecular states $|\chi_n\rangle$ and $|\chi_{n'}\rangle$ due to tunneling of an electron associated with the qth electrode can be defined as

$$W^q_{\chi_{n'},\chi_n} = \sum_{k\sigma\in q} \Big\{ \mathcal{W}^{|k\sigma;\chi_n\rangle}_{|0;\chi_{n'}\rangle} f_q(\varepsilon^q_{k\sigma}) + \mathcal{W}^{|0;\chi_n\rangle}_{|k\sigma;\chi_{n'}\rangle} \left[1 - f_q(\varepsilon^q_{k\sigma})\right] \Big\}, \tag{2.13}$$

where $f(\varepsilon^q_{k\sigma})_q$ is the Fermi function of the qth electrode, given by Eq. (2.5). The composite state of the molecule and the electrode q reads as

$$|k\sigma;\chi_n\rangle \equiv |k\sigma\rangle_q \otimes |\chi_n\rangle\,. \tag{2.14}$$

Equation (2.13) illustrates the two possible electron tunneling pathways between a molecule and leads. An electron can either tunnel into the molecule (*first* term) or tunnel out of the molecule (*second* term). As an instructive example, the detailed calculation of a *tunneling-in* event is given here, whereas the *tunneling-out* rate can be derived in a similar manner. For the *tunneling-in* process, the initial state of the system (molecule plus electrode) reads $|i\rangle = |k\sigma\rangle_q \otimes |\chi_N\rangle$, whereas the final state is defined as $|f\rangle = |0\rangle_q \otimes |\chi_{N+1}\rangle$. Using Eq. (2.12), the transition rate from a neutral molecular state $|\chi_N\rangle$ to a charged one $|\chi_{N+1}\rangle$ can be written as

$$\begin{aligned} \mathcal{W}^{|i\rangle}_{|f\rangle} &= \frac{2\pi}{\hbar}\left| \langle f| \hat{\mathcal{H}}_{\text{tun}} |i\rangle \right|^2 \delta(E_f - E_i) \\ &= \frac{2\pi}{\hbar}\left| \langle 0|_q \langle \chi_{N+1}| \sum_{q'lk'\sigma'} t_l^{q'}\, \hat{d}^\dagger_{l\sigma'} \hat{a}^{q'}_{k\sigma'}\; |k\sigma\rangle_q |\chi_N\rangle \right|^2 \delta\big(\varepsilon_{\chi_{N+1}} - (\varepsilon_{\chi_N} + \varepsilon^q_{k\sigma})\big), \end{aligned} \tag{2.15}$$

where the tunneling matrix element $t_l^{q'}$ is assumed to be spin independent. Rearranging the expression, we arrive at

$$\begin{aligned} \mathcal{W}^{|i\rangle}_{|f\rangle} =& \frac{2\pi}{\hbar}\left| \sum_{q'lk'\sigma'} t_l^{q'}\, \langle 0|_q\, \hat{a}^{q'}_{k'\sigma'} |k\sigma\rangle_q \langle \chi_{N+1}| \hat{d}^\dagger_{l\sigma'} |\chi_N\rangle \right|^2 \delta\big(\varepsilon_{\chi_{N+1}} - (\varepsilon_{\chi_N} + \varepsilon^q_{k\sigma})\big) \\ &= \frac{2\pi}{\hbar}\left| \sum_{q'lk'\sigma'} t_l^{q'}\; \delta_{qq'}\delta_{kk'}\delta_{\sigma\sigma'}\; \langle \chi_{N+1}| \hat{d}^\dagger_{l\sigma'} |\chi_N\rangle \right|^2 \delta\big(\varepsilon_{\chi_{N+1}} - (\varepsilon_{\chi_N} + \varepsilon^q_{k\sigma})\big) \\ &= \frac{2\pi}{\hbar}\left| \sum_{l} t_l^{q}\, \langle \chi_{N+1}| \hat{d}^\dagger_{l\sigma} |\chi_N\rangle \right|^2 \delta\big(\varepsilon_{\chi_{N+1}} - (\varepsilon_{\chi_N} + \varepsilon^q_{k\sigma})\big). \end{aligned} \tag{2.16}$$

Using Eq. (2.7), the molecular states are defined in the basis of the S_z spin projections as follows

$$
\begin{aligned}
|\chi_N\rangle &= \sum_{M_N} a_{M_N} |S_N, M_N\rangle\,, \\
|\chi_{N+1}\rangle &= \sum_{M_{N+1}} b_{M_{N+1}} |S_{N+1}, M_{N+1}\rangle\,.
\end{aligned}
\tag{2.17}
$$

By plugging the molecular states into Eq. (2.16), the result reads

$$
\mathcal{W}_{|f\rangle}^{|i\rangle} = \frac{2\pi}{\hbar}\left|\sum_l t_l^q \sum_{M_{N+1}} \sum_{M_N} a_{M_N} b^*_{M_{N+1}} \langle S_{N+1}, M_{N+1}|\, \hat{d}^\dagger_{l\sigma}\, |S_N, M_N\rangle\right|^2 \delta\big(\varepsilon_{\chi_{N+1}} - (\varepsilon_{\chi_N} + \varepsilon^q_{k\sigma})\big).
\tag{2.18}
$$

Here, we encounter the issue that the creation operator of the molecule $\hat{d}^\dagger_{l\sigma}$ is represented in terms of the molecular orbital l, whereas we define the molecular states $|\chi_n\rangle$ based on the S_z spin projections; hence, we are faced with the cumbersome matrix element $\langle S_{N+1}, M_{N+1}|\, \hat{d}^\dagger_{l\sigma}\, |S_N, M_N\rangle$. However, this complication can be circumvented by using the *Wigner-Eckart* theorem [51], which splits this matrix element into a product of two factors. First, a *reduced matrix element* that does not depend on the orientation of the angular momentum. In other words, this reduced matrix element is independent of the magnetic quantum number of the molecular states $|\chi_n\rangle$. The second factor is the *Clebsch-Gordan coefficients* which are the expansion coefficients resulting from the addition of angular momenta [52]. To give an illustration, the state $|SM\rangle$ resulting from combining two states $|S_1M_1\rangle$ and $|S_2M_2\rangle$ can be written as linear combinations of the composite state $|S_1M_1\rangle\,|S_2M_2\rangle$ with the Clebsch-Gordan coefficients as the linear expansion coefficients in the following form

$$
|SM\rangle = \sum_{M_1+M_2=M} \langle S_1, M_1; S_2, M_2|\, S, M\rangle\, |S_1M_1\rangle\, |S_2M_2\rangle\,.
\tag{2.19}
$$

Going back to the transition rate in Eq. (2.18) and employing Wigner-Eckart theorem, the resulting expression reads as

$$
\begin{aligned}
\mathcal{W}_{|f\rangle}^{|i\rangle} = \frac{2\pi}{\hbar}&\left|\sum_l t_l^q \sum_{M_{N+1}} \sum_{M_N} a_{M_N} b^*_{M_{N+1}} \big\langle S_N, M_N; 1/2, \sigma\big|S_{N+1}, M_{N+1}\big\rangle\, \langle S_{N+1}|\,|\hat{d}^\dagger_l|\,|S_N\rangle\right|^2 \\
&\times \delta\big(\varepsilon_{\chi_{N+1}} - (\varepsilon_{\chi_N} + \varepsilon^q_{k\sigma})\big),
\end{aligned}
\tag{2.20}
$$

where we can see that the magnetic quantum numbers σ, M_N and M_{N+1} are decoupled from the reduced matrix element $\langle S_{N+1}|\,|\hat{d}^\dagger_l|\,|S_N\rangle$. The constants $\big\langle S_N, M_N; 1/2, \sigma\big|S_{N+1}, M_{N+1}\big\rangle$ are the Clebsch-Gordan coefficients signifying the addition of an electron with a magnetic quantum number σ to a molecule with a spin S_N and a magnetic quantum number M_N as a result of a *tunneling-in* process of an electron from the leads to the molecule. The Clebsch-Gordan coefficients are a central consequence of using the molecular spin-state basis and they act as selection rules that allow or forbid transitions between the molecular states $|\chi_n\rangle$. Since electrons are half-spin particles, each electron-tunneling process must change the S_z spin projection of the molecular state by half, i.e., $M_{N+1} - M_N = \pm 1/2$. Finally, the transition rate can be written as

$$
\mathcal{W}_{|f\rangle}^{|i\rangle} = \frac{2\pi}{\hbar}\big|\mathbb{T}^q_{S_N S_{N+1}}\big|^2 \big|\mathcal{T}^\sigma_{a_N b_{N+1}}\big|^2 \delta\big(\varepsilon_{\chi_{N+1}} - (\varepsilon_{\chi_N} + \varepsilon^q_{k\sigma})\big),
\tag{2.21}
$$

with

$$\mathcal{T}^{\sigma}_{a_N b_{N+1}} = \sum_{M_{N+1}} \sum_{M_N} a_{M_N} b^{*}_{M_{N+1}} \big\langle S_N, M_N; 1/2, \sigma \big| S_{N+1}, M_{N+1} \big\rangle, \tag{2.22}$$

and $\mathbb{T}^{q}_{S_N S_{N+1}} = \sum_l t^{q}_{l} \, \langle S_{N+1} | \, |\hat{d}^{\dagger}_{l}| \, | S_N \rangle$ is considered as a free parameter in the calculations that determines the coupling strength between the molecule and the leads, as explained below. Inserting Eq. (2.21) into Eq. (2.13), it can be seen that to obtain the final expression for the tunneling rate, one has to sum over the electronic states in the electrodes, that is,

$$W^{q}_{\chi_{N+1}, \chi_N} = \sum_{k\sigma \in q} \frac{2\pi}{\hbar} |\mathbb{T}^{q}_{S_N S_{N+1}}|^2 |\mathcal{T}^{\sigma}_{a_N b_{N+1}}|^2 f^{q}(\epsilon^{q}_{k\sigma}) \delta\big(\varepsilon_{\chi_{N+1}} - (\varepsilon_{\chi_N} + \varepsilon^{q}_{k\sigma})\big). \tag{2.23}$$

By converting the momentum summation into an integral over the density of states, the final expression of the transition rate from a neutral molecular state $|\chi_N\rangle$ into a charged one $|\chi_{N+1}\rangle$ can be given by

$$W^{q}_{\chi_{N+1}, \chi_N} = \frac{1}{\hbar} \sum_{\sigma} \Gamma^{\sigma}_{q} |\mathcal{T}^{\sigma}_{a_N b_{N+1}}|^2 f^{q}(\varepsilon_{\chi_{N+1}} - \varepsilon_{\chi_N}), \tag{2.24}$$

where the tunnel-coupling strength reads

$$\Gamma^{\sigma}_{q} = 2\pi \rho^{q}_{\sigma} |\mathbb{T}^{q}_{S_N S_{N+1}}|^2, \tag{2.25}$$

with ρ^{q}_{σ} denoting the density of states of an electrode q for the spin σ population. It should be emphasized that, in order to perform the integral resulting from the momentum summation in Eq. (2.23), we assumed that the density of state in the leads is constant, i.e., the density of states is the same regardless of the energy of the tunneling electron. This assumption is commonly known as the flat-band approximation.

2.3.1 Spin Polarized Electrodes

In the previous discussion, we have seen that, for a *tunneling-in* process, the resultant (*final*) molecular state $|\chi_{N+1}\rangle$ is determined based on the *initial* molecular state $|\chi_N\rangle$ and, importantly, the spin of the tunneling electron σ. Consequently, one way to modify the occupations of the molecular states $|\chi_n\rangle$ and, hence, impact the transport properties through the molecule, is to manipulate the spin population of the tunneling electrons via the use of *ferromagnetic electrodes*. For instance, we can favor the tunneling of spin-up (↑) electrons over spin-down (↓) ones, or *vice versa*. Accordingly, in this section, we address the spin-dependence of the tunnel-coupling strength Γ, given in Eq. (2.25), from the theoretical perspective, whereas in Sec. 2.4.4, examples of spin-polarized transport through a single magnetic molecule are discussed.

On the one hand, in case of *nonmagnetic* electrodes such as gold, the density of states of spin-up (↑) and spin-down (↓) electrons near the Fermi level E_f is the same [22]. As a result, the tunnel-coupling strength is independent of the spin of the tunneling electrons. However, in case of *ferromagnetic* electrodes, e.g. nickel, there exists a relative difference between the spin-up (↑) and down (↓) density of states near the Fermi level, which renders the tunnel-coupling spin-dependent. Accordingly, a spin polarization P^q for an electrode q can be defined by [53, 54]

$$P^{q} = \frac{\rho^{q}_{+}(E_f) - \rho^{q}_{-}(E_F)}{\rho^{q}_{+}(E_f) + \rho^{q}_{-}(E_f)}, \tag{2.26}$$

where $\rho^{q}_{+}(E_f)$ denotes the density of states of the majority spin population (+) at the Fermi level, whereas ρ^{q}_{-} refers to the minority spin population (−). The total density of states for

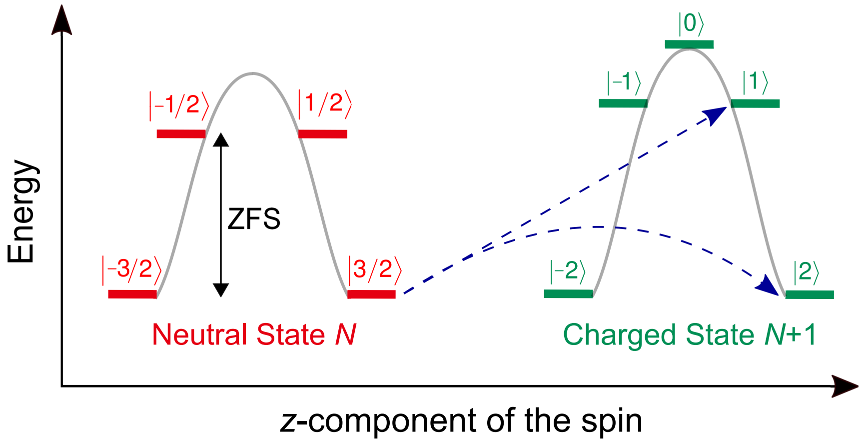

Figure 2.2: Energy spectrum for a magnetic molecule in the neutral and charged states. A molecule with spin $S_N = 3/2$ in the neutral state and $S_{N+1} = 2$ in the charged state is considered. The molecular states $|\chi_n\rangle$ are split into $2S + 1$ states as a result of the uniaxial anisotropy. In the absence of the transverse magnetic anisotropy, the molecular states are given by the S_z spin projections. The difference between the lowest two energy states in the neutral (charged) state is referred to as zero-field splitting ZFS_N (ZFS_{N+1}). However, in this example, the zero-field splitting of the neutral state will be referred to as ZFS for the sake of brevity, as indicated on the plot. The two blue arrows indicate the possible tunneling pathways from the neutral to the charged states. These two transitions correspond to the two lines in the stability diagram in Fig. 2.3.

the qth electrode, now, reads $\rho^q = \rho^q_+ + \rho^q_-$. Consequently, we can now rewrite the tunnel-coupling strength Γ as

$$\Gamma^{\pm}_q = 2\pi\frac{\rho^q}{2}(1 \pm P^q)|\mathbb{T}^q_{S_N S_{N+1}}|^2. \tag{2.27}$$

2.4 Examples of transport through a magnetic molecule

In order to illustrate the use of the Fermi golden rule formalism with the classical rate equations and to gain an insight into how the molecular spin states $|\chi_n\rangle$ manifest in the transport through magnetic molecules, two transport examples (in the absence of molecular vibrations) are discussed in this section. The first example assumes a magnetic molecule with *only uniaxial* magnetic anisotropy, i.e., $E = 0$. In contrast, the second example considers a molecule with *both uniaxial and transverse* magnetic anisotropy. Furthermore, at the end of this section, we study the effect of *asymmetrically* coupling the molecule to the left and right electrodes on the transport properties. Finally, the issue of spin-polarized transport is addressed by assuming a molecule embedded between two ferromagnetic electrodes.

2.4.1 Molecule with *uniaxial* magnetic anisotropy only

In this example, we consider a molecule with only uniaxial magnetic anisotropy ($D > 0$ and $E = 0$). As previously explained, the magnetic anisotropy along the z-direction splits the eigenstates of the molecule into $2S + 1$ states where S is the total spin of the molecule. The energetic preference to align the spin moment along the z-axis (easy axis) results in a parabolic energy spectrum in which

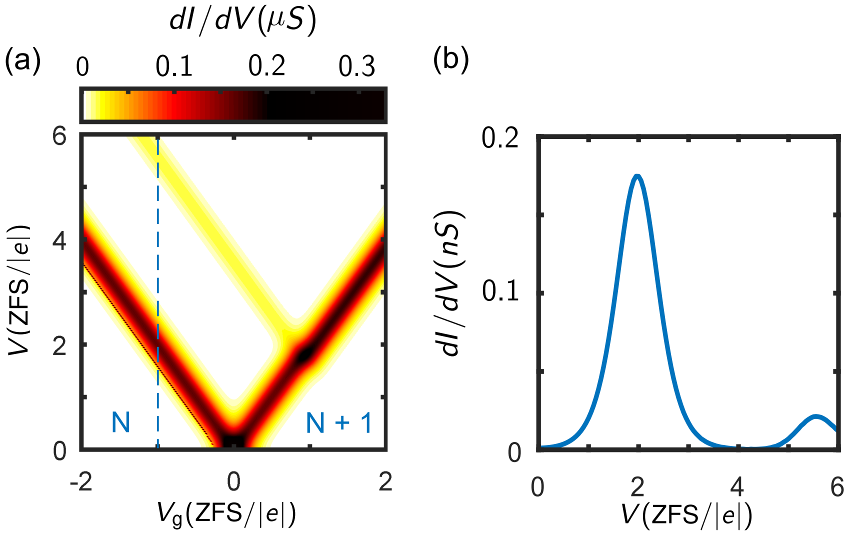

Figure 2.3: Differential conductance plots of a molecule with uniaxial magnetic anisotropy only. **(a)** A stability diagram of the molecule given in Fig. 2.2. The molecule exists in the stable charge state N $(N+1)$ in the lower *left* (*right*) corner of the diagram, whereas it alternates its charge state in the sequential tunneling region in the middle as electrons hop from the source to the drain via the molecule. The two parallel lines represent the four possible transitions from a neutral molecular state $|\chi_N\rangle$ to a charged molecular state $|\chi_{N+1}\rangle$. **(b)** A differential conductance plot is presented by taking a cut at a gate voltage $V_g = -1$ (ZFS/$|e|$), as indicated by the vertical dashed line in (a). Analogously to the two parallel lines in (a), the two peaks represent the allowed tunneling events from the neutral to the charged state.

the molecular states with highest magnetic quantum number constitute the ground state of the molecule. For the example at hand, we study a magnetic molecule with a total spin $S_N = 3/2$ in the neutral state and a spin $S_{N+1} = 2$ in the charged state, as depicted in the energy spectrum in Fig. 2.2. Referring to Eq. (2.2), we see that the anisotropy parameter can be charge-dependent. Accordingly, for the calculations performed here, we assume $D_N = 100$ μeV for the neutral state and $D_{N+1} = 120$ μeV for the charged state, with a difference of 20% between both parameters. The order of magnitude of both parameters was adopted based on magnetic molecules with similar properties such as the Fe_4 SMM studied in Ref. [30, 31]. The calculations were conducted for a temperature $T = 0.16$ K ($k_B T = 14$ μeV). The temperature T is chosen considerably lower than the zero-field splitting to allow for resolving the transitions between the molecular states $|\chi_n\rangle$. Moreover, the tunneling-coupling strength to both left and right electrodes are assumed to be equal to 1 μeV to satisfy the condition $\Gamma \ll k_B T$ for the weak-coupling regime. Finally, we should remark that, in order to gain a clear physical interpretation from the differential conductance plots, all the energy units are represented in terms of the zero-field splitting (ZFS) of the *neutral* state as indicated on Fig. 2.2.

Following the recipe of Fermi golden rule with the stationary-state rate equations, the charge current and also the differential conductance dI/dV are calculated through this symmetrically tunnel-coupled molecule. Figure 2.3(a) illustrates a differential conductance map, which is the typical result of conductance measurement through a *three-terminal* single-molecule junction. By tuning the capacitively applied gate voltage V_g, we can alter the charge state of the molecule. At large positive gate voltage and small bias voltage [lower *right* corner of Fig. 2.3(a)], the molecule exists only in the charged state $N+1$, whereas at large negative gate voltage [lower *left* corner of Fig. 2.3(a)], the molecule remains in the neutral state N, as indicated on the stability diagram. The region in-between represents the sequential tunneling region where the molecule alternates between the two charge states as electrons tunnel from the source to the drain via the molecule.[1]

When an electron tunnels into the molecule from the leads, the molecule makes a transition from a neutral molecule state $|\chi_N\rangle$ to a charged molecular state $|\chi_{N+1}\rangle$. For the molecule at hand, there exists four possible pathways for such a transition. At low bias voltage, the molecule can either make a transition from the state $|3/2\rangle$ to the state $|2\rangle$ (*cf.* Fig. 2.2) or from the state $|-3/2\rangle$ to the state $|-2\rangle$. It should be noted that, for the sake of brevity, we refer to the molecular states using the magnetic quantum number only, i.e., $|S_n, M_n\rangle \equiv |M_n\rangle$. As the bias voltage increases, additional transitions become accessible, namely the transition from the state $|3/2\rangle$ to the state $|1\rangle$ (*cf.* Fig. 2.2) and from the state $|-3/2\rangle$ to the state $|-1\rangle$. Due to the degeneracy between molecular states with the same absolute value of the magnetic quantum number, for instance the states $|1\rangle$ and $|-1\rangle$, these four transitions appear only as two lines in the differential conductance plot, as in Fig. 2.3(a). Importantly, we note that there is no transition to the state $|0\rangle$ since such transition requires changing the spin moment by an amount larger than 1/2, which is more than the spin of a single tunneling electron. This can be attributed to the spin conservation selection rule, imposed by the Clebsch-Gordan coefficients which forbid any transition if $M_{N+1} - M_N \neq 1/2$. For this reason, there exists only two possible transitions from a charged molecular state $|\chi_{N+1}\rangle$ to a neutral one $|\chi_N\rangle$. Particularly, from the states $|2\rangle$ and $|-2\rangle$ to the states $|3/2\rangle$ and $|-3/2\rangle$, respectively.

In addition to the stability diagram in Fig. 2.3(a), we can also keep track of the transitions between the molecular states via one-dimensional differential conductance plots such as Fig. 2.3(b). These plots are typically obtained in a *two-terminal* configuration such as using a scanning tunneling microscope (STM) on a molecule that lies on a substrate (*cf.* Fig. 1.2). The two terminals, here, refer to the source and the drain, i.e., there is no gate electrode to manipulate the charge state of the molecule through adjusting the energy level of the charged state. For the molecule under consideration, Fig. 2.3(b) illustrates a cut along a constant gate voltage $V_\mathrm{g} = -1$ ZFS/$|e|$. The two differential conductance peaks correspond to the two lines in Fig. 2.3(a), representing the transitions between the neutral molecular states $|\chi_N\rangle$ to the charged molecular states $|\chi_{N+1}\rangle$.

2.4.2 Molecule with both *uniaxial* and *transverse* magnetic anisotropy

In the following example, a molecule with both uniaxial and transverse magnetic anisotropy components is studied. Unlike the previous example, we assume a molecule with a total spin $S_N = 1/2$ in the neutral state and $S_{N+1} = 1$ in the charged state. The reason for choosing this particular molecule is twofold. First, the eigenvalues and eigenstates of the spin $S = 1$ molecule can be obtained analytically, which is not the case for larger spin values ($S > 1$). Thus, this example is appealing for understanding the details of the molecular Hamiltonian given in Eq. (2.2). Second, for the spin-vibron interaction discussed in Chap. 3, it will be shown that the molecular Hamiltonian cannot be diagonalized except for a molecule with $S = 1$. Accordingly, it is instructive to get familiar with this molecule in the present section, since it is central to the discussion of spin-vibron interaction that follows in Chap. 3.

Our goal now is to determine the eigenstates and energies of the aforementioned molecule. To begin with, for the neutral state N, one should notice that the notion of uniaxial magnetic

---

[1] It should be emphasized that the gate voltage is chosen such that the ground state of the neutral N and charged $N+1$ states are degenerate at $V_\mathrm{g} = 0$, as indicated in the energy spectrum in Fig. 2.2.

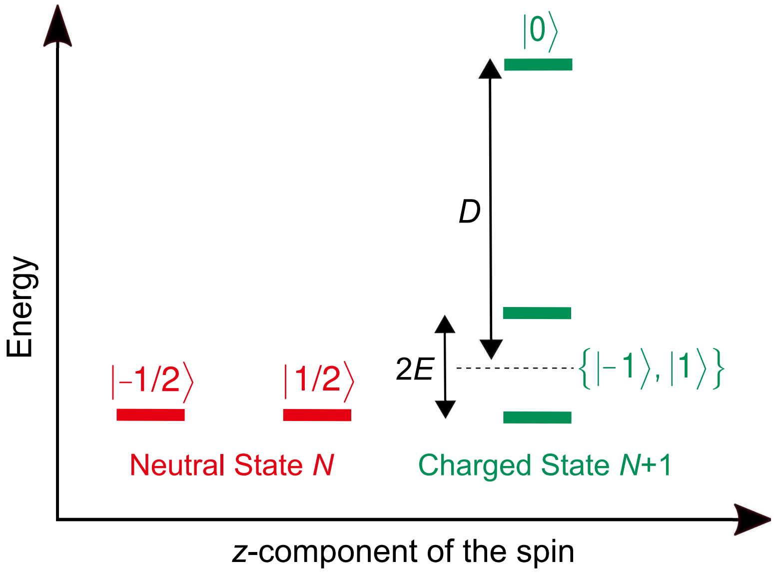

Figure 2.4: Energy spectrum for a magnetic molecule in the neutral and charged states. A molecule with spin $S_N = 1/2$ in the neutral state and $S_{N+1} = 1$ in the charged state is considered. For the neutral state, the energy spectrum consists of two degenerate molecular states since the uniaxial and transverse magnetic anisotropy do not influence spin-half systems. For the charged state $N+1$, the transverse magnetic anisotropy breaks the rotational symmetry around the z-axis. As a result, the eigenstates of the charged molecule become an admixture of the pure S_z projections of the spin, and the ground state doublet becomes split.

anisotropy does not apply since the molecule behaves as an electron with either spin up or down. Additionally, the eigenvalues of $\left(\hat{S}_n^+\right)^2$ and $\left(\hat{S}_n^-\right)^2$ are zeros since these quadratic ladder operators couple every other state. As a result, the neutral molecule is also not affected by the transverse magnetic anisotropy and, hence, its energy spectrum consists of two degenerate molecular states, namely $|\chi_{1/2}\rangle = |1/2\rangle$ and $|\chi_{-1/2}\rangle = |-1/2\rangle$. By contrast, for the charged state $N+1$, the transverse magnetic anisotropy splits the S_z spin projections into two time-reversed sets, $\left\{\, |0\rangle \,\right\}$ and $\left\{\, |-1\rangle, |1\rangle \,\right\}$. Significantly, the molecular states $|\chi_{N+1}\rangle$ become an admixture of the S_z projections belonging to one of these two sets. In order to obtain these molecular states and their corresponding energies, we write down the charged state spin Hamiltonian

$$\hat{\mathcal{H}}_{\text{spin},N+1} = \begin{pmatrix} -D & 0 & E \\ 0 & 0 & 0 \\ E & 0 & -D \end{pmatrix}, \tag{2.28}$$

where the constants E and D are the transverse and uniaxial anisotropy parameters for the charged molecule, respectively. Diagonalization of the matrix in Eq. (2.28) yields the following eigenfunctions with the corresponding eigenvalues, as illustrated in the energy spectrum given in Fig. 2.4,

$$|\chi_0\rangle = |0\rangle \quad \rightarrow \quad \varepsilon_0 = 0, \tag{2.29}$$

$$|\chi_+\rangle = \frac{1}{\sqrt{2}}|1\rangle + \frac{1}{\sqrt{2}}|-1\rangle \quad \rightarrow \quad \varepsilon_+ = -D + E, \tag{2.30}$$

$$|\chi_-\rangle = \frac{1}{\sqrt{2}}|1\rangle - \frac{1}{\sqrt{2}}|-1\rangle \quad \rightarrow \quad \varepsilon_- = -D - E. \tag{2.31}$$

Similar to the previous example, we wish to obtain the differential conductance dI/dV through the molecule, which gives us an insight into the transitions between the molecular states $|\chi_n\rangle$. For the calculations conducted here, we assume a uniaxial magnetic anisotropy constant $D = 100\ \mu$eV at a temperature $T = 0.05$ K ($k_\mathrm{B}T = 4.5\ \mu$eV) with the same tunnel-coupling strength used in Sec. 2.4.1. The temperature, here, is assumed to be even lower than the previous example to allow for resolving the small energy difference between the molecular states $|\chi_+\rangle$ and $|\chi_-\rangle$,

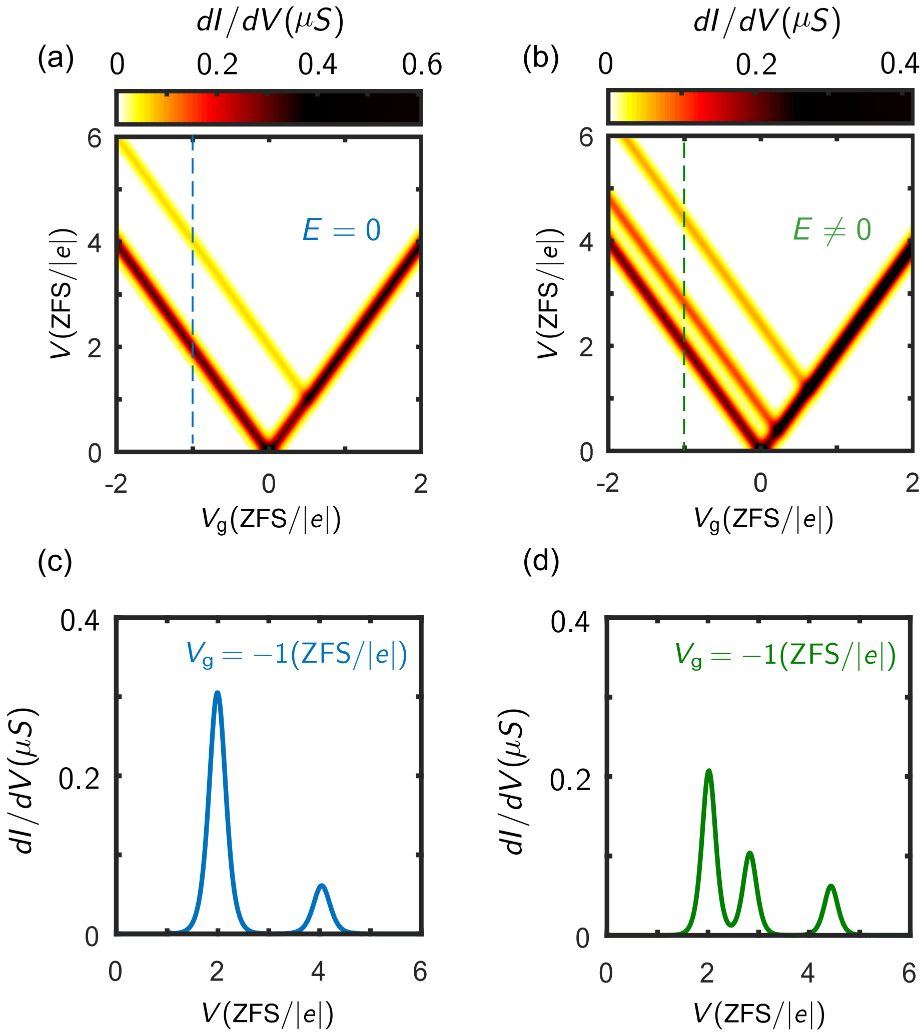

Figure 2.5: Differential conductance plots of a molecule with both uniaxial and transverse magnetic anisotropy. **(a) - (b)** A stability diagram of the molecule given in Fig. 2.2 in the absence (a) and presence (b) of transverse magnetic anisotropy. The transverse anisotropy component leads to splitting of the degenerate ground state of the system, which can be seen by the additional line that appears in (b). **(c) - (d)** A differential conductance plot is presented by taking a cut at a constant gate voltage $V_\mathrm{g} = -1$ (ZFS/$|e|$), as depicted by the vertical dashed lines in (a) and (b). Analogous to the additional line in (b), the leftmost differential conductance peak in (c) splits into two peaks, as seen in part (d).

referred to as the tunnel-splitting Δ. The energies are represented in terms of the zero-field splitting of the charged state $N+1$ (ZFS $= 100\ \mu$eV).

Using the formalism of Sec. 2.3, the differential conductance through this molecule has been calculated twice, in the absence ($E=0$) and presence ($E=0.2D$) of transverse magnetic anisotropy. When $E=0$, there are four possible transitions from the neutral to the charged molecular states. The first two transitions occur from the state $|1/2\rangle$ to the states $|1\rangle$ and $|0\rangle$. Additionally, we have two other transitions from $|-1/2\rangle$ to the states $|-1\rangle$ and $|0\rangle$. Due to the degeneracy between states, these four transitions appear as two peaks in the differential conductance plots (or equivalently, two lines in the stability diagrams) in left-hand side of Fig. 2.5. By contrast, in the presence of transverse magnetic anisotropy $E=0.2D$, the degeneracy between the two states $|-1\rangle$ and $|1\rangle$ is lifted and they split into the two states $|\chi_-\rangle$ and $|\chi_+\rangle$, as demonstrated in Fig. 2.4. Consequently, the line corresponding to transitions to the degenerate states $|-1\rangle$ and $|1\rangle$ in Fig. 2.5(a) splits into two lines as demonstrated in Fig. 2.5(b), with the vertical height between these lines denoting the energy difference between the two states $|\chi_-\rangle$ and $|\chi_+\rangle$, that is $2E$. The same effect can be seen from the one-dimensional differential conductance plots. By comparing Fig. 2.5(c) and (d), it is clear that the leftmost peak in (c) splits into two peaks whose summation gives the same height as the original one. To sum up, the mixing of the S_z states, owning to the transverse magnetic anisotropy, results in additional transitions between the neutral and charged states that can be observed on the stability diagrams obtained from conductance measurements.

2.4.3 Asymmetric tunnel-coupling

So far, we have restricted our attention to molecules placed in a *symmetric* junction. In other words, the tunnel-coupling strength to the left and right electrodes have been assumed to be equal, $\Gamma_\mathrm{R} = \Gamma_\mathrm{L}$. In this section, however, our goal is to investigate the effect of *asymmetric* coupling between the left and right electrodes on transport properties through single magnetic molecules. One should note that using scanning tunneling microscopy (STM) is desirable here since this technique allows for a tunable coupling strength Γ (*cf.* Fig. 1.2). Accordingly, in this section, the results are presented using the one-dimensional differential conductance plot which are typically

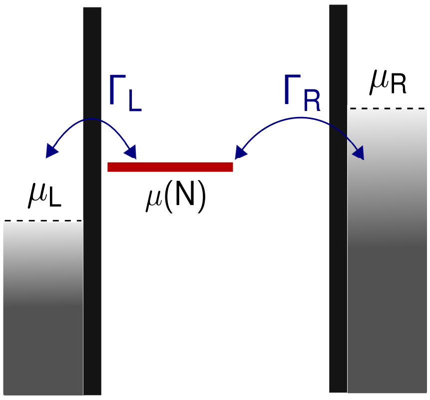

Figure 2.6: Asymmetric molecular junction. Electrochemical diagram of an *asymmetrically* coupled molecule. Due to the application of a bias voltage $V>0$, the chemical potential of the *left* electrode is shifted by $eV/2$, whereas the *right* one is shifted by $-eV/2$, where $e<0$, as defined earlier. The tunnel-coupling strength to the left electrode Γ_L is higher than that to the right one Γ_R, i.e., $\Gamma_\mathrm{L} > \Gamma_\mathrm{R}$.

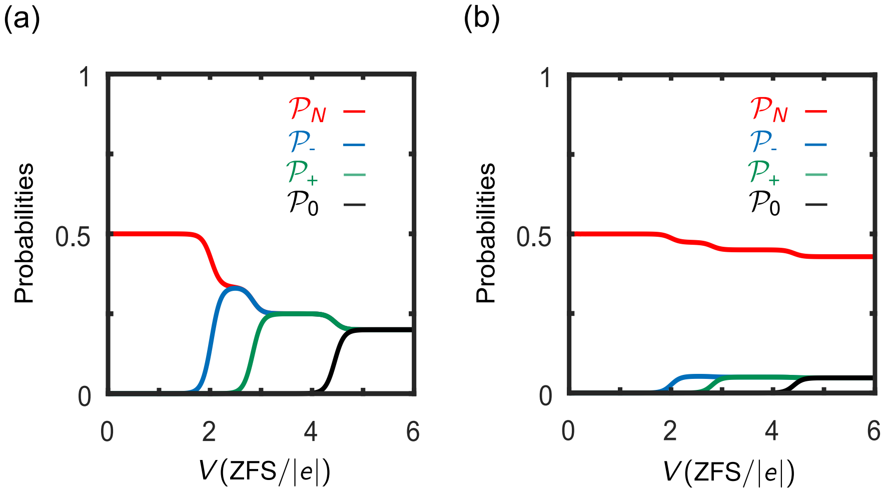

Figure 2.7: Probabilities of molecular states for a symmetrically and asymmetrically coupled molecules. The probabilities of the molecular states $|\chi_n\rangle$ are plotted as a function of bias voltage V at a constant gate voltage $V_\mathrm{g} = -1$ (ZFS/$|e|$), which corresponds to the cut in the stability diagrams in Fig. 2.5. For the calculations performed here, $\Gamma_\mathrm{L} = 9\Gamma_\mathrm{R}$. The tunnel-coupling strengths are chosen such that the total coupling $\Gamma_\mathrm{L} + \Gamma_\mathrm{R}$ is consistent with the example in Sec. 2.4.2 **(a)** Probabilities of the spin states of the molecule given in Fig. 2.4 in the symmetric coupling case. The probability $\mathcal{P}_N = \mathcal{P}_{1/2} = \mathcal{P}_{-1/2}$. When the bias voltage V is high enough for all transitions to take place, the probabilities of all the molecular spin states become equal to 0.2. **(b)** Probabilities for an asymmetrically coupled molecule, where the molecule prefers the neutral charge state N, even at high bias voltage.

obtained with such a two-terminal configuration. Now, in order to examine this asymmetry, we consider the same molecule as in Sec. 2.4.2 while varying the tunneling-coupling strengths, $\Gamma_\mathrm{L} \neq \Gamma_\mathrm{R}$. In the previous examples, only the positive bias range $V > 0$ was considered since stability diagrams were symmetric around $V = 0$. By contrast, when $\Gamma_\mathrm{R} \neq \Gamma_\mathrm{L}$, this symmetry is broken. Thus, to demonstrate the full picture, two cases are considered for $V > 0$, namely $\Gamma_\mathrm{L} > \Gamma_\mathrm{R}$ and $\Gamma_\mathrm{L} < \Gamma_\mathrm{R}$. The first case is discussed here, whereas the latter can be found in App. C.1.

The main consequence of asymmetric coupling of a molecule to the left and right electrodes is that either the charging or the discharging process of the molecule is favored. To give an illustration, for the asymmetrically coupled molecule in Fig. 2.6, the coupling to the left electrode Γ_L is assumed to be stronger than to the right one Γ_R ($\Gamma_\mathrm{L} > \Gamma_\mathrm{R}$). As a result, the charging rate of the molecule ($W^\mathrm{R}_{\chi_{N+1},\chi_N} \propto \Gamma_\mathrm{R}$) is lower than the discharging rate ($W^\mathrm{L}_{\chi_N,\chi_{N+1}} \propto \Gamma_\mathrm{L}$) [*cf.* Eq. (2.24)], assuming that the bias voltage V is applied as captured in the electrochemical diagram in Fig. 2.6. Thus, the molecule preferably exists in the neutral charge state N. This effect is demonstrated by the change in the occupation probabilities between the symmetric and asymmetric cases, as plotted in Fig. 2.7. In the *symmetric* case, when the bias voltage V is high enough for all transitions to occur, the molecular spin states are equiprobable, each with a probability of 0.2. In contrast, for the *asymmetric* case, the molecule prefers the neutral state N, which is indicated by the dominant probability of the neutral state $\mathcal{P}_N$.

To examine the impact of asymmetric coupling on transport observables, we calculate the current I and the differential conductance dI/dV for $\Gamma_\mathrm{L} = 9\Gamma_\mathrm{R}$. We choose the tunnel-coupling strengths such that the total coupling strength Γ, defined as $\Gamma = \Gamma_\mathrm{L} + \Gamma_\mathrm{R}$, is the same as in

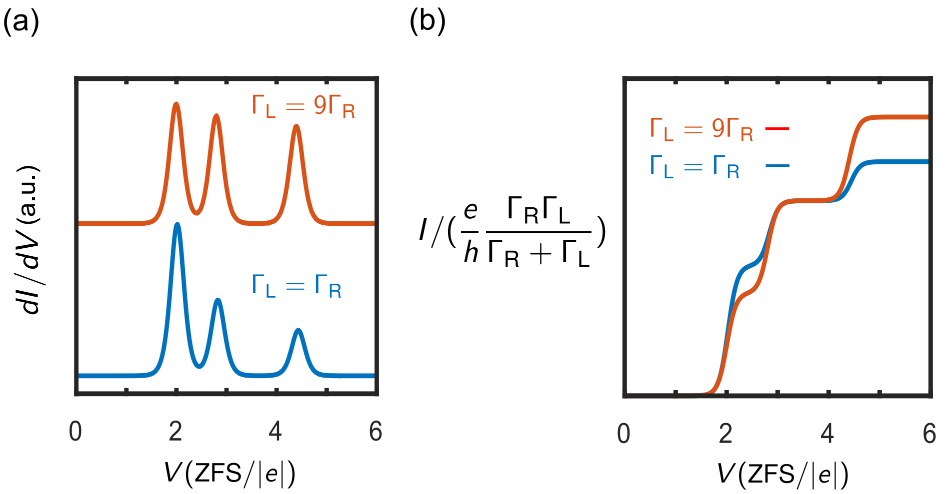

Figure 2.8: Differential conductance (a) and current (b) of a molecule in the symmetric and asymmetric coupling cases. These two plots were obtained at a gate voltage $V_g = -1$ (ZFS/$|e|$). The asymmetric coupling magnifies the weak transitions that occur at higher bias voltage, in contrast to the symmetric case where the differential conductance is dominated by the transition to the ground state of the charged molecule, that is the molecular state $|\chi_-\rangle$ (the leftmost peak). As indicated on the plot, the current and, hence, the differential conductance, is normalized by a factor $(e/\hbar)\ \Gamma_L\Gamma_R/(\Gamma_L + \Gamma_R)$ to allow for comparing the two coupling scenarios.

Sec. 2.4.2 for the sake of comparison. For the *symmetric* case in Fig. 2.8(a), we can see that the dominant transition, i.e., the highest differential conductance peak, correspond to the transitions from the two degenerate neutral molecular states $|1/2\rangle$ and $|-1/2\rangle$ to the ground state of the charged molecule $|\chi_-\rangle$. However, for the *asymmetric* case in Fig. 2.8(a), it is clear that all transitions, including those allowed at higher bias voltage, now occur with approximately equal amplitudes. This behavior can be understood as follows: By referring to Eq. (2.10) for the charge current, we infer that the contribution of each transition to the current depends on two factors, the transition rate W and the occupation of the initial molecular state of the transition $\mathcal{P}$. First, since all the three peaks correspond to transitions from a neutral molecule state $|\chi_N\rangle$ to a charged one $|\chi_{N+1}\rangle$, all the involved transition rates are proportional to the tunnel-coupling strength to the right electrode, i.e., $(W^{\mathrm{R}}_{\chi_{N+1},\chi_N} \propto \Gamma_{\mathrm{R}})$. Secondly, as indicated by the probability plot in Fig. 2.7(b), the occupation of the neutral molecular states $|1/2\rangle$ and $|-1/2\rangle$ varies only slightly when increasing the bias voltage V, which guarantees that the occupation of the initial states for the three peaks is almost the same. In the light of these two factors, the transitions from the neutral molecular states $|1/2\rangle$ and $|-1/2\rangle$ to the *three* charged molecular states $|\chi_-\rangle$, $|\chi_+\rangle$ and $|\chi_0\rangle$ give rise to a similar current contribution, as evident by the steps in the red curve in Fig. 2.8(b).

Based on this illustrative example, we conclude that *asymmetric coupling of individual magnetic molecules can magnify weak transitions that take place at high bias voltages.* Thus, this can be a valuable tool for experimental studies on magnetic molecule to observe the various transitions between the molecular spin states.

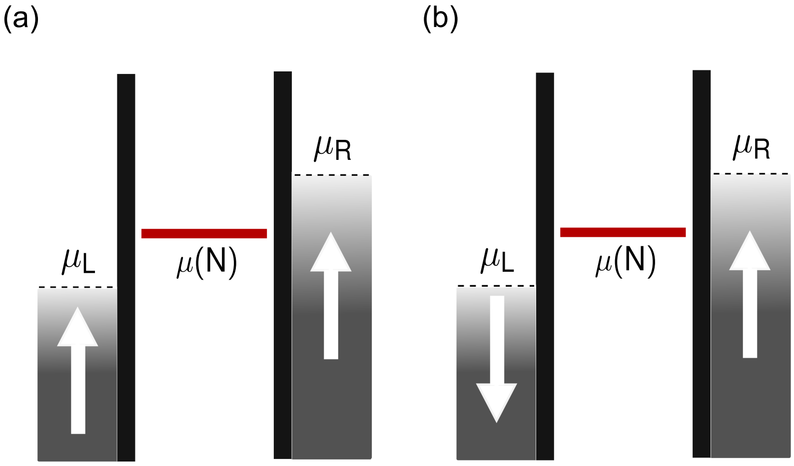

Figure 2.9: Spin-valve molecular junction in the *parallel* (a) and *antiparallel* (b) configuration. Electrochemical diagram of a molecule coupled to ferromagnetic electrodes. Due to the application of a bias voltage $V > 0$, the chemical potential of the *left* electrode is shifted by $eV/2$, whereas the *right* one is shifted by $-eV/2$. (**a**) The depicted molecular junction is in the parallel configuration, i.e., the spin of the majority population of electrons is the same in the left and right electrodes. (**b**) For the antiparallel configuration, the majority population of the right electrode consists of spin-up (↑) electrons, whereas for the left one it consists of spin-down (↓) electrons.

2.4.4 Spin-polarized transport

Another important degree of freedom in the leads is the spin polarization. As established in Sec. 2.3.1, for ferromagnetic electrodes, there exists a difference between the density of states of spin-up and down electrons near the Fermi level. In this section, the impact of spin polarization is explored by considering a molecule trapped between two ferromagnetic electrodes. For the sake of consistency, we consider the same magnetic molecule studied in the previous section with a spin $S_N = 1/2$ in the neutral state and $S_{N+1} = 1$ in the charged state.

In order to characterize how the spin-polarization of the electrodes can alter the occupation of molecular states and, hence, affect transport observables, we study two opposite cases. In the first case, the spin of the majority population of electrons in the left and right electrodes is the same, which we refer to as the *parallel* magnetic configuration (P), as depicted in Fig. 2.9(a). By contrast, for the second case, the majority spin is different in both electrodes, which we denote by the *antiparallel* magnetic configuration (AP) [*cf.* Fig. 2.9(b)].

Prior to comparing the parallel and antiparallel magnetic configurations, we start by analyzing the *spin-resolved current* in the case of nonmagnetic electrodes, that is the spin polarization in the left and right electrodes equal zero ($P_{\mathrm{R}} = P_{\mathrm{L}} = P = 0$). The transition rate in Eq. (2.13) can be rewritten as

$$W^{q,\sigma}_{\chi_{n'},\chi_n} = \sum_{k\in q} \left\{ \mathcal{W}^{|k\sigma;\chi_n\rangle}_{|0;\chi_{n'}\rangle} f_q(\varepsilon^q_{k\sigma}) + \mathcal{W}^{|0;\chi_n\rangle}_{|k\sigma;\chi_{n'}\rangle} \left[1 - f_q(\varepsilon^q_{k\sigma})\right] \right\}, \tag{2.32}$$

where, compared to Eq. (2.13), the summation over the spin σ is omitted, i.e., the transition rate is derived for a specific electronic spin orientation, either up or down. Accordingly, the charge current entering into an electrode with an index q due to the flow of electrons with a spin σ can be given by

$$I_q^\sigma = e \sum_{n,\chi_n} \sum_{n',\chi_{n'}} (n' - n) W^{q,\sigma}_{\chi_{n'},\chi_n} \mathcal{P}_{\chi_n} \; . \tag{2.33}$$

The symmetrized charge current for a specific electronic spin orientation σ, then, reads as

$$I^\sigma = \frac{I_{\mathrm{R}}^\sigma - I_{\mathrm{L}}^\sigma}{2}. \tag{2.34}$$

In turn, the total charge current, given in Eq. (2.11), can be written as $I = I^{(\sigma=\uparrow)} + I^{(\sigma=\downarrow)}$, which means that the total charge current through the molecule can be decomposed into two contributions for spin-up and spin-down electrons. To give an illustration, Fig. 2.10(a) shows the spin-resolved current for the molecule studied in Sec. 2.4.2 in the case of nonmagnetic electrodes. We can see that spin-up and spin-down electrons contribute equally to the total current I. That is to say, the current through the molecule can be thought of as two independent channels of spin-up and spin-down electrons. Furthermore, each of these two channels give rise to the same amount of current ($I^\uparrow = I^\downarrow$) owning to the non-polarized electrodes, i.e., the density of states for spin-up and down electrons are identical near the Fermi level.

For the *parallel* magnetic configuration, we choose the majority population to be spin-up (↑) electrons with a spin polarization $P = 0.7$ ($P_{\mathrm{L}} = P_{\mathrm{R}} = P = 0.7$). The reason for choosing such a large polarization value is to ensure that the impact of the ferromagnetic electrodes on transport observables is manifest for the purpose of illustration. Unlike in the *non-polarized* case, the current contribution from the spin-up and spin-down channels are not equal in the *parallel* case. In particular, the spin-up electrons contribute more to the total current, as shown in Fig. 2.11(a). Furthermore, one should note that, in case of the *parallel* magnetic configuration, the probabilities of the molecular states $|1/2\rangle$ and $|-1/2\rangle$ are equal, similar to the case of *non-polarized* electrodes, which could be understood as follows: First, for the sake of the argument, we ignore transitions to the state $|0\rangle$ since they occur at high bias only. Next, considering the transition between the state $|-1/2\rangle$ and the two states $|\chi_+\rangle$ and $|\chi_-\rangle$, we can see that, since such transitions require a spin-down electron (minority), the tunneling rate into and out of the state $|-1/2\rangle$ will be relatively low, compared to the transitions between the state $|1/2\rangle$ and the same two charged states $|\chi_\pm\rangle$ which requires a spin-up electron (majority). In other words, the tunneling rate into and out of the state $|-1/2\rangle$ is low, whereas, for the state $|1/2\rangle$ the rate is high. As a result, both states end up with equal probabilities in the steady state.

Finally, we address the issue of the *antiparallel* magnetic configuration where the majority population of the right electrode is chosen to be spin-up electrons, unlike in the left one where the majority of electrons are spin-down, as schematically illustrated in Fig. 2.9(b). Comparing Fig. 2.10(a) and Fig. 2.11(a), we infer that the total charge current I is identical in the non-polarized and parallel cases, whereas, for the *antiparallel* case, the total current behaves differently as shown in Fig. 2.12(a). Such a dissimilarity is also displayed in the occupations of the molecular states, given in Fig. 2.12(b). In contrast to the parallel configuration, the probabilities of the molecular states $|1/2\rangle$ and $|-1/2\rangle$ are not equal in the antiparallel case, due to the conservation of spin momentum which determines the allowed and forbidden transitions between the molecular states $|\chi_n\rangle$.

The difference in the probabilities of the two states $|1/2\rangle$ and $|-1/2\rangle$, as well as, the behavior of the total current I can be understood via the following two-fold argument. First, let us consider a charged molecule at a bias voltage greater than zero ($V > 0$), as depicted in Fig. 2.9(b). Since for the left electrode $\Gamma_{\mathrm{L}}^{\downarrow} > \Gamma_{\mathrm{L}}^{\uparrow}$, the majority of the tunneling-out electrons have a down spin. As a result, the tunneling rate from the two charged molecular states $|\chi_{\pm}\rangle$ to the neutral state $|{-1/2}\rangle$, i.e., $W_{|-1/2\rangle,|\chi_{\pm}\rangle}^{\mathrm{L},\downarrow} \propto \Gamma_{\mathrm{L}}^{\downarrow}$, is relatively higher than the rate to the state $|1/2\rangle$, that is $W_{|1/2\rangle,|\chi_{\pm}\rangle}^{\mathrm{L},\uparrow} \propto \Gamma_{\mathrm{L}}^{\uparrow}$ [*cf.* Eq. (2.32)]. Secondly, starting with a neutral molecule in the state $|-1/2\rangle$, we note that the majority of tunneling-in electrons are spin-up electrons due to the fact that $\Gamma_{\mathrm{R}}^{\uparrow} > \Gamma_{\mathrm{R}}^{\downarrow}$. Thus, the favorable charging transition is from the neutral molecular state $|-1/2\rangle$ to the charged molecular state $|0\rangle$. However, this transition is only available at bias of $V \approx 4$ (ZFS$/|e|$). Now, in the light of the previous argument, we conclude that at a bias voltage $V < 4$ (ZFS$/|e|$) the tunneling rate out of the state $|-1/2\rangle$ is substantially lower than the tunneling rate into it and, hence, it acts almost as a *dark state* that *absorbs* much more than it *emits*, leading to a suppression of the total current through the molecule. In consequence, the total current I, shown in Fig. 2.12(a), is significantly lower than in the parallel configuration at low bias. Only when the bias is high enough for the transition from the state $|-1/2\rangle$ to $|0\rangle$ to occur, the total current through the molecule increases to catch up with the parallel case. This sudden increase in current corresponds to the sharp drop in the occupation of the state $|-1/2\rangle$.

The above discussion is summarized in Fig. 2.13, where the differential conductance for the non-polarized electrodes, parallel and antiparallel magnetic configurations is plotted. It can be seen that the transition from the molecular state $|-1/2\rangle$ to the state $|0\rangle$ (rightmost peak) is the dominant one in the antiparallel case. Moreover, it is clear that the non-polarized and parallel cases behave similarly. The only difference, as mentioned before, are the contributions of the spin-up and down channels to the total current I.

To conclude, *ferromagnetic electrodes can lead to the magnification of certain magnetic transitions which, in turn, amplifies the magnitude of the corresponding differential conductance peaks*, as it was demonstrated in the case of the antiparallel configuration. This magnification can allow one

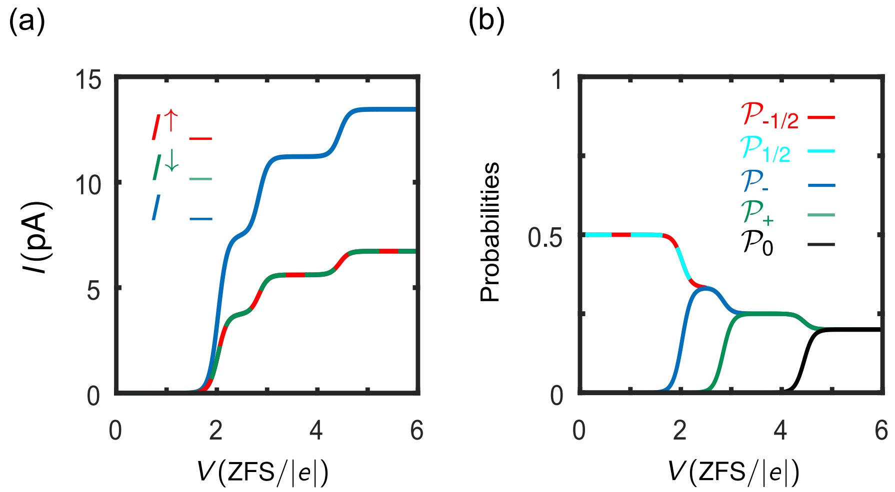

Figure 2.10: Transport through a molecule attached to *non-polarized* electrodes **(a)** Current through the molecule, given in Fig. 2.4, in the non-polarized case at a gate voltage $V_{\mathrm{g}} = -1$ (ZFS$/|e|$). The spin resolved current I^{σ} shows equal contributions from spin-up $I^{(\sigma=\uparrow)}$ and spin-down $I^{(\sigma=\downarrow)}$ to the total current I. **(b)** Probabilities of the molecular states $|\chi_n\rangle$ of the molecule. The probabilities of the states $|1/2\rangle$ and $|-1/2\rangle$ are equal (*cf.* Fig. 2.12).

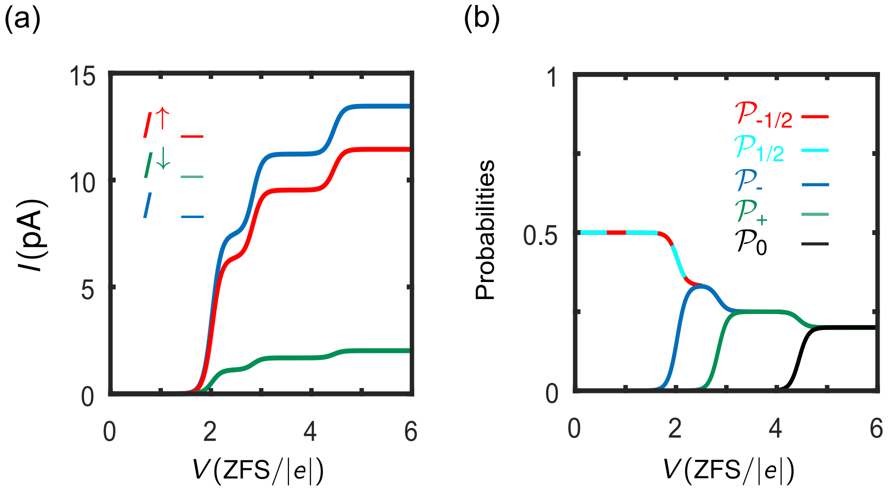

Figure 2.11: Transport through a molecule attached to ferromagnetic electrodes in the *parallel* magnetic configuration (a) Current through the molecule, given in Fig. 2.4, in the parallel case at a gate voltage $V_g = -1$ (ZFS/$|e|$). The majority population of electrons are chosen to be with a spin up in the left and right electrodes. Thus, the total current I is dominantly composed of spin-up electrons. **(b)** Similar to the non-polarized case, probabilities of the molecular states $|1/2\rangle$ and $|-1/2\rangle$ are equal (*cf.* Fig. 2.12). A spin polarization $P = 0.7$ was used for these calculations, i.e., $P_L = P_R = P = 0.7$.

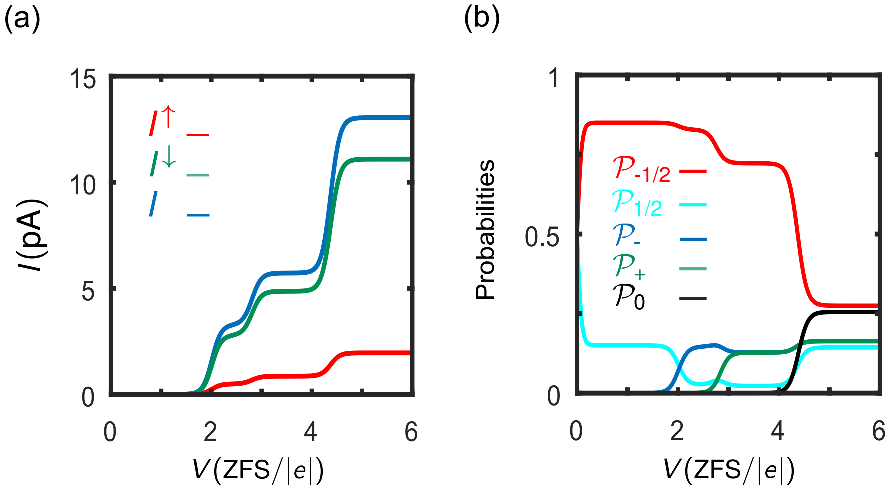

Figure 2.12: Transport through a molecule attached to ferromagnetic electrodes in the *antiparallel* configuration (a) Current through the molecule, given in Fig. 2.4, in the antiparallel case at a gate voltage $V_g = -1$ (ZFS/$|e|$). Due to the conservation of spin momentum, the state $|-1/2\rangle$ acts as a *dark state*, leading to a suppression of current at low bias compared to the parallel case. Only when the bias voltage V is high enough for the transition from $|-1/2\rangle$ to $|0\rangle$ to occur, the transport suppression is lifted and the current exhibits a sharp step. This increase of the current corresponds to the substantial drop in the probability of the state $|-1/2\rangle$ in **(b)**. It should be emphasized that, unlike the parallel and non-polarized cases, the probabilities of the states $|-1/2\rangle$ and $|1/2\rangle$ are not equal.

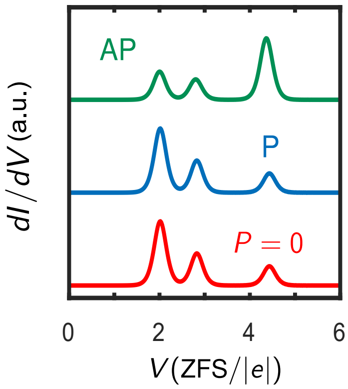

Figure 2.13: Differential conductance plot in the antiparallel (AP), parallel (P) and non-polarized ($P = 0$) cases. This differential conductance is obtained at a gate voltage $V_\mathrm{g} = -1$ (ZFS/$|e|$), as indicated by the bias cut in Fig. 2.5. The parallel and non-polarized cases exhibit the same differential conductance amplitudes. Whereas, the antiparallel configuration results in magnification of the transition from the molecular state $|-1/2\rangle$ to the state $|0\rangle$.

to gain insights into the energy spectrum of the molecule and, hence, it is of particular relevance to the spin-vibron coupling discussion in Sec. 3.2.1.

2.5 Charge-vibron interaction in magnetic molecules

Up to this point, the molecules were considered only as a magnetic core without taking into account additional degrees of freedom that stem from their molecular nature. In fact, molecules embedded in single-molecule junctions can vibrate with discrete frequencies, which are a characteristic fingerprint for these molecules [35]. Importantly, *molecular vibrations can couple to the degrees of freedom of the tunneling electrons, namely the charge and the spin*, as established in Sec. 1.3.1 [47]. In this section, we address the interaction between charge and molecular vibrations in magnetic molecules along with examples to illustrate its impact on transport properties, whereas the coupling between spin and molecular vibrations will be discussed in Chap. 3.

2.5.1 Integration of molecular vibrations in transport model

The effect of charge-vibron interaction in magnetic molecules can be incorporated into the model presented in Sec. 2.1 by adopting an Anderson-Holstein-like model [55, 56]. Recently, this effect has been experimentally and theoretically discussed for magnetic molecules in Refs. [35, 47] and it is instructive to review the model here before building upon it to include the spin-vibron interaction in Chap. 3. In general, a magnetic molecule trapped in a single-molecule junction, in the presence of molecular vibrations, can be described by the Hamiltonian

$$\hat{\mathcal{H}}_\mathrm{mol} = \sum_n \hat{\mathcal{H}}_{\mathrm{spin},n} + (\varepsilon - eV_\mathrm{g})\hat{n}_d + \sum_i \hbar\omega_i \hat{b}_i^\dagger \hat{b}_i + \sum_i \lambda_i \hbar\omega_i \big(\hat{b}_i^\dagger + \hat{b}_i\big)\hat{n}_d, \tag{2.35}$$

where a short-hand notation $\hat{n}_d \equiv \sum_{l\sigma} \hat{d}_{l\sigma}^\dagger \hat{d}_{l\sigma}$ has been introduced for the number operator of the molecule, which quantifies the presence of an additional electron. The last two terms in the equation above describe molecular vibrations, with the operator $\hat{b}_i^\dagger$ ($\hat{b}_i$) creating (annihilating) the ith quantized vibrational mode. In particular, the penultimate term represents energies of the various vibrational states of a molecule in terms of a set of independent harmonic oscillators characterized by vibrational angular frequencies ω_i. The last term, on the other hand, accounts for the coupling between electronic charge and vibrational modes with the dimensionless coupling strength λ_i. It can be seen that due to the coupling between molecular vibrations and the charge of the molecule, the molecular Hamiltonian $\hat{\mathcal{H}}_{\mathrm{mol}}$, in the Hilbert space of the molecular spin states, now possesses off-diagonal terms. Consequently, the S_z projections of the spin are no longer a good quantum number and, hence, we wish to apply a canonical transformation to diagonalize the Hamiltonian (2.35). Before discussing the details of the diagonalization method, we should emphasize that it is of particular relevance to work in the S_z basis since it allows for tracking the transitions between the various molecular states $|\chi_n\rangle$, which is essential to understand the differential conductance plots for magnetic molecules.

2.5.2 Diagonalization of molecular Hamiltonian: Lang-Firsov transformation

In order to eliminate the charge-vibron coupling from the molecular Hamiltonian $\hat{\mathcal{H}}_{\mathrm{mol}}$, which is the source of the off-diagonal terms, the Lang-Firsov canonical transformation is performed [57], which basically results in a change of basis to quasi-particles referred to as *polarons*, i.e., electrons surrounded by clouds of vibrations. This canonical transformation has the form

$$\hat{\mathcal{H}}'_{\mathrm{mol}} = \hat{U}\ \hat{\mathcal{H}}_{\mathrm{mol}}\ \hat{U}^{-1} = \mathrm{e}^{\hat{\mathcal{S}}}\hat{\mathcal{H}}_{\mathrm{mol}}\mathrm{e}^{-\hat{\mathcal{S}}} \quad \text{with} \quad \hat{\mathcal{S}} = \sum_i \lambda_i \big(\hat{b}_i^\dagger - \hat{b}_i\big)\hat{n}_d. \tag{2.36}$$

It should be remarked that the transformation given in Eq. (2.36) is unitary, $\hat{U}^\dagger = \hat{U}^{-1}$, in order to maintain the Hermiticity of the molecular Hamiltonian, that is, the transformation kernel $\hat{\mathcal{S}}$ must be anti-Hermitian, $\hat{\mathcal{S}}^\dagger = -\hat{\mathcal{S}}$. Now, using the Baker-Hausdorff formula [57]

$$\mathrm{e}^{\hat{A}}\hat{B}\mathrm{e}^{-\hat{A}} = \sum_{n=0}^{\infty}\frac{1}{n!}\big[\hat{A},\hat{B}\big]_n = \hat{B} + \big[\hat{A},\hat{B}\big] + \frac{1}{2}\big[\hat{A},\big[\hat{A},\hat{B}\big]\big] + \frac{1}{6}\big[\hat{A},\big[\hat{A},\big[\hat{A},\hat{B}\big]\big]\big] + \text{h.o.}, \tag{2.37}$$

the operators can be transformed, one by one, resulting in the total diagonalized Hamiltonian, $\hat{\mathcal{H}}' = \mathrm{e}^{\hat{\mathcal{S}}}\hat{\mathcal{H}}\mathrm{e}^{-\hat{\mathcal{S}}}$. Here, we only present the resultant operators, denoted by tildes, whereas the details of the transformation can be found in App. A.1. The transformed creation and annihilation operators of the molecule read

$$\hat{\tilde{d}}_{l\sigma}^\dagger = \hat{X}^\dagger\hat{d}_{l\sigma}^\dagger \quad \text{and} \quad \hat{\tilde{d}}_{l\sigma} = \hat{X}\hat{d}_{l\sigma}, \tag{2.38}$$

where $\hat{X}^\dagger = \exp\Big[-\sum_i \lambda_i\big(\hat{b}_i - \hat{b}_i^\dagger\big)\Big]$. Since the number operator commutes with other number operators, e.g., $[\hat{n}'_d, \hat{n}_d] = 0$, they remain unchanged upon this canonical transformation. Likewise, the creation and annihilation operator for the leads remain unchanged due to vanishing commutations with $\hat{\mathcal{S}}$. As for the molecular vibrations, the creation and annihilation operators are changed into the new basis as follows

$$\hat{\tilde{b}}_i^\dagger = \hat{b}_{i'}^\dagger - \lambda_i\hat{n}_d \quad \text{and} \quad \hat{\tilde{b}}_{i'} = \hat{b}_{i'} - \lambda_i\hat{n}_d. \tag{2.39}$$

The transformed molecular Hamiltonian, obtained by substituting the aforementioned operators into Eq. (2.35), can be then written as

$$\hat{\mathcal{H}}'_{\text{mol}} = \sum_{n} \hat{\mathcal{H}}_{\text{spin},n} + \big(\varepsilon - eV_{\text{g}} + \sum_{i} \hbar\omega_i \lambda_i^2\big)\, \hat{n}_d \; + \sum_{i} \hbar\omega_i \hat{b}_i^\dagger \hat{b}_i. \tag{2.40}$$

It can be seen that the Lang-Firsov transformation eliminated the off-diagonal terms, representing electron-vibron coupling. Thus, the molecular Hamiltonian becomes diagonal with respect to the creation and annihilation operators of vibrations, in addition to the spin projection operator $\hat{S}_z$. Moreover, the transformation also shifts the energy of the charged state of the molecule by an amount $\hbar\omega_i\lambda_i^2$, which is dependent on the coupling strength λ_i. However, this constant energy shift is neglected in our calculations since it can be absorbed in the energy shift induced by the capacitively applied gate voltage V_{g}.

Since the coupling between vibrations and electronic charge is now eliminated, the transformed molecular Hamiltonian $\hat{\mathcal{H}}'_{\text{mol}}$ is diagonal in the eigenstates of the S_z projections of the spin. Accordingly, the new states that characterize the system are a product of the molecular spin states and the eigenstates of a harmonic oscillator, $|S_N M_N\rangle \otimes |n_q\rangle$, where $|n_q\rangle$ is the vibrational eigenstate of a molecule with $n_q = \sum_i n_i$ where n_i represents how many energy quanta, vibrons, are placed in the ith vibrational mode. Since vibrons are bosonic excitations, the number of energy quanta in an arbitrary vibrational mode is not restricted, as vibrons are not subject to the Pauli exclusion principle.

Similar to the molecular Hamiltonian, the tunneling Hamiltonian $\hat{\mathcal{H}}_{\text{tun}}$ can be changed into the new basis by substituting the transformed creation and annihilation operators of the molecule, given in Eq. (2.38), as follows

$$\hat{\mathcal{H}}'_{\text{tun}} = \sum_{qlk\sigma} \Big\{ t^q_{l\sigma} \hat{X}^\dagger \, \hat{d}^\dagger_{l\sigma} \hat{a}^q_{k\sigma} + t^q_{l\sigma} \hat{X} \, \hat{a}^{\dagger q}_{k\sigma} \hat{d}_{l\sigma} \Big\}. \tag{2.41}$$

Significantly, the coupling between charge and molecular vibrations reappears in the tunneling Hamiltonian via the factor $\hat{X}$. Now, the transition rates, calculated by Fermi golden rule, consist of two distinctive parts. The first is an *electronic* part as previously derived in Eq. (2.24), whereas the second is a *vibronic* part defined as $|\langle n'_q| \hat{X} |n_q\rangle|^2 \equiv |\mathcal{J}_{n_q,n'_q}|^2$, where $|n'_q\rangle$ and $|n_q\rangle$ are the final and initial vibrational states, respectively and $\mathcal{J}_{n_q,n'_q}$ is the overlap integral between the wave functions of the initial and final states. Accordingly, building upon Eq. (2.24), the transition rate from a neutral molecular state $|\chi_N\rangle$ with $|n_q\rangle$ vibrons to a charged molecular state $|\chi_{N+1}\rangle$ with $|n'_q\rangle$ vibrons can be written as

$$W^q_{f,i} = \frac{1}{\hbar} \sum_{\sigma} \Gamma^\sigma_q |\mathcal{T}^\sigma_{a_N b_{N+1}}|^2 |\mathcal{J}_{n_q,n'_q}|^2 f^q(\varepsilon_{\chi_{N+1}} + n'_q\hbar\omega - \varepsilon_{\chi_N} - n_q\hbar\omega), \tag{2.42}$$

with the composite states $|i\rangle$ and $|f\rangle$ defined as

$$|i\rangle = |\chi_N\rangle \otimes |n_q\rangle\,, \tag{2.43}$$

and

$$|f\rangle = |\chi_{N+1}\rangle \otimes |n'_q\rangle\,. \tag{2.44}$$

The squared matrix element $|\mathcal{J}_{n_q,n'_q}|^2$ in Eq. (2.42) is typically referred to as the *Franck-Condon* factor, $\mathcal{F}_{n_q,n'_q} \equiv |\mathcal{J}_{n_q,n'_q}|^2$, and it acts as a new selection rule for the transitions between the various vibrational states. Franck-Condon factors are the main consequences of the interaction between charge and vibrations in molecules and can result in drastic implications, such as transport blockade as illustrated later in Sec. 2.5.4.

The question now arises, how does the coupling between electronic charge and molecular vibration affect the transport through a single magnetic molecule? In the next section, an illustrative example is discussed to demonstrate the implications of the aforementioned coupling, which mainly comes from the Franck-Condon factors in the transition rates and the vibrational energy in the molecular Hamiltonian $\hat{\mathcal{H}}'_{\mathrm{mol}}$.

2.5.3 Example of transport through a magnetic molecule with charge-vibron interaction

In the example at hand, we examine the same molecule as that discussed in Sec. 2.4.1 while taking into consideration the effect of charge-vibron interaction. For the sake of illustration, we assume only one vibrational mode of an energy $\hbar\omega = 2$ meV with a coupling strength $\lambda = 1.3$. These two values were obtained based on similar magnetic molecule studied in [35, 47]. With this in mind, it is instructive to note that the typical frequencies of molecular vibrations range from tens of gigahertz (≈ 0.04 meV) to hundreds of terahertz (≈ 400 meV) [58]. Contrary to the previous sections, the energy units are kept in meV, which allows for comparing the transitions on the stability diagram with the vibrational energies. However, this comes at the expense of missing the details of the magnetic transitions, which happens at a smaller energy scale in this particular example (*cf.* Sec. 2.4.1 for the values of the anisotropy parameter, thermal energy and tunnel-coupling strength).

The fundamental difference arising due to molecular vibrations is that, instead of two parabolas for the neutral and charged states (*cf.* Fig. 2.2), the energy spectrum of the molecule consists now of infinite repetitions of these two parabolas, separated by the vibrational energy quanta $\hbar\omega$, as schematically depicted in Fig. 2.14(b). The two bottommost parabolas refer to the vibrational ground state of the molecule $|n_q = 0\rangle$, whereas the two on top of them refer to the first vibrationally excited state $|n_q = 1\rangle$, and so on till infinity. However, in practice, it is not possible to excite an infinite number of vibrons at a limited bias voltage V. Thus, it is only relevant to allow for a certain number of vibrational quanta that is attainable within the applied bias V. For instance, in the present example, only four vibrational quanta are considered. The resultant differential conductance is shown in Fig. 2.14(a). It can be seen that the differential conductance pattern is repeated at a bias voltage $V = 4$ meV, which corresponds to a vibrational energy $\hbar\omega = 2$ meV since the applied bias is symmetric $V/2$. As a result, for each magnetic transition, there exists corresponding ones that involve excitation of molecular vibrations. These excitations can be thought of as parallel transport channels attainable at higher bias voltages.

To give an illustration, the three blue arrows on Fig. 2.14(b) represent the same magnetic transition from the neutral molecular state $|3/2\rangle$ to the charged one $|2\rangle$, but they differ in terms of how many vibrations are excited due to the tunneling of an electron into the molecule. The occurrence of these three transitions is determined by two factors. Most evidently, in order to populate a vibrationally excited state, a certain bias voltage is required. For instance, the first vibrational excitation $|n_q = 1\rangle$ happens at $eV/2 = \hbar\omega = 2$ meV. Accordingly, due to the charge-vibron coupling, we can see that the transition from the state $|3/2\rangle$ to $|2\rangle$, can take place at $eV = 2m\hbar\omega$ with $m = 0, 1, 2, 3, \ldots$. Secondly, the vibronic part of the transition rates gives rise to Franck-Condon selection rules and, hence, an additional weighting factor is imposed on transitions to the multiple vibrational states. That is to say, the three blues lines on Fig. 2.14(b) indicating identical transitions from the perspective of the spin part of the states, are now weighted based on the wave

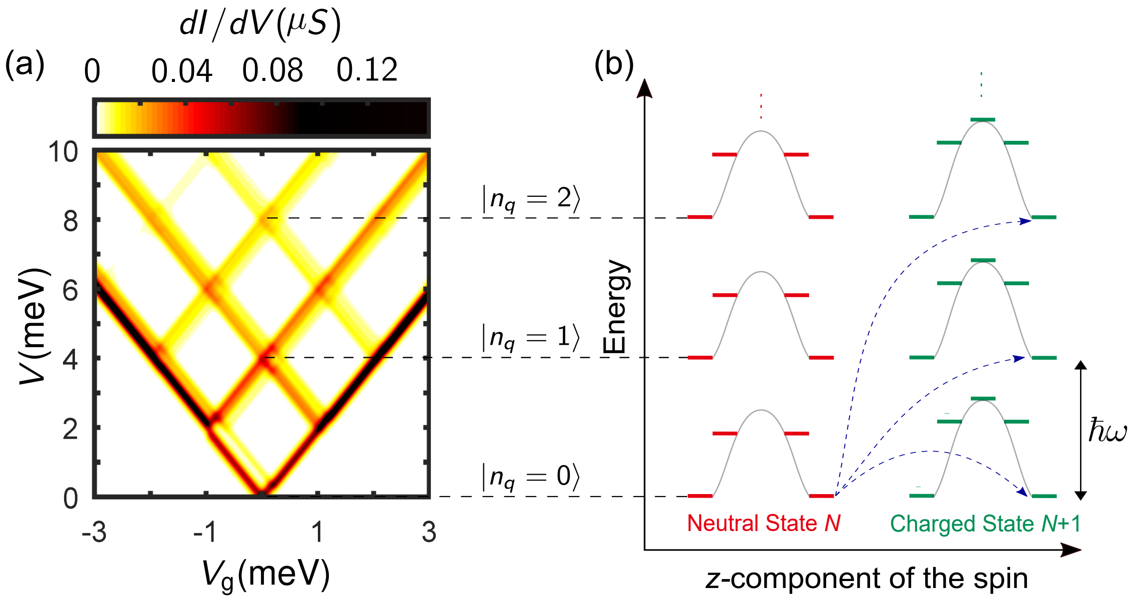

Figure 2.14: Differential conductance plot and energy spectrum of a magnetic molecule, with molecular vibrations included. (a) A stability diagram of the molecule given in Fig. 2.2. Due to the presence of molecular vibrations, the edges of the sequential tunneling regions are repeated at a bias voltage $V = 4$ meV, corresponding to a vibrational energy $\hbar\omega = 2$ meV since a bias of $\pm V/2$ is applied to the electrodes. It should be noted that the magnetic transitions observed before in Fig. 2.3 are not easily resolved here owning to the energy scale used in this example. **(b)** Energy spectrum of a magnetic molecules where the two charge state parabolas are repeated an infinite number of times based on the number of excited vibrations. (a) and (b) are linked by horizontal lines that shows the correspondence between the repeated pattern in the differential conductance and the repeated energy spectrum due to the excited vibrational states.

function overlap between the initial neutral state N and the various vibrational excitations of the charged state $N + 1$.

2.5.4 Franck-Condon blockade

Interestingly, the interaction between charge and molecular vibrations can result in more drastic effects on transport through a single magnetic molecule. For a strong charge-vibron coupling ($\lambda_i \gg 1$), it is favorable to alter the charge state of the molecule by a transition via a vibrationally excited state, rather than via the vibrational ground state [46]. As mentioned before, this can be attributed to the wave function overlap, which comes about in the transition rates as Franck-Condon factors. Consequently, if the bias voltage V is not large enough to excite a vibrational state ($eV < \hbar\omega_i$), tunneling of electrons is prohibited and, hence, the transport is blocked. This blockade, referred to as *Franck Condon blockade*, takes place at low bias voltage, and cannot be lifted with gate voltage V_g. Recently, this blockade has been observed in the context of magnetic molecules, specifically the Fe$_4$ SMM, which emphasizes that molecular vibrations play a fundamental role in transport properties of single molecules, in general, and magnetic molecules, in particular [47].

Now, to examine the Franck-Condon blockade, we calculated the differential condutance through an individual magnetic molecule for different values of the charge-vibron coupling strength λ.

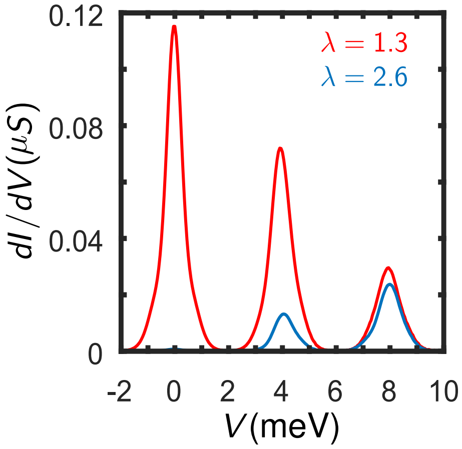

Figure 2.15: Franck-Condon blockade. Differential conductance plot, at a gate voltage $V_\mathrm{g} = 0$ meV, for the two coupling strength, $\lambda = 1.3$ and $\lambda = 2.6$. For the strong coupling case, $\lambda = 2.6$, a blockade of transport takes place at low-bias voltage because transitions that involve excited vibrational states are favorable. By contrast, at $\lambda = 1.3$ transport dominantly occurs through the vibrational ground state, as evident by the magnitude of the leftmost peak.

For the purpose of illustrating the blockade effect, we simply double the charge-vibron coupling strength λ used in the previous example (*cf.* Sec. 2.5.3). Yet, it should be remarked that this new coupling strength ($\lambda = 2.6$) is close to the fitting parameter obtained in Ref. [47] for the Franck-Condon blockade in the Fe_4 SMM ($\lambda \approx 2.21$). Using these two values, the differential conductance was acquired at a constant gate voltage equal to zero meV, as shown in Fig. 2.15. At a coupling strength $\lambda = 1.3$, the transitions through the vibrational ground states are favored, as evident by the dominant leftmost peak (red curve). However, upon doubling the coupling strength ($\lambda = 2.6$), transitions via the vibrational ground state are suppressed. Thus, a blockade of transport at low-bias occurs since the vibrationally excited states are not accessible. At higher bias voltages, the tunneling electrons possess energy high enough to excite vibrational states and, hence, the blockade is lifted, as represented by the two blue peaks in Fig. 2.15 which correspond to transitions to the first ($eV = 2\hbar\omega$) and second ($eV = 4\hbar\omega$) excited states.

3

Spin-vibron interaction in magnetic molecules

As already established, a single molecule embedded in a junction can vibrate with discrete frequencies. Importantly, not only do molecular vibrations couple to the charge of tunneling electrons, but they can also couple to the spin of the molecule, which impacts its magnetic properties. Although the charge-vibron coupling has been recently studied by McCaskey *et al.* [35], the interaction between spin and vibrations and its effect on transport properties of magnetic molecules has not been investigated in literature so far. Consequently, in this chapter, we provide and scrutinize a model for transport through a single magnetic molecule that takes into account the spin-vibron coupling. It is shown that this coupling results in renormalization of both the transverse and the uniaxial magnetic anisotropy of the molecule.

This chapter is divided into two parts. First, the spin-vibron coupling is incorporated into the model Hamiltonian for a molecule with only *uniaxial* magnetic anisotropy. For this purpose, a solution by canonical transformation is derived along with examples to demonstrate the implications of the spin-vibron coupling on transport characteristics. The second part extends the model by assuming a molecule with both *uniaxial* and *transverse* magnetic anisotropy and addresses the cases for which there is an exact solution. Finally, we present an example for a molecule where the vibrations couple to the magnetic anisotropy along the *uniaxial* and *transverse* directions.

3.1 The coupling of molecular vibrations to the *uniaxial* component of molecular spin

The coupling between the spin and the vibrational degrees of freedom of individual molecules can occur along the uniaxial, as well as, the transverse direction of the magnetic anisotropy. In order to simplify our analysis of this coupling, in this section we consider a molecule without a transverse anisotropy component, i.e., $E = 0$. The question then to be addressed is: how to describe the spin-vibron interaction in the model Hamiltonian used in Sec. 2.5? Building upon the spin-vibron interaction term discussed in Refs. [48, 59, 60], the molecular Hamiltonian in Eq. (2.35) can be extended as follows:

$$\hat{\mathcal{H}}_{\text{mol}} = \sum_n \hat{\mathcal{H}}_{\text{spin},n} + (\varepsilon - eV_{\text{g}})\hat{n}_d + \hat{\mathcal{H}}_{\text{vib}} + \hat{\mathcal{H}}_{\text{ch-vib}} + \hat{\mathcal{H}}_{\text{sp-vib}}, \tag{3.1}$$

with

$$\hat{\mathcal{H}}_{\text{sp-vib}} = \sum_n \sum_i \Lambda_n^i \hbar\omega_i \big(\hat{S}_n^z\big)^2 (\hat{b}_i^\dagger + \hat{b}_i). \tag{3.2}$$

In Eq. (3.1), $\hat{\mathcal{H}}_{\text{vib}}$ denotes the energy of molecular vibrations, whereas $\hat{\mathcal{H}}_{\text{ch-vib}}$ accounts for the charge-vibron interaction term, as introduced in Sec. 2.5.1. Significantly, the newly added term in Eq. (3.1), $\hat{\mathcal{H}}_{\text{sp-vib}}$, represents the coupling between molecular vibrations and the total effective spin of the molecule, quantified by the dimensionless coupling strength Λ_n^i, which can be thought of as an induced anisotropy due to coupling to the ith vibrational mode. It should be mentioned that the derivation of that additional term is primarily based on how molecular vibrations modify the ligand field, generating additional magnetic anisotropy in the molecule [48].

It can be seen that the S_z spin projections are no longer a good quantum number for describing the state of a vibrating molecule since the molecular Hamiltonian (3.1) possesses now two forms of interaction leading to off-diagonal terms. The *first* one, captured by $\hat{\mathcal{H}}_{\text{ch-vib}}$, is due to the charge-vibron coupling, as discussed in Sec. 2.5.1, whereas the *second* one, given in Eq. (3.2), arises from the interaction between molecular vibrations and spin. Thus, we aim to apply *two successive canonical transformations to eliminate the threefold coupling between charge, spin and molecular vibrations.* The Lang-Firsov transformation, which eliminates the charge-vibron coupling, was already discussed in Sec. 2.5.2. Consequently, the goal of the next section is to find a similar transformation that decouples the new spin-vibron interaction term $\hat{\mathcal{H}}_{\text{sp-vib}}$.

Before proceeding to the diagonalization of the molecular Hamiltonian, it should be emphasized that Ref. [59] discusses a similar system in which vibrations couple only to the uniaxial magnetic anisotropy. However, the main limitation of that study is that it only addresses the case of a molecular spin $S = 1$. Moreover, the discussed model in Ref. [59] does not take into consideration the charge-vibron coupling.

3.1.1 Solution by canonical transformation

In order to eliminate the spin-vibron coupling in the molecular Hamiltonian (3.1), we wish to find a transformation

$$\hat{\mathcal{H}}'_{\text{mol}} = \hat{U}\ \hat{\mathcal{H}}_{\text{mol}}\ \hat{U}^{-1} = \mathrm{e}^{\hat{\mathcal{S}}}\hat{\mathcal{H}}_{\text{mol}}\mathrm{e}^{-\hat{\mathcal{S}}}, \tag{3.3}$$

such that $\hat{\mathcal{H}}'_{\text{mol}}$ is diagonal with respect to the charge, spin and vibronic operators. For this purpose, we derived a transformation kernel $\hat{\mathcal{S}}$, based on a recipe given in Ref. [61], by projecting the spin-vibron interaction term $\hat{\mathcal{H}}_{\text{sp-vib}}$ on the eigenstates of the Hamiltonian $\hat{\mathcal{H}}_0$, defined as $\hat{\mathcal{H}}_0 = \hat{\mathcal{H}}_{\text{mol}} - \hat{\mathcal{H}}_{\text{sp-vib}}$, which is the original molecular Hamiltonian without the new coupling term between spin and vibrations (the Hamiltonian $\hat{\mathcal{H}}_0$ is referred to as the equilibrium Hamiltonian throughout the present chapter). Accordingly, for the molecular Hamiltonian $\hat{\mathcal{H}}_{\text{mol}} = \hat{\mathcal{H}}_0 + \hat{\mathcal{H}}_{\text{sp-vib}}$ given in Eq. (3.1), the transformation kernel $\hat{\mathcal{S}}$ can be written as

$$\hat{\mathcal{S}} = \sum_{\chi_n \neq \chi'_n} \frac{1}{E^0_{\chi_n} - E^0_{\chi'_n}}\ \left|\chi_n\right\rangle \left\langle\chi_n\right| \hat{\mathcal{H}}_{\text{sp-vib}} \left|\chi'_n\right\rangle \left\langle\chi'_n\right|, \tag{3.4}$$

where $E^0_{\chi_n}$ and $E^0_{\chi'_n}$ are the eigenvalues of the equilibrium Hamiltonian $\hat{\mathcal{H}}_0$. One should recall that Eq. (3.4) is primarily for diagonalizing the molecular Hamiltonian $\hat{\mathcal{H}}_{\text{mol}}$ in the first order to obtain a Schrieffer-Wolff-like transformation [61]. However, in the case of coupling between molecular vibrations and the uniaxial component of the spin, we can obtain a transformation kernel $\hat{\mathcal{S}}$ that gives an exact solution. The reason for this can be understood as follows: In terms of the spin operators, both the equilibrium Hamiltonian $\hat{\mathcal{H}}_0$ and the interaction term $\hat{\mathcal{H}}_{\text{sp-vib}}$ are expressed in terms of the same spin projection operator, namely $\left(\hat{S}_n^z\right)^2$. Now, since any operator commutes with itself, the commutator $\left[\hat{\mathcal{H}}_{\text{spin}}, \hat{\mathcal{H}}_{\text{sp-vib}}\right]$ equals zero. This essentially means that there exist common S_z states for both Hamiltonians. As for the vibronic operators, we note that the commutators $\left[(\hat{b}_i^\dagger+\hat{b}_i), \hat{b}_i^\dagger \hat{b}_i\right]$ and $\left[(\hat{b}_i^\dagger+\hat{b}_i), (\hat{b}_i^\dagger+\hat{b}_i)\right]$ equal zero. As a result, the three terms $\hat{\mathcal{H}}_{\text{vib}}$, $\hat{\mathcal{H}}_{\text{sp-vib}}$ and $\hat{\mathcal{H}}_{\text{ch-vib}}$ commute with each other. In light of these vanishing commutators, we conclude that the equilibrium Hamiltonian $\hat{\mathcal{H}}_0$ commutes with the interaction term $\hat{\mathcal{H}}_{\text{sp-vib}}$. Consequently, a transformation generator $\hat{\mathcal{S}}$ can be acquired such that the molecular Hamiltonian $\hat{\mathcal{H}}_{\text{mol}}$ becomes diagonal in both $\hat{\mathcal{H}}_0$ and $\hat{\mathcal{H}}_{\text{sp-vib}}$ *simultaneously.*

Employing Eq. (3.4), the derived transformation kernel $\hat{\mathcal{S}}$ is found to take the form

$$\hat{\mathcal{S}} = -\sum_i \sum_n \Lambda_n^i \left(\hat{S}_n^z\right)^2 \left(\hat{b}_i - \hat{b}_i^\dagger\right), \tag{3.5}$$

with the details of the derivation given in App. A.2. It should be remembered that in order to conserve the Hermiticity of the operators, the transformation must be unitary and, hence, $\hat{\mathcal{S}}$ is anti-Hermitian ($\hat{\mathcal{S}}^\dagger = -\hat{\mathcal{S}}$). Now, using the Baker-Hausdorff formula given in Eq. (2.37), we can transform the operators of the molecule, electrode and vibrations. Due to the vanishing commutations between charge and spin operators, the charge operators of the molecule and electrodes remain intact upon this transformation. Thus, the tunneling $\hat{\mathcal{H}}_{\text{tun}}$ and leads $\hat{\mathcal{H}}_{\text{leads}}$ Hamiltonians are untouched. Likewise, $\hat{S}_n^z$ commutes with $\hat{\mathcal{S}}$, and that is why it is unchanged as well. Regarding the vibronic operators, we start by evaluating the first order commutator

$$\begin{aligned}\left[\hat{\mathcal{S}}, \hat{b}_{i'}^\dagger\right] &= \left[-\sum_i \sum_n \Lambda_n^i \left(\hat{S}_n^z\right)^2 \left(\hat{b}_i - \hat{b}_i^\dagger\right), \hat{b}_{i'}^\dagger\right] \\ &= -\sum_i \sum_n \Lambda_n^i \left(\hat{S}_n^z\right)^2 \left[\left(\hat{b}_i - \hat{b}_i^\dagger\right), \hat{b}_{i'}^\dagger\right] \\ &= -\sum_n \Lambda_n^{i'} \left(\hat{S}_n^z\right)^2.\end{aligned} \tag{3.6}$$

Equation (3.6) implies that only the first two terms of the expansion in Eq. (2.37) survives. Thus, the transformed vibronic creation operator reads

$$\hat{\hat{b}}_i^\dagger = \hat{b}_i^\dagger - \sum_n \Lambda_n^i \left(\hat{S}_n^z\right)^2. \tag{3.7}$$

Similarly, we can transform the annihilation operator as follows

$$\hat{\hat{b}}_i = \hat{b}_i - \sum_n \Lambda_n^i \left(\hat{S}_n^z\right)^2. \tag{3.8}$$

Inserting Eq. (3.7) and (3.8) into Eq. (3.1), the transformed molecular Hamiltonian for a charge state n can be written as

$$\begin{aligned}\hat{\mathcal{H}}'_{\text{mol},n} = \hat{\mathcal{H}}_{\text{spin},n} + (\varepsilon - eV_{\text{g}})\hat{n}_d + \sum_i \hbar\omega_i \left(\hat{b}_i^\dagger - \Lambda_n^i \left(\hat{S}_n^z\right)^2\right)\left(\hat{b}_i - \Lambda_n^i \left(\hat{S}_n^z\right)^2\right) \\ + \sum_i \lambda_i \hbar\omega_i \left(\hat{b}_i^\dagger + \hat{b}_i - 2\Lambda_n^i \left(\hat{S}_n^z\right)^2\right)\hat{n}_d + \sum_i \Lambda_n^i \hbar\omega_i \left(\hat{S}_n^z\right)^2 \left(\hat{b}_i^\dagger + \hat{b}_i - 2\Lambda_n^i \left(\hat{S}_n^z\right)^2\right),\end{aligned} \tag{3.9}$$

where the molecular Hamiltonian is defined as $\hat{\mathcal{H}}'_{\text{mol}} = \sum_n \hat{\mathcal{H}}'_{\text{mol},n}$. Simplifying the expression, we arrive at

$$\hat{\mathcal{H}}'_{\mathrm{mol},n} = \hat{\mathcal{H}}_{\mathrm{spin},n} + \Big(\varepsilon - eV_{\mathrm{g}} - 2\sum_i \lambda_i \Lambda_n^i \hbar\omega_i \big(\hat{S}_n^z\big)^2 \Big)\, \hat{n}_d - \sum_i \big(\Lambda_n^i\big)^2 \hbar\omega_i \big(\hat{S}_n^z\big)^4 + \hat{\mathcal{H}}_{\mathrm{vib}} + \hat{\mathcal{H}}_{\text{ch-vib}}. \tag{3.10}$$

Careful examination of the above Hamiltonian shows that the coupling between spin and vibronic operators is now eliminated at the expense of modifying the magnetic properties of the molecule. In particular, the uniaxial magnetic anisotropy of the molecule is renormalized via *two new terms*. The *first* term simply modulates the uniaxial anisotropy constant D_n such that, in the presence of spin-vibron coupling, it can be rewritten as

$$D'_n = D_n + 2\Big(\sum_i \lambda_i \Lambda_n^i \hbar\omega_i\Big)\hat{n}_d \tag{3.11}$$

The renormalization in Eq. (3.11) is not solely due to the spin-vibron coupling, but rather arises from the *threefold* coupling between charge, spin and molecular vibrations. That is to say, if the charge-vibron coupling strength $\lambda_i = 0$, this term vanishes. In addition, it should be noted that this term only affects the anisotropy constant of the charged state $N+1$ of the molecule owning to the number operator $\hat{n}_d$, which yields zero when acting on the neutral state N.

Moreover, the interaction between spin and vibrations results in a *second* renormalization term which contains the quartic spin projection operator $\big(\hat{S}_n^z\big)^4$. In contrast to Eq. (3.11), this term modifies the uniaxial magnetic anisotropy of both the neutral N and the charged $N+1$ states of the molecule. Yet, it can be seen from Eq. (3.10) that such term depends *quadratically* on the coupling strength Λ_n^i between spin and vibrations. Thus, in case of weak spin-vibron coupling ($\Lambda_n^i \ll 1$), it can be ignored and the anisotropy renormalization only affects the charged state as indicated by Eq. (3.11). The typical values for the spin-vibron coupling strengths are discussed in Sec. 3.1.2.

Although the coupling between spin and molecular vibrations is now eliminated, Hamiltonian (3.10) still includes an off-diagonal term due to the charge-vibron coupling. In a similar manner to Sec. 2.5.2, the Lang-Firsov transformation is carried out next to eliminate this coupling. The resulting Hamiltonian, then, reads as

$$\hat{\mathcal{H}}'_{\mathrm{mol},n} = \hat{\mathcal{H}}_{\mathrm{spin},n} + \Big(\varepsilon - eV_{\mathrm{g}} - 2\sum_i \lambda_i \Lambda_n^i \hbar\omega_i \big(\hat{S}_n^z\big)^2 \Big)\, \hat{n}_d - \sum_i \big(\Lambda_n^i\big)^2 \hbar\omega_i \big(\hat{S}_n^z\big)^4 + \hat{\mathcal{H}}_{\mathrm{vib}}, \tag{3.12}$$

where the interaction between charge and molecular vibrations is transfered into the tunneling Hamiltonian $\hat{\mathcal{H}}_{\mathrm{tun}}$, as given in Eq. (2.41).

As indicated by the molecular Hamiltonian in Eq. (3.12), the presence of molecular vibrations modulates the magnetic anisotropy of the molecule. Now, although it is possible, based on electronic transport measurements, to determine the effective anisotropy of the molecule such as in Refs. [30, 31], it is not a straightforward task to detect the renormalization due to spin-vibron coupling. This stems from the difficulty to distinguish between the equilibrium anisotropy of the molecule in the absence of molecular vibrations and the spin-vibron induced anisotropy. Accordingly, it would be desired to vary the anisotropy component resulting from the coupling between spin and molecular vibrations to allow for a direct observation of this coupling in transport measurement. Experimentally, this could be realized by bending or vibrating the substrate that the molecule is lying on, so that the molecule can couple to a different vibrational mode, that is $\hbar\omega$ is varied and, hence, the induced anisotropy changes. Now, from a theoretical perspective, we can imitate this effect by varying the spin-vibron coupling strength in our calculations. This explains why for each of the examples discussed throughout the present chapter, we obtain the differential conductance for different spin-vibron coupling strengths to gain insights on the renormalization of magnetic anisotropy.

In summary, the threefold coupling between charge, spin and molecular vibrations is eliminated via two successive canonical transformations. Importantly, *the elimination of spin-vibron interaction comes at the expense of modulating the uniaxial magnetic anisotropy of the molecule.* In the next section, we explore the consequences of this anisotropy renormalization by presenting two examples of transport through an individual magnetic molecule embedded in a junction.

3.1.2 Examples of the renormalization of *uniaxial* magnetic anisotropy

In this section, two examples are given to illustrate the impact of the renormalization of uniaxial magnetic anisotropy, induced by spin-vibron interaction, on transport through a single magnetic molecule. For the sake of conceptual simplicity, only one vibrational mode is considered throughout the present section and, hence, we drop the index i. As one can see from Eq. (3.12), this renormalization depends on the vibrational frequency ω, the coupling strengths λ and Λ_n and also the equilibrium anisotropy parameter of the molecule D_n. Accordingly, based on the molecule under consideration, the magnetic anisotropy renormalization can lead to diverse effects, as discussed throughout this section.

For this purpose, two examples that lie on the opposite limits of the parameter space are discussed to demonstrate how the presence of the spin-vibron coupling manifests in spectroscopic transport measurements. In the first example, we assume a molecule with spin $S_N = 3/2$ in the neutral state and $S_{N+1} = 2$ in the charged state. Moreover, a positive anisotropy constant ($D_n > 0$) is considered (the *easy-axis* type of magnetic anisotropy) along with a vibrational energy comparable to the zero-field splitting in both the charged and neutral states ($\hbar\omega \approx \mathrm{ZFS}_n$). By contrast, in the second example, a similar molecule is discussed, yet the uniaxial anisotropy constant is assumed to be negative ($D_n < 0$), that is, a molecule with the *easy-plane* type of magnetic anisotropy. In addition, the vibrational energy is chosen to be significantly higher than the scale of all transitions between the molecular spin states $|\chi_n\rangle$, which means $\hbar\omega \gg \mathrm{ZFS}_n$.

Before proceeding to the transport examples, it is instructive here to discuss the typical values for the spin-vibron coupling strengths. First of all, we note that the reported values in literature, such as Refs. [62–65], were obtained in the context of bare molecules where nuclear magnetic resonance (NMR) spectroscopy was used to study the various vibrational modes and their coupling strength. In addition, the model used in these studies is different from the model discussed in the present work. However, we can still obtain the appropriate order of magnitude for the spin-vibron coupling strengths to be used in our illustrative examples throughout Chap. 3. Accordingly, we can conclude that the product $\Lambda_n\hbar\omega$ is typically in the same order of magnitude as the anisotropy constant $|D_n|$ [23]. Now, since in the thesis at hand we usually assume the anisotropy constants to be approximately 100 μeV, plus the considered vibrational energies ($\hbar\omega$) range from hundreds of μeV to few meV, it is legitimate to presume that the spin-vibron coupling strength Λ_n varies from 0.01 up to 1.

a) A molecule with the *easy-axis* type of magnetic anisotropy

In this example, a molecule identical to the one in Sec. 2.4 is considered along with a vibrational energy $\hbar\omega = 800$ μeV and charge-vibron coupling strength $\lambda = 1.3$. The calculations were carried

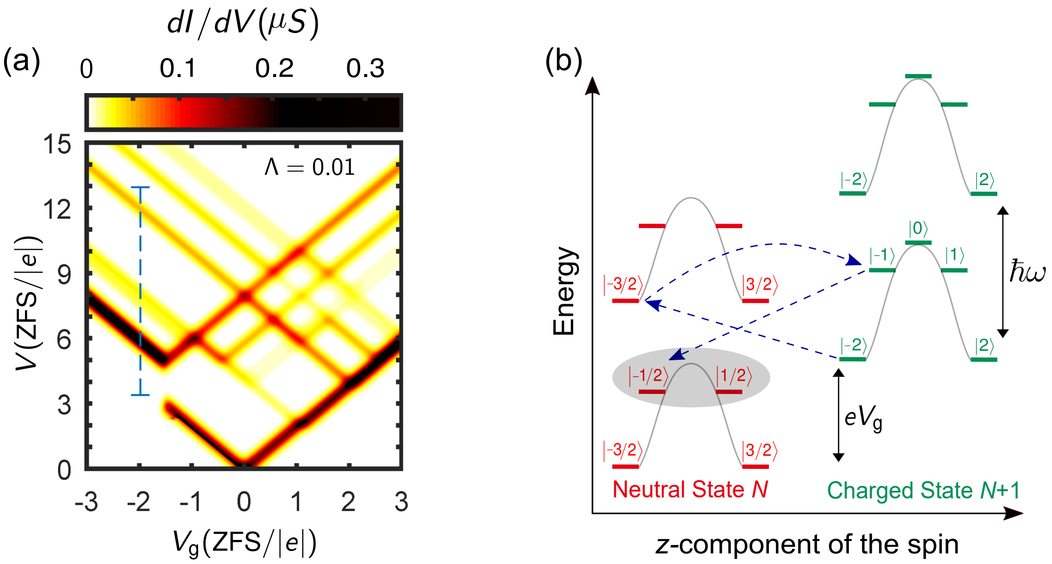

Figure 3.1: Stability diagram and energy spectrum of a molecule with the easy-axis type of magnetic anisotropy in the presence of spin-vibron coupling. **(a)** A differential conductance plot for the molecule whose energy spectrum is given in Fig. 2.2 in the presence of the threefold coupling between charge, spin and molecular vibrations. Since the energy of the vibrational mode under consideration $\hbar\omega$ is comparable to the zero-field splitting (note ZFS here denotes ZFS_N for brevity), the shown transitions are due to both magnetic and vibrational excitations. The discontinuity in the bottom-left corner is attributed to a blockade of transport due to the presence of *dark states*. The dashed line represents a bias cut along a constant gate voltage, which is used to generate the one-dimensional differential conductance plot in Fig. 3.3(a) **(b)** A schematic energy spectrum at a gate voltage $V_\mathrm{g} = -2$ ZFS/|e|, corresponding to the cross-section along the dashed line in (a). Since electrons cannot tunnel out of the states $|\pm 1/2\rangle$, the transport is blocked until a higher bias voltage is reached to enable the transition from $|\pm 1/2\rangle$ to $|\pm 1\rangle$. For this reason, the states $|\pm 1/2\rangle$ are referred to as *dark states.*

out for a temperature $T = 0.18$ K ($k_\mathrm{B}T = 16$ μeV). The spin-vibron coupling strength of both charge states is assumed to be equal ($\Lambda_N = \Lambda_{N+1} = \Lambda = 0.01$).

For the molecule under consideration, the vibrational energy $\hbar\omega$ is comparable to the energy difference between the molecular states $|\chi_n\rangle$ (the zero-field splitting for the neutral state equals 200 μeV, whereas for the charged state it is 300 μeV). Consequently, in contrast to the case discussed in Sec. 2.5.3, the transitions between molecular spin states $|\chi_n\rangle$ involving ground and excited vibrational states can be resolved simultaneously. Using the Fermi golden rule formalism, presented in Sec. 2.3, coupled with the transition rates given in Eq. (2.42), the differential conductance dI/dV was calculated at a coupling strength $\Lambda = 0.01$, as shown in the stability diagram in Fig. 3.1(a).

It is instructive here to recall the layout of this differential conductance plot. At large positive gate voltages $V_\mathrm{g} \gg 0$, the molecule exists in the charged state $N+1$, whereas for $V_\mathrm{g} \ll 0$, the molecule becomes neutral, that is $n = N$. The region in between, bounded by the two black lines, is referred to as the sequential tunneling region where the molecule alternates between both charge states as electrons hop from the source to the drain via the molecule. The edges of the sequential tunneling region represent the transitions between the ground state of both the neutral N and the

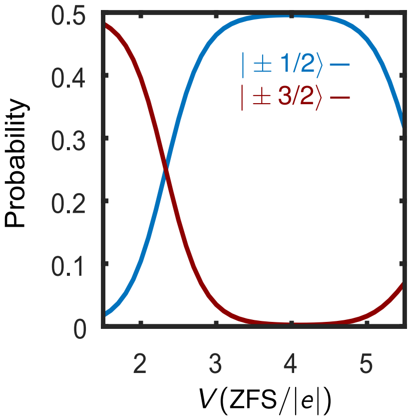

Figure 3.2: Occupation probability for the molecular states $|\pm 1/2\rangle$ and $|\pm 3/2\rangle$. A plot for the occupation probability as a function of the bias voltage V at a constant gate voltage $V_\mathrm{g} = -2$ ZFS/|e|, corresponding to the vertical cut along the dashed line in Fig. 3.1(a). At low bias voltage, the molecule exists in the ground neutral state $|\pm 3/2\rangle$. As the bias voltage increases, the molecule is expected to enter the sequential tunneling region where it alternates between both the neutral and the charged states. However, the presence of *dark states* absorbs all the probability leading to blockade of transport.

charged states $N+1$. In particular, the edge in the bottom-left corner of Fig. 3.1(a) corresponds to the transition from the two neutral molecular states $|3/2, n_q = 0\rangle$ and $|-3/2, n_q = 0\rangle$ to the charged ones $|2, n_q = 0\rangle$ and $|-2, n_q = 0\rangle$, respectively, whereas the bottom-right edge corresponds to the same transition but in the opposite direction, i.e., from the charged $N+1$ to the neutral N molecular states.[1]

Evidently, the first thing to observe in the stability diagram shown Fig. 3.1(a) is the discontinuity in the edge of the sequential tunneling region [the bottom-left corner of Fig. 3.1(a)], which can be attributed to a blockade of transport. The underlying mechanism for the transport blockade can be understood by investigating the transition rates involving the two neutral molecular state $|1/2\rangle$ and $|-1/2\rangle$. Fig. 3.1(b) depicts the energy spectrum of the molecule at a constant gate voltage $V_\mathrm{g} = -2$ ZFS/|e|, where ZFS denotes the zero-field splitting of the neutral state, i.e., ZFS = ZFS$_N$. At the gate and bias voltages where the discontinuity takes place, transitions to the molecular states $|1/2\rangle$ and $|-1/2\rangle$ are allowed, as indicated by the blue arrows. Nevertheless, the bias voltage is not high enough to permit a transition out of these two states. As a result, these two states act as *dark states* [*cf.* shaded states in (b)]. This basically means that the transition rates from other molecular states to these two states are non-zero, whereas the transition rates out of them are vanishing. These vanishing transition rates manifest in the occupation of the molecular states, as shown in Fig. 3.2, where the sequential transport is blocked and the molecule exists solely in the two states $|1/2\rangle$ and $|-1/2\rangle$ for the bias range from $3-5$ ZFS/|e|. Finally, it is noteworthy that even though transport blockade is not a direct consequence of spin-vibron coupling, it is enabled by the energy spectrum reconstruction stemming from the magnetic anisotropy renormalization.

---

[1] Recall that an arbitrary molecular state can be defined as $|\chi_n, n_q\rangle \equiv |\chi_n\rangle \otimes |n_q\rangle$, with $|\chi_n\rangle$ denoting the spin state of the molecule, whereas n_q denotes the number of vibrational energy quanta in the molecule. For instance $|n_q = 0\rangle$ stands for the vibrational ground state and $|n_q = 1\rangle$ represents the first excited state, and so on. For the sake of brevity, vibrational ground states will be denoted only by the molecular spin state, i.e., $|\chi_n, n_q = 0\rangle \equiv |\chi_n\rangle$.

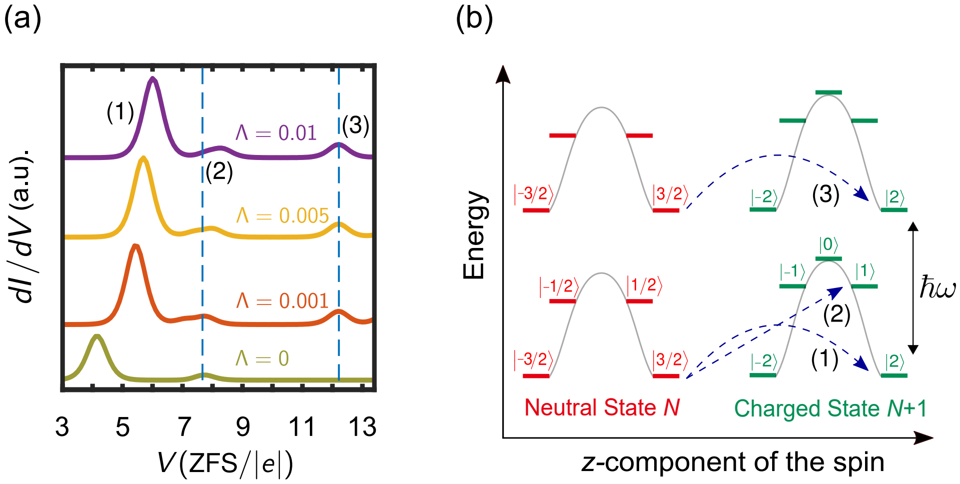

Figure 3.3: Differential conductance plot of a molecule with the easy-axis type of magnetic anisotropy. **(a)** The differential conductance is calculated at different spin-vibron coupling strengths at a constant gate voltage $V_\text{g} = -2$ ZFS/|e|, corresponding to the vertical cut along the dashed line in Fig. 3.1(a). **(b)** The energy spectrum is depicted at zero gate voltage $V_\text{g} = 0$ where the transitions corresponding to the three peaks are marked with blue arrows. The position of the leftmost peak (1) in (a) shifts due to blockade of transport, whereas the rightmost peak (3) in (a) is fixed since it only depends on the vibrational energy $\hbar\omega$. The anisotropy renormalization of the charged state $N+1$ of the molecule can be obtained based on the position shift of the middle peak (2) in (a), as discussed in the text.

Now, in order to shed some light on how the magnetic anisotropy of the molecule is renormalized, the differential conductance is calculated for different values of spin-vibron coupling Λ. Moreover, we isolate three differential conductance peaks by taking a bias cut along a constant gate voltage $V_\text{g} = -2$ ZFS/|e|, as shown by the dashed line in Fig. 3.1(a). The resultant one-dimensional differential conductance plot is shown in Fig. 3.3(a), where the three peaks correspond to the transitions marked on the energy spectrum in Fig. 3.3(b). Particularly, the leftmost (1) and middle peaks (2) represent a transitions from the neutral molecular states $|\pm 3/2\rangle$ to the charged states $|\pm 2\rangle$ and $|\pm 1\rangle$, respectively. On the other hand, the rightmost peak (3) is associated with the transition within the first vibrationally excited states ($|\pm 3/2, n_q = 1\rangle$ to $|\pm 2, n_q = 1\rangle$). It should be noted that the rightmost peak is not present in the bottom curve for $\Lambda = 0$, since we assume the absence of molecular vibrations all-together in this case, that is the charge-vibron coupling strength λ also equals zero. Our aim here is to gain insights into how the modulation of magnetic anisotropy reconstructs the energy spectrum of the molecule by tracking the position (the bias at which they occur) of the differential conductance peaks. Accordingly, whenever useful a vertical dashed line is added to help resolve the position of the peaks, as shown for instance in Fig. 3.3(a).

First, for the rightmost peak (3) in Fig. 3.3(a), we can see that its position is fixed regardless of the coupling strength between spin and vibrations. This is because the position of the first excited vibrational state is not affected by the magnetic anisotropy of the molecule, but rather depends solely on the vibrational mode energy $\hbar\omega$. Thus, for the molecule at hand, the position of this peak is fixed at $eV = 2\hbar\omega$. Similarly, it is justified to expect that the position of the leftmost peak (1) would also not shift as the spin-vibron coupling strength increases since it occurs at the degeneracy point between the neutral N and charged states $N+1$, which we typically guarantee by adjusting the gate voltage V_{g}. Nevertheless, Fig. 3.3(a) shows that the peak actually shifts which can be attributed to the transport blockade discussed above.

Finally, the renormalization of magnetic anisotropy can be extrapolated from the position shift of the middle peak (2) in Fig. 3.3(a). In this example, the coupling strength $\Lambda \ll 1$. Consequently, we can ignore any effects stemming from the penultimate term in Eq. (3.12) since it depends on the coupling strength Λ quadratically. Thus, the dominant renormalization is captured by Eq. (3.11), where the uniaxial anisotropy constant of the charged state D_{N+1} is modified. Accordingly, the magnitude of the position shift between the bottom and topmost middle peaks can be given by $e\Delta V = 2\lambda\Lambda\hbar\omega$.

b) A molecule with the *easy-plane* type of magnetic anisotropy

In the example at hand, the same molecule is considered, yet with a negative magnetic anisotropy constant $D_n < 0$. Consequently, the parabolic energy spectrum shown before is now inverted, as illustrated in Fig. 3.4(b). Here, we consider only one mode with a vibrational energy $\hbar\omega = 2$ meV. As already explained, in order to encompass the diverse effects that arise from magnetic anisotropy renormalization, we study two examples at the opposite limits of the parameter space. Unlike, the previous example, the vibrational energy is assumed here significantly larger than the energy difference between molecular spin states. Thus, we expect that on the stability diagram, we can only resolve the transitions between molecular spin states. The calculations were conducted for a temperature $T = 0.08$ K (the thermal energy $k_{\mathrm{B}}T = 8$ μeV). It should be noted that the zero-field splitting energy units used here are based on the previous example for the sake of consistency, i.e., ZFS is equal to 200 μeV.

Analogously to the previous example, we wish to investigate the implications of spin-vibron coupling and, hence, the coupling strength Λ is varied. However, before including the vibrational degree of freedom, let us first attempt to understand the dynamics of the molecule in the absence of the coupling between spin, charge and vibrations, i.e., λ and Λ equal zero. Figure. 3.4 shows the differential conductance dI/dV in (a) along with the energy spectrum of the molecule in (b). The three differential conductance lines on the lower-left corner of the stability diagram correspond to transitions from the neutral state N to the charge state $N+1$. In particular, the two bottom line refer to transitions from the neutral molecular states $|\pm 1/2\rangle$ to the charged molecular states $|0\rangle$ and $|\pm 1\rangle$, whereas the third line refers to a transition from the neutral molecular state $|\pm 3/2\rangle$ to the charged one $|\pm 2\rangle$. By contrast, the two lines in the lower-right corner stand for transitions from the charged molecular states $|\chi_{N+1}\rangle$ to the neural molecular states $|\chi_N\rangle$, namely the two transitions $|0\rangle$ to $|\pm 1/2\rangle$ and $|\pm 1\rangle$ to $|\pm 3/2\rangle$. It can be seen from Fig. 3.4(a) that there exists a *negative differential conductance* (NDR) region, indicated by the blue line segment. The presence of this NDR indicates that the current I through the molecule decreases as the bias voltage V is increased, leading to a dip (negative peak) in the differential conductance plot, which could be thought of as a partial blockade of transport. For the molecule under discussion, the NDR occurs because the transition from the charged molecular state $|\pm 1\rangle$ to the neutral one $|\pm 3/2\rangle$ occurs before the bias voltage is high enough to allow for the transition out of the neutral state $|\pm 3/2\rangle$ to the charged one $|\pm 2\rangle$. That is to say, once an electron tunnels off a charged molecule resulting in a transition from $|\pm 1\rangle$ to $|\pm 3/2\rangle$, it is forbidden for another electron to tunnel into the molecule until the bias voltage is further increased, which results in a decrease in the current that flows through the molecule. It should be emphasized that this is not a complete transport blockade, but rather a decrease in the tunneling current since the molecule is also likely to exist in other molecular states that give rise to current. Specifically, current through the molecule is still enabled by the transitions between the states the two states $|0\rangle$ and $|\pm 1/2\rangle$.

Now, taking into consideration the interaction between charge, spin and molecular vibrations, the differential conductance is acquired at a coupling strength $\Lambda = 0.05$, as shown in Fig. 3.5(a). Evidently, the presence of molecular vibrations drastically impacts the transport properties of the molecule. Importantly, we can see from Fig. 3.5(a) that the transport is blocked at low bias voltage. Interestingly, the origin of this blockade can be traced back to the renormalization of magnetic anisotropy of the molecule. As discussed in Sec. 3.1.1, if the coupling strength $\Lambda \ll 1$, the second order term in Eq. (3.12) can be neglected. Moreover, the anisotropy renormalization is dominated by Eq. (3.11), which indicates that the uniaxial anisotropy parameter of the *charged* state D_{N+1} is modified due to the threefold coupling between spin, charge and molecular vibrations. Since the induced anisotropy in Eq. (3.11) is positive, for vibrational modes with large energy such as the one under consideration, the negative anisotropy parameter can change sign, that is $D'_{N+1} > 0$. In other words, the charged molecule switches from the *easy-plane* to the *easy-axis* type of magnetic anisotropy (*cf.* Sec. 1.3). Figure 3.5(b) shows the reconstructed energy spectrum of the molecule in the presence of molecular vibrations. It can be seen that the parabolic energy spectrum of the charged state $N+1$ becomes inverted, that is, the spin moments now prefer to orient along the z-axis (easy-axis). In fact, it is now straightforward to understand the underlying reason for the transport blockade. As already established, spin selection rules, imposed by the Clebsch Gordon coefficients, forbid transitions between the neutral ground state $|\pm 1/2\rangle$ and the charged ground

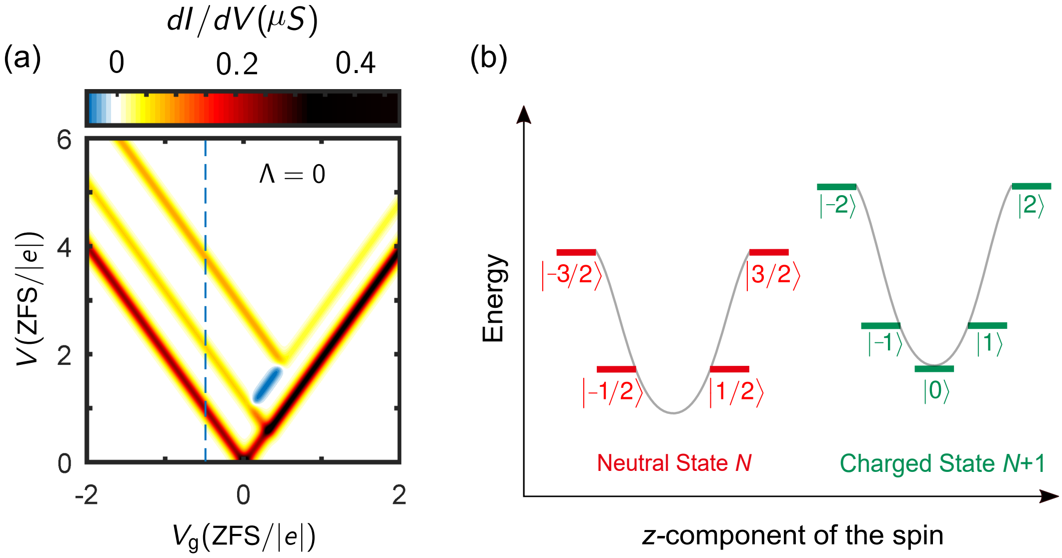

Figure 3.4: Differential conductance plot and energy spectrum of a molecule with the easy-plane type of magnetic anisotropy in the absence of molecular vibrations. **(a)** A stability diagram in the absence of molecular vibrations (λ and $\Lambda = 0$). The blue segment indicates a negative differential conductance region where the current through the molecule drops due to a partial blockade of transport. The vertical dashed line stands for a bias cut at a constant gate voltage as plotted in Fig. 3.6. **(b)** An energy spectrum of the molecule under consideration. In comparison to Fig. 3.3(b), the parabolic energy spectrum is inverted since for $D < 0$, the spin moment prefers to orient in the plane perpendicular to the easy axis (easy-plane anisotropy).

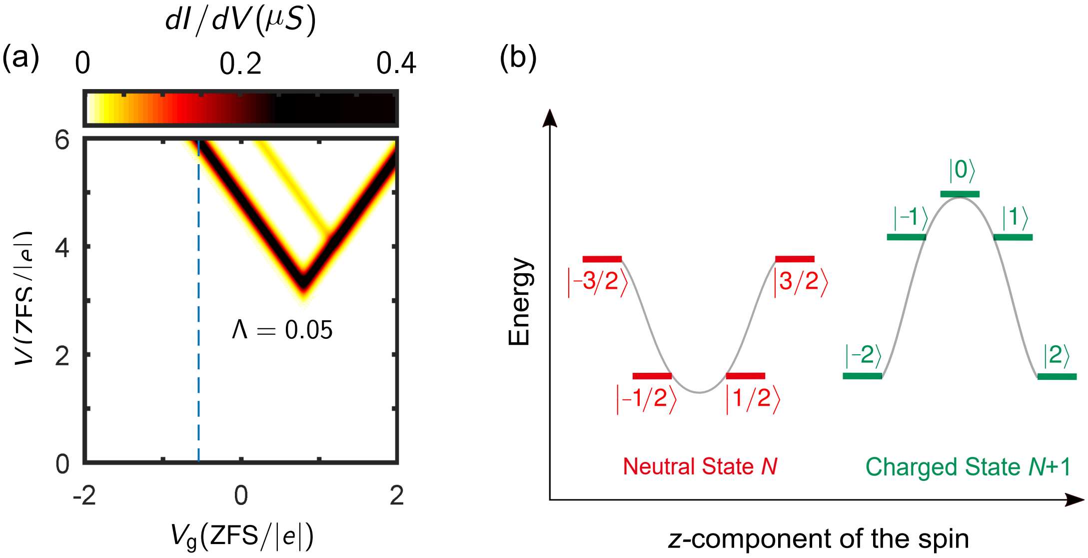

Figure 3.5: Differential conductance plot and energy spectrum of a molecule with the easy-plane type of magnetic anisotropy in the presence of spin-vibron coupling. **(a)** A stability diagram at a spin-vibron coupling strength $\Lambda = 0.05$ and a charge-vibron coupling strength $\lambda = 1.3$. Spin selection rules leads to blockade of transport since there is no transitions allowed between the neutral and charged ground states. The vertical dashed line stands for a bias cut at a constant gate voltage as plotted in Fig. 3.6. **(b)** A reconstructed energy spectrum of the molecule due to spin-vibron interaction. The energy spectrum of the molecule in the charged state $N+1$ becomes flipped because the effective anisotropy constant of the charged state changes its sign.

state $|\pm 2\rangle$ since it would require changing the spin state of the molecule by an amount more than the spin of the tunneling electron, that is, $1/2$. Consequently, the transport is blocked until the bias voltage is high enough to allow transitions between the two states $|\pm 2\rangle$ and $|\pm 3/2\rangle$, which correspond to the two black lines in Fig. 3.5(a).

In order to investigate the sign change in the uniaxial anisotropy parameter of the charged state $N+1$, a bias cut at a constant gate voltage $V_{\mathrm{g}} = -0.5$ ZFS/$|e|$ is taken while varying the spin-vibron coupling strength Λ, as plotted in Fig. 3.6. The bottom blue curve simply reflects the bias cut in Fig. 3.4(a) where the differential conductance is plotted in the absence of molecular vibrations. At a coupling strength $\Lambda = 0.02$, the three transitions in Fig. 3.4(a) merge into one, which implies that all the charged molecular states $|\chi_{N+1}\rangle$ are now degenerate. That is to say, the molecule is *isotropic*, i.e., $D'_{N+1} = 0$ and, hence, there is no longer a preferential direction for the spin moment to orient along. For spin-vibron coupling strength greater than 0.02, the energy spectrum of the charged state becomes inverted and a blockade of transport takes place.

In conclusion, *the spin-vibron induced anisotropy can result in suppression of the total magnetic anisotropy of the molecule or even changing the ground state of the molecule.* The later could lead to spin-vibron induced blockade since transitions between the ground states are forbidden by the conservation of spin momentum.

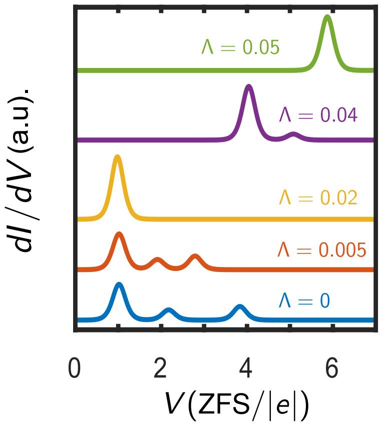

Figure 3.6: Differential conductance plot for various spin-vibron couping strengths. The differential conductance is plotted as a function of the bias voltage V at a constant gate voltage $V_{\mathrm{g}} = -0.5$ ZFS/$|e|$, indicated by the cut in the stability diagrams in Fig. 3.4(a) and Fig. 3.5(a). The effective anisotropy constant of the molecule changes its sign from negative to positive leading to a spin-vibron induced blockade. At a coupling strength $\Lambda \approx 0.02$, the effective anisotropy constant equals zero. Thus, the charged molecule becomes isotropic, which is indicated by the disappearance of the peaks since the charged molecular stats $|\chi_{N+1}\rangle$ are, now, degenerate.

3.2 The coupling of molecular vibrations to the *uniaxial* and *transverse* component of molecular spin

In Sec. 3.1, we have limited our discussion to molecules with only uniaxial magnetic anisotropy. Our goal now is to address a more general case where the molecular vibrations couple to both the *uniaxial* and *transverse* directions of magnetic anisotropy. Accordingly, this section starts by extending the molecular Hamiltonian (3.1) to incorporate the spin-vibron coupling along the transverse direction. Next, we explore the conditions under which this model is exactly solvable. Finally, we present an illustrative example to explore the impact of the aforementioned coupling on electronic transport through a single magnetic molecule.

By including an additional coupling term to the molecular Hamiltonian (3.1), the full Hamiltonian that captures the coupling of molecular vibrations to the uniaxial and the transverse magnetic spin components, as well as charge-vibron coupling, can be written as

$$\hat{\mathcal{H}}_{\mathrm{mol}} = \sum_n \hat{\mathcal{H}}_{\mathrm{spin},n} + (\varepsilon - eV_{\mathrm{g}})\hat{n}_d + \hat{\mathcal{H}}_{\mathrm{vib}} + \hat{\mathcal{H}}_{\text{ch-vib}} + \hat{\mathcal{H}}_{\text{sp-vib}}, \tag{3.13}$$

where

$$\hat{\mathcal{H}}_{\text{sp-vib}} = \sum_n \hbar\omega\Big(\Lambda_n^{\mathrm{u}}\big(\hat{S}_n^z\big)^2 + \Lambda_n^{\mathrm{t}}\Big[\big(\hat{S}_n^+\big)^2 + \big(\hat{S}_n^-\big)^2\Big]\Big)(\hat{b}^\dagger + \hat{b}), \tag{3.14}$$

with Λ_n^{u} and Λ_n^{t} as the coupling strength of vibrations to the uniaxial and transverse components of the magnetic anisotropy, respectively. It should be noted that, for the sake of brevity, the summation over the various vibrational modes denoted by i is dropped. In other words, Eq. (3.13) is written for a single vibrational mode. However, we should emphasize that this does not limit the generality of the model Hamiltonian given in Eq. (3.13). In comparison to Eq. (3.1), the molecular

Hamiltonian (3.13), in the S_z spin projection basis, also possesses two off-diagonal terms due to the threefold interaction between charge, spin and vibrations. Thus, it would be ideal to follow the same procedure as in Sec. 3.1.1, where a canonical transformation was derived in order to eliminate the spin-vibron coupling. Unfortunately, there exists no general canonical transformation that exactly eliminates the off-diagonal coupling. The reason is that, on the contrary to Sec. 3.1.1, the interaction term $\hat{\mathcal{H}}_{\text{sp-vib}}$ does not commute in the present case with the equilibrium Hamiltonian $\hat{\mathcal{H}}_0$ since the commutator

$$\big[\hat{\mathcal{H}}_{\text{sp-vib}},\hat{\mathcal{H}}_{\text{spin}}\big]=\sum_n\hbar\omega(\hat{b}^\dagger+\hat{b})\Big[\Lambda_n^{\text{u}}\big(\hat{S}_n^z\big)^2+\Lambda_n^{\text{t}}\Big(\big[\hat{S}_n^+\big]^2+\big[\hat{S}_n^-\big]^2\Big),-D_n\big(\hat{S}_n^z\big)^2+\frac{E_n}{2}\Big(\big[\hat{S}_n^+\big]^2+\big[\hat{S}_n^-\big]^2\Big)\Big] \tag{3.15}$$

is not equal to zero owning to the fact that the squared ladder operators do not commute with the $\hat{S}_z$ projection operator, $\big[\big(\hat{S}_n^z\big)^2,\big(\hat{S}_n^+\big)^2+\big(\hat{S}_n^-\big)^2\big]\neq 0$. This basically means that, both Hamiltonians do not have common eigenstates. As a result, the molecular Hamiltonian $\hat{\mathcal{H}}_{\text{mol}}$ in Eq. (3.13) *cannot be diagonal in the spin Hamiltonian* $\hat{\mathcal{H}}_{\text{spin}}$ *and in the interaction term* $\hat{\mathcal{H}}_{\text{sp-vib}}$ *terms simultaneously.* However, as we shall see in the next section, there are two scenarios for which Hamiltonian (3.13) can be exactly diagonalized.

3.2.1 Exactly solvable models

As mentioned above, in order to eliminate the coupling between spin and molecular vibrations exactly, the commutator $\big[\hat{\mathcal{H}}_{\text{sp-vib}},\hat{\mathcal{H}}_{\text{spin}}\big]$ has to vanish. In fact, there are two scenarios that allow for a cancellation of this commutator. The first one ensures this by imposing a restriction on the magnetic anisotropy parameters of the molecule, whereas the second scenario is based on the fact that the commutator $\big[\hat{\mathcal{H}}_{\text{sp-vib}},\hat{\mathcal{H}}_{\text{spin}}\big]=0$ for a molecular spin $S=1$.[2] The latter is of particular interest to the present work since, though limited to a molecular spin $S=1$, the solution is generally applicable without the need to impose further conditions on the properties of the molecule. Accordingly, for the sake of completeness, we will briefly discuss the first scenario below, while the rest of this section is devoted to discuss the second case.

a) Solution by parameter restriction

In order to eliminate the spin-vibron coupling, we assume a transformation generator $\hat{\mathcal{S}}$ in the form

$$\hat{\mathcal{S}}=-\sum_n\Big[\Lambda_n^{\text{u}}\big(\hat{S}_n^z\big)^2+\Lambda_n^{\text{t}}\Big(\big(\hat{S}_n^+\big)^2+\big(\hat{S}_n^-\big)^2\Big)\Big](\hat{b}-\hat{b}^\dagger). \tag{3.16}$$

Now, we recall that the bottleneck for eliminating the spin-vibron coupling here is that the commutator $\big[\hat{\mathcal{H}}_{\text{sp-vib}},\hat{\mathcal{H}}_{\text{spin}}\big]\neq 0$. This means that if we devise a transformation generator $\hat{\mathcal{S}}$ that eliminates the spin-vibron coupling in the transformed interaction term $\hat{\mathcal{H}}'_{\text{sp-vib}}$, the coupling will reappear in the Hamiltonian $\hat{\mathcal{H}}'_{\text{spin}}$. However, this complexity is circumvented by enforcing a condition on the anisotropy constants of the molecule such that the spin-vibron coupling does not appear in the transformed spin Hamiltonian $\hat{\mathcal{H}}'_{\text{spin}}$. To illustrate this in more detail, we carry out the canonical transformation for $\hat{\mathcal{H}}_{\text{spin}}$ using the Baker-Hausdorff formula, given in Eq. (2.37), as follows

---

[2] It should be recalled that for a molecule with a spin $S=1/2$, the molecular states consist of the degenerate molecular states $|1/2\rangle$ and $|-1/2\rangle$ since both the uniaxial and transverse magnetic anisotropy play no role. As a result, the commutator $\big[\hat{\mathcal{H}}_{\text{sp-vib}},\hat{\mathcal{H}}_{\text{spin}}\big]$ equals zero, too.

$$\hat{\mathcal{H}}'_{\text{spin}} = \mathrm{e}^{\hat{\mathcal{S}}}\hat{\mathcal{H}}_{\text{spin}}\mathrm{e}^{-\hat{\mathcal{S}}} = \hat{\mathcal{H}}_{\text{spin}} + \big[\hat{\mathcal{S}}, \hat{\mathcal{H}}_{\text{spin}}\big] + \text{h.o.} \tag{3.17}$$

To make progress with this, we start by evaluating the first order commutation between the giant spin Hamiltonian and the transformation generator $\hat{\mathcal{S}}$,

$$\begin{aligned}\big[\hat{\mathcal{S}}, \hat{\mathcal{H}}_{\text{spin}}\big] &= \sum_n \Big[\hat{\mathcal{S}}, -D_n\big(\hat{S}_n^z\big)^2 + \frac{E_n}{2}\Big(\big(\hat{S}_n^+\big)^2 + \big(\hat{S}_n^-\big)^2\Big)\Big] \\ &= -\sum_n \big(D_n\Lambda_n^{\text{t}} + \frac{E_n}{2}\Lambda_n^{\text{u}}\big)\Big[\big(\hat{S}_n^z\big)^2, \big(\hat{S}_n^+\big)^2 + \big(\hat{S}_n^-\big)^2\Big](\hat{b} - \hat{b}^\dagger).\end{aligned} \tag{3.18}$$

Now, by imposing the condition

$$D_n\Lambda_n^{\text{t}} = -\frac{E_n}{2}\Lambda_n^{\text{u}}, \tag{3.19}$$

we ensure that the commutation in Eq. (3.17) vanishes. Accordingly, the transformed spin Hamiltonian $\hat{\mathcal{H}}'_{\text{spin}} = \hat{\mathcal{H}}_{\text{spin}}$ which means that the spin-vibron coupling can be eliminated. We should, however, remark that this condition is not of direct experimental relevance since for this particular model to work, we need to find a molecule with tailored magnetic anisotropy constants and spin-vibron coupling strengths.

b) Solution for a molecular spin $S \leq 1$

Now, we turn our attention to the *second* case for which the molecular Hamiltonian in Eq. (3.13) is exactly solvable, that is, the case of a molecule with a spin $S_N = 1/2$ in the neutral state and a spin $S_{N+1} = 1$ in the charged state, or vice versa. For this case, we can use the transformation generator $\hat{\mathcal{S}}$, given in Eq. (3.16), to eliminate the spin-vibron coupling since for the charged state with $S_{N+1} = 1$, the commutator $\big[\big(\hat{S}_n^z\big)^2, \big(\hat{S}_n^+\big)^2 + \big(\hat{S}_n^-\big)^2\big] = 0$. In other words, the mixed eigenstates of $S = 1$, given in Eq. (2.29), are still eigenfunctions of the operator $\big(\hat{S}_n^z\big)^2$. As for the neutral state with $S = 1/2$, we already established that the above commutator also equals zero since the transverse magnetic anisotropy does not influence the neutral molecular states. This is because the ladder operators $\big(\hat{S}_n^+\big)^2$ and $\big(\hat{S}_n^-\big)^2$ mix every other state and, hence, their eigenvalues are zeros for half-spin systems.

Accordingly, we can proceed to diagonalize the molecular Hamiltonian by carrying out *two* successive canonical transformations; the *first* for eliminating the spin-vibron coupling using Eq. (3.16) (*cf.* Sec. 3.1.1 for a similar transformation), whereas the *second* for the charge-vibron coupling (*cf.* Lang-Firsov transformation in Sec. 2.5.2). Employing these two transformation, the transformed molecular Hamiltonian[3] reads

$$\hat{\mathcal{H}}'_{\text{mol},n} = \hat{\mathcal{H}}_{\text{spin},n} + \big(\,\varepsilon - eV_{\text{g}} - 2\hbar\omega\lambda\gamma\big)\,\hat{n}_d - \hbar\omega\gamma^2 + \hat{\mathcal{H}}_{\text{vib}}, \tag{3.20}$$

where

$$\gamma = \Lambda_n^{\text{u}}\big(\hat{S}_n^z\big)^2 + \Lambda_n^{\text{t}}\Big[\big(\hat{S}_n^+\big)^2 + \big(\hat{S}_n^-\big)^2\Big]. \tag{3.21}$$

Using Eq. (3.20) and (3.21), we can write now the shifted eigenvalues for the neutral and charged states of the molecule. For the *neutral* state with spin $S_N = 1/2$, the energy of the spin doublet $|1/2\rangle$ and $|-1/2\rangle$ is shifted by $-(\hbar\omega/4)(\Lambda_N^{\text{u}})^2$. However, as before, this constant energy

---

[3] Recall that the molecular Hamiltonian is defined as $\hat{\mathcal{H}}_{\text{mol}} = \sum_n \hat{\mathcal{H}}_{\text{mol},n}$

normalization is typically left out in the calculation since it can be incorporated in the energy shifts induced by the applied gate voltage V_g.

As for the *charged* molecule with a spin $S_{N+1} = 1$, Eq. (3.20) can be rewritten in the form of the spin Hamiltonian $\hat{\mathcal{H}}_\mathrm{spin}$ by replacing the anisotropy constants D_{N+1} and E_{N+1} with the effective ones, namely D_eff and E_eff, which include the effects of the threefold coupling between charge, spin and molecular vibrations. Accordingly, Eq. (3.20) reduces to the following Hamiltonian

$$\hat{\mathcal{H}}'_{\mathrm{mol},N+1} = -D_\mathrm{eff}\big(\hat{S}^z_{N+1}\big)^2 + \frac{E_\mathrm{eff}}{2}\Big[\big(\hat{S}^+_{N+1}\big)^2 + \big(\hat{S}^-_{N+1}\big)^2\Big] + (\varepsilon - eV_\mathrm{g})\hat{n}_d + \hat{\mathcal{H}}_\mathrm{vib}, \tag{3.22}$$

where

$$D_\mathrm{eff} = D_{N+1} + 2\hbar\omega\lambda\Lambda^\mathrm{u}_{N+1} + \hbar\omega(\Lambda^\mathrm{u}_{N+1})^2 + 4\hbar\omega(\Lambda^\mathrm{t}_{N+1})^2, \tag{3.23}$$

and

$$E_\mathrm{eff} = E_{N+1} - 4\hbar\omega\lambda\Lambda^\mathrm{t}_{N+1} - 4\hbar\omega\Lambda^\mathrm{u}_{N+1}\Lambda^\mathrm{t}_{N+1}. \tag{3.24}$$

In comparison to Eq. (2.29)-(2.31), the eigenvectors and energies of the molecular Hamiltonian for the charged state take then the form

$$|\chi_0\rangle = |0\rangle \quad \rightarrow \quad \varepsilon_0 = 0, \tag{3.25}$$

$$|\chi_+\rangle = \frac{1}{\sqrt{2}}|1\rangle + \frac{1}{\sqrt{2}}|-1\rangle \quad \rightarrow \quad \varepsilon_+^{'} = -D_\mathrm{eff} + E_\mathrm{eff}. \tag{3.26}$$

$$|\chi_-\rangle = \frac{1}{\sqrt{2}}|1\rangle - \frac{1}{\sqrt{2}}|-1\rangle \quad \rightarrow \quad \varepsilon_-^{'} = -D_\mathrm{eff} - E_\mathrm{eff}. \tag{3.27}$$

Evidently, we obtain the same expression for energies as given in Eq. (2.29)-(2.31), only with renormalized magnetic anisotropy constants. Now, to scrutinize how the energy spectrum of a charged molecule with S_{N+1} is modified due to the spin-vibron coupling, we write an explicit expression of the energies of the molecular states $|\chi_-\rangle$ and $|\chi_+\rangle$ in terms of the ratio between coupling strengths along the uniaxial and transverse directions. Accordingly, for the ratio ζ defined as $\zeta = \Lambda^\mathrm{t}_{N+1}/\Lambda^\mathrm{u}_{N+1}$, Eq. (3.26) and (3.27) can be reformulated as

$$\varepsilon_+^{'} = -D_\mathrm{eff} + E_\mathrm{eff} = \varepsilon_+ - 2\hbar\omega\lambda\Lambda^\mathrm{u}_{N+1}(2\zeta + 1) - \hbar\omega(\Lambda^\mathrm{u}_{N+1})^2(2\zeta + 1)^2, \tag{3.28}$$

$$\varepsilon_-^{'} = -D_\mathrm{eff} - E_\mathrm{eff} = \varepsilon_- + 2\hbar\omega\lambda\Lambda^\mathrm{u}_{N+1}(2\zeta - 1) - \hbar\omega(\Lambda^\mathrm{u}_{N+1})^2(2\zeta - 1)^2. \tag{3.29}$$

Equation (3.28) shows that the energy of the molecular state $|\chi_+\rangle$ always decreases as the coupling strength between spin and vibrations increases. By contrast, Eq. (3.29) indicates that at $\zeta = 1/2$, the energy of the state $|\chi_-\rangle$ is independent of the coupling strength and equals the eigenvalue in the absence of molecular vibrations, namely $\varepsilon'_- = \varepsilon_- = -D_{N+1} - E_{N+1}$. Moreover, in case of weak spin-vibron coupling $\Lambda^\mathrm{u}_{N+1} \ll 1$[4], the first-order terms of Λ^u_{N+1} dominate. Thus, the energy of the molecular state $|\chi_-\rangle$ falls into three regimes, as illustrated in Fig. 3.7 . For $\zeta < 1/2$, $\varepsilon_-^{'}$ decreases as Λ^u_{N+1} increases, whereas for $\zeta > 1/2$, it increases as the coupling strength increases.

---

[4] Note that we refer only to the uniaxial coupling strength since the coupling along the transverse direction is directly related to it via the ratio ζ.

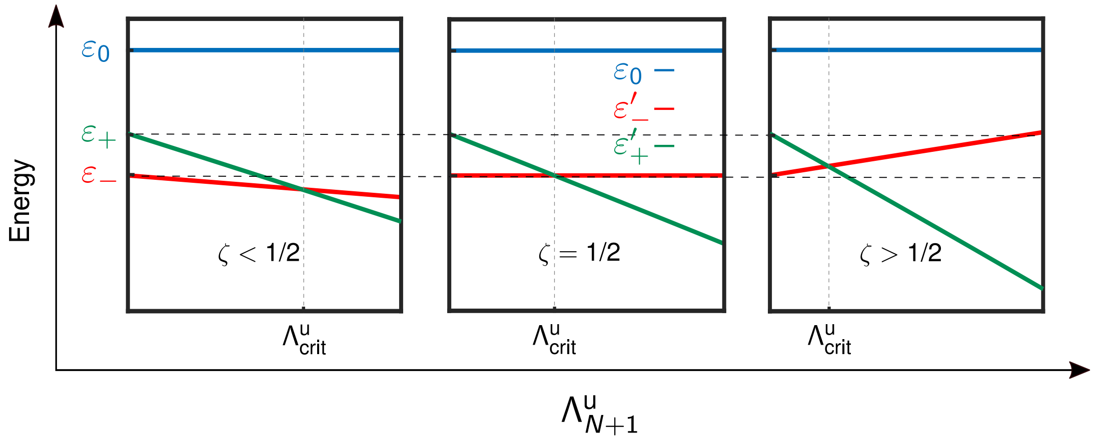

Figure 3.7: Energy spectrum for the charged state with $S_{N+1} = 1$ as a function of spin-vibron coupling strength $\Lambda^{\mathrm{u}}_{N+1}$. Based on the ratio ζ between the coupling strength in the uniaxial and transverse directions, one can distinguish three regimes, $\zeta < 0.5$ (left), $\zeta = 0.5$ (middle) and $\zeta > 0.5$ (right), where $\zeta = \Lambda^{\mathrm{t}}_{N+1}/\Lambda^{\mathrm{u}}_{N+1}$. For $\zeta = 0.5$, the energy of the state $|\chi_-\rangle$ is independent of the spin-vibron coupling strength. Moreover, for $\zeta > 0.5$, ε'_- increases and eventually it can cross the energy of the state $|\chi_0\rangle$ which reverses the order of the eigenstates of the system. The coupling strength at which the transverse magnetic anisotropy is suppressed, i.e., the two states $|\chi_-\rangle$ and $|\chi_+\rangle$ become degenerate, is referred to as the *critical* coupling strength given by $\Lambda^{\mathrm{u}}_{\mathrm{crit}} = (\lambda/2) - \sqrt{(\lambda^2/4) - (E_{N+1}/4\hbar\omega\zeta)}$.

Interestingly, for modes with large vibrational energy quanta $\hbar\omega$, the energy of the molecular state $|\chi_-\rangle$ can actually become higher than the state $|\chi_0\rangle$, provided that $\zeta > 1/2$. This scenario is of particular relevance since it can allow for observing the effect of spin-vibron coupling in transport measurements. Recalling the discussion on spin-polarized transport in Sec. 2.4.4, we have illustrated that using *ferromagnetic* electrodes in the *antiparallel* magnetic configuration, we can amplify the differential conductance peak corresponding to transitions to the state $|\chi_0\rangle$ (*cf.* the rightmost peak in Fig. 2.13). This magnification can, in turn, facilitate keeping track of that particular peak in electronic transport experiments. Accordingly, if we can observe that this peak occurs at a bias voltage V lower than that required for the transition to the state $|\chi_-\rangle$, it will be a clear indication that the coupling of spin and molecular vibrations reconstructed the energy spectrum so that the state $|\chi_0\rangle$ lies within the tunnel splitting window of the two states $|\chi_+\rangle$ and $|\chi_-\rangle$.

In light of Eq. (3.23) and (3.24), it is evident that *the interaction between spin and molecular vibrations results in renormalization of both the uniaxial and transverse magnetic anisotropy constants.* This renormalization depends on the coupling strength along both spin directions, the interaction strength between charge and vibrations λ and the vibrational energy $\hbar\omega$. Thus, the manifestation of the anisotropy renormalization on transport properties can take various forms based on the molecule and the coupling parameters. In the next section, we present one particular example where it is shown that spin-vibron coupling can result in suppression of the transverse magnetic anisotropy.

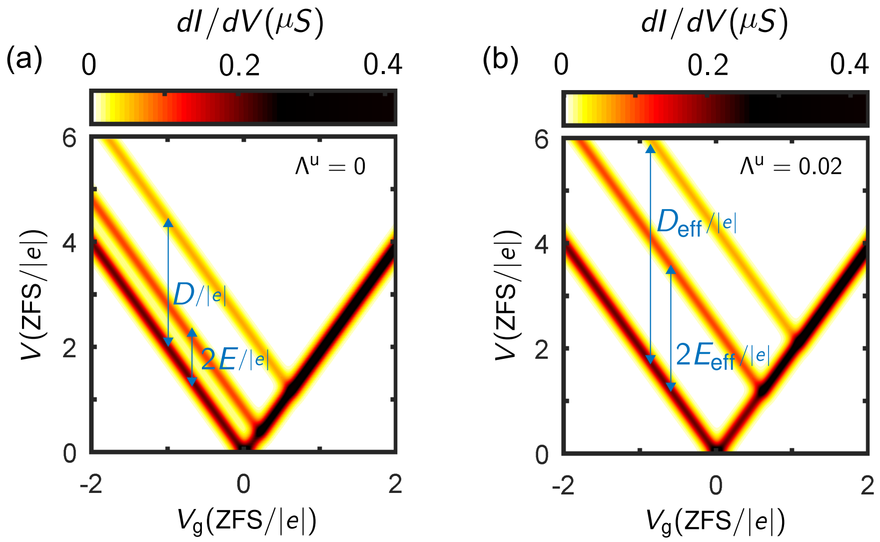

Figure 3.8: Two Differential conductance maps in the absence (a) and presence (b) of spin-vibron coupling .(a) Stability diagram obtained in the absence of molecular vibrations, that is, $\Lambda^{\mathrm{u}} = 0$ and $\lambda = 0$. The anisotropy constants of the molecule, E and D, are marked on the plot. **(b)** In the presence of molecular vibrations, $\Lambda^{\mathrm{u}} = 0.02$ and $\lambda = 1.3$, a stability diagram similar to (a) is obtained, but the magnetic anisotropy of the molecule is modulated. The renormalized magnetic anisotropy constants, D_{eff} and E_{eff} are illustrated on the diagram.

3.2.2 Example of the renormalization of *uniaxial* and *transverse* magnetic anisotropy

The example to be considered involves the same molecule as discussed above with $S_N = 1/2$ and $S_{N+1} = 1$. Since the neutral state N of the molecule is neither affected by the magnetic anisotropy nor by the spin-vibron coupling, in the present analysis, for the sake of notational clarity, we drop the charge index of the anisotropy constants and the spin-vibron coupling strengths. That is, the parameters $D, E, \Lambda^{\mathrm{u}}$ and Λ^{t} refer now to the charged state of the molecule $N + 1$. The anisotropy constants and the thermal energy were chosen in accordance with the example discussed in Sec. 2.4.2 to allow for comparing the cases in the presence and absence of molecular vibrations. As before, for illustrative purposes, we account for a single vibrational mode with $\hbar\omega = 1$ meV. Similar to all previous examples, a charge-vibron coupling strength $\lambda = 1.3$ is used. Based on Fig. 3.7, we established that, depending on the ratio ζ, the energy spectrum of the charged $N + 1$ state falls into three distinctive regimes. In the example under consideration, we set ζ to 3/4 to focus on the rightmost case in Fig. 3.7 while varying the spin-vibron coupling strength along the uniaxial direction Λ^{u}. The values of Λ^{u} were chosen to be in the same order as in Sec. 3.1.2.

Before addressing the implications of the spin-vibron coupling, let us first recall the details of the stability diagram obtained for the molecule at hand in the absence of molecular vibrations, as shown in Fig. 3.8(a). In particular, the three lines on the left corner of the plot, from bottom to top, indicate the transitions from the neutral molecular states $|\pm 1/2\rangle$ to the charged molecular states $|\chi_-\rangle$, $|\chi_+\rangle$ and $|\chi_0\rangle$, respectively. Accordingly, based on the energy spectrum given in Fig. 2.4, the uniaxial and transverse magnetic anisotropy constants can be marked on the differential conductance plot as shown on Fig. 3.8(a). Now, accounting for the molecular vibrations, the magnetic anisotropy constants become normalized as given by Eq. (3.23) and (3.24). Similarly, we

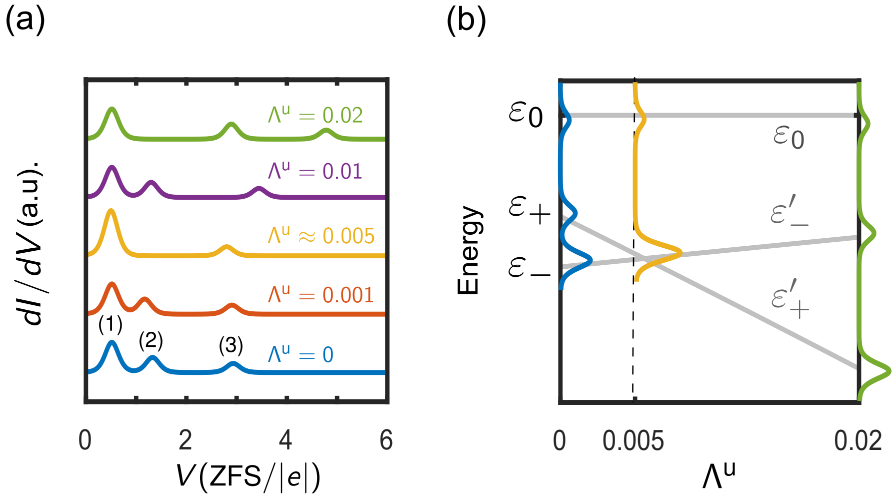

Figure 3.9: Differential conductance plot and energy spectrum as a function of the spin-vibron coupling strength. **(a)** Differential conductance dI/dV as a function of bias voltage for different spin-vibron coupling strength. This plot is obtained at a fixed gate voltage $V_g = -0.5$ ZFS/$|e|$. At a coupling strength $\Lambda^u \approx 0.005$, the transverse anisotropy of the molecule is suppressed and, hence, the peaks (1) and (2) representing transitions to $|\chi_-\rangle$ and $|\chi_+\rangle$, respectively, merge. At stronger coupling strengths, the effective transverse anisotropy becomes positive and the ground state of the charged molecule changes from $|\chi_-\rangle$ to $|\chi_+\rangle$. **(b)** Energy spectrum of the charged molecule with spin $S_{N+1} = 1$ as a function of spin-vibron coupling strength. The crossing between the lowest two energy states at a coupling strength $\Lambda^u \approx 0.005$ is shown, indicating a suppression of transverse anisotropy. The differential conductance peaks are superimposed over the spectrum at $\Lambda^u = 0$, 0.005 and 0.02.

acquire the differential conductance plot, presented in Fig. 3.8(b), where we can see that the three transitions mentioned above are also visible, but they occur at different bias voltages. Moreover, we can obtain the *effective* anisotropy constants E_{eff} and D_{eff} as shown on the stability diagram in Fig. 3.8(b).

Although Fig. 3.8 shows, in the absence (a) and presence (b) of molecular vibrations, three lines representing transitions from the neutral N to the charged state $N+1$, the molecular states $|\chi_n\rangle$ involved in these transitions are, in fact, not the same. To examine these three lines and the corresponding transitions in more detail, the spin-vibron coupling strength along the uniaxial direction Λ^u is varied while keeping the ratio ζ fixed. Additionally, we take a cut through the two stability diagrams in Fig. 3.8 at a constant gate voltage, so that we can compare the resultant differential conductance peaks with the energy spectrum of the molecule at different spin-vibron coupling strengths, as shown in Fig. 3.9. The three differential conductance peaks in Fig. 3.9(a), plotted at a gate voltage $V_g = -0.5$ ZFS/$|e|$, correspond to the three lines in the stability diagrams given in Fig. 3.8. From the energy spectrum in Fig. 3.9(b), we can see that as the coupling strength increases, the tunnel-splitting Δ, defined as $|\varepsilon'_- - \varepsilon'_+|$, first decreases, which indicates that the effective transverse magnetic anisotropy constant E_{eff} is lowered. Ultimately, at a coupling strength of approximately 0.005, the splitting of the ground state doublet, $|\chi_-\rangle$ and $|\chi_+\rangle$, in the charged state is suppressed. This, in turn, means that E_{eff} equals zero as evident by the merging of the first two peaks, i.e., (1) and (2), representing transitions to the states $|\chi_-\rangle$ and $|\chi_+\rangle$. That is to say, *the renormalization of magnetic anisotropy, triggered by spin-vibron interaction, led to a suppression* *of the transverse magnetic anisotropy of the molecule.* For coupling strengths greater than 0.005, the ground state of the charged molecule changes from the state $|\chi_-\rangle$ to the state $|\chi_+\rangle$. For this reason, while the bottom-left line in Fig. 3.8(a) stands for to a transition from $|\pm 1/2\rangle$ to $|\chi_-\rangle$, the corresponding line in Fig. 3.8(b) indicates a transition to $|\chi_+\rangle$. The swap of the ground state of the charged molecule is clearly demonstrated in the energy spectrum schematically depicted in Fig. 3.9(b) along with the differential conductance peak overlaid on top of the energy spectrum.

Based on this example and the one given in Sec. 3.1.2, we come to the conclusion that the interaction between the molecular vibrations and the spin results in renormalization of magnetic anisotropy along the uniaxial and transverse directions. Moreover, depending on the molecule under consideration, the vibrational energy and the coupling strengths, this interaction can result in diverse effects ranging from a suppression of magnetic anisotropy to a blockade of transport.

4

The role of quantum coherences in transport through magnetic molecules

The quantum state of a molecule embedded between two electrodes can be fully described by its reduced density matrix (*cf.* Sec. 2.2). In particular, the diagonal elements represent the occupation probabilities of the molecular states $|\chi_n\rangle$, whereas the off-diagonal ones denote the coherent superpositions between these states. In Chap. 2, we used Fermi golden rule to calculate the probabilities of the molecular states, while neglecting their superpositions. In this chapter, however, we aim for a full quantum mechanical treatment by using a technique that captures the dynamics of the diagonal, as well as, the off-diagonal elements of the reduced density matrix. Accordingly, the *real-time diagrammatic technique*, introduced in Ref. [66–68], is used to examine the role of quantum coherences in transport through magnetic molecules.

This chapter is organized as follows: Section 4.1 presents an overview of the technical aspects of the real-time diagrammatic technique, focusing on the *generalized master equation*, whereas, in Sec. 4.2, it is employed to study first-order transport through a single magnetic molecule, taking into consideration the full dynamics of the reduced density matrix. In Sec. 4.3, an illustrative example is presented to show that the off-diagonal elements play no role in first-order transport through a magnetic molecule embedded between *nonmagnetic* electrodes.

4.1 Real-time diagrammatic technique

The purpose of this section is to illustrate the use of the real-time diagrammatic technique to obtain the charge current through a molecule coupled to two electrodes. The details of the technique can be found in Ref. [66–69]. In the present section, however, we only focus on the central result of this technique, namely a generalized master equation, and how to use it to calculate both the diagonal and the off-diagonal elements of the reduced density matrix[1]. Within the framework of the real-time diagrammatic technique, the time evolution of a matrix element of the reduced density matrix $\mathcal{P}^{\chi_1}_{\chi_2} \equiv \langle\chi_1|\, \rho^{\mathrm{red}}\, |\chi_2\rangle$ can be written as

$$\frac{d\mathcal{P}^{\chi_1}_{\chi_2}}{dt} = (\varepsilon_{\chi_1} - \varepsilon_{\chi_2})\mathcal{P}^{\chi_1}_{\chi_2} + \sum_{\chi_1'\chi_2'} \Sigma^{\chi_1\chi_1'}_{\chi_2\chi_2'} \mathcal{P}^{\chi_1'}_{\chi_2'}, \tag{4.1}$$

---

[1] Recall from Sec. 2.2 that by taking a trace over the degrees of freedom in the leads, we can obtain the reduced density matrix of the molecule where the occupations of the molecular states are on the diagonal elements, whereas the off-diagonal terms represent superpositions between these states.

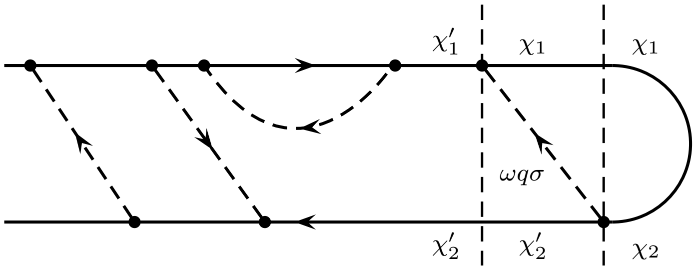

Figure 4.1: Time evolution of the reduced density matrix. The time evolution of the reduced density matrix is depicted by the *Keyldysh contour* where the upper and lower lines represent the forward and backward propagators in time, respectively, as indicated by the arrows. The dashed lines connecting different parts of the propagator correspond to tunneling events to the left and right electrodes. The cross-section on the right-hand side represent one of the irreducible diagrams for the self-energy $\Sigma^{\chi_1\chi_1'}_{\chi_2\chi_2'}$. In particular, this diagram stands for a transition from a matrix element $\mathcal{P}^{\chi_1'}_{\chi_2'}$ to $\mathcal{P}^{\chi_1}_{\chi_2}$ due to the tunneling of an electron with spin σ from an electrode with an index q.

where ε_{χ_1} and ε_{χ_2} are the energies of the molecular states $|\chi_1\rangle$ and $|\chi_2\rangle$, respectively. The self-energies $\Sigma^{\chi_1\chi_1'}_{\chi_2\chi_2'}$ describe the transitions between the elements of the reduced density matrix. Each self-energy, also referred to as generalized transition rate, corresponds to the sum of all irreducible diagrams that stand for transitions between two elements of the reduced density matrix. For instance, the irreducible diagram obtained by taking a cross section of the *Keldysh contour* in Fig. 4.1 represents one of the possible transitions between the elements $\mathcal{P}^{\chi_1}_{\chi_2}$ and $\mathcal{P}^{\chi_1'}_{\chi_2'}$. It is noteworthy that the first term in Eq. (4.1) represents the intra-molecule dynamics, where only off-diagonal elements (coherences) play a role since this term vanishes for diagonal elements ($\varepsilon_{\chi_1} - \varepsilon_{\chi_1} = 0$). On the other hand, the second term signifies the evolution due to coupling to the left and right electrodes.

Based on Eq. (4.1), it is evident that calculating the self-energies is a prerequisite to obtain the elements of the reduced density matrix of the molecule. In the real-time diagrammatic technique, the self-energies can be evaluated diagrammatically using the rules in App. B.1.1. With the knowledge of the self-energies and the elements of the reduced density matrix, the tunneling current through the molecule can be calculated as [67]

$$I = -\frac{\imath e}{2\hbar}\boldsymbol{e}^T\boldsymbol{\Sigma}^I\boldsymbol{\mathcal{P}}, \tag{4.2}$$

where $\boldsymbol{\Sigma}^I$ is a matrix containing the *current* self-energies, evaluated diagrammatically in a similar manner to the self-energies in Eq. (4.1). The main difference, however, is that, in the case of first-order transport, the current self-energy carries an additional multiplicative factor that accounts for the direction of the electron tunneling process corresponding to that self-energy. As a result of this multiplicative factor, the current flowing into the left electrode I_L acquires a negative sign, whereas the current flowing into the right electrode I_R is kept positive such that the total current formula reads as $I = (I_\mathrm{R} - I_\mathrm{L})/2$. The details of calculating the current self-energies are summarized in App. B.1.3. The vector $\boldsymbol{\mathcal{P}}$ contains the diagonal elements of the reduced density matrix (probabilities) followed by the off-diagonal ones (coherences). Finally, The vector $\boldsymbol{e}^T$ is non-zero for the diagonal elements of the vector $\boldsymbol{\mathcal{P}}$ and zero otherwise.

To sum the technique up, the procedure for calculating the tunneling current through the molecule starts by drawing the set of all irreducible diagrams which characterize the possible transitions between the elements of the reduced density matrix. Next, for each diagram, a self-energy is obtained based on the energy-space diagrammatic rules provided in App. B.1.1. Using the generalized master equation, given in Eq. (4.1), the diagonal and off-diagonal elements of the reduced density matrix can be acquired at the steady state. In turn, the tunneling current through the molecule can be calculated with the help of Eq. (4.2).

4.2 First-order transport through a magnetic molecule

In this section, the formalism of the real-time diagrammatic technique is employed to study first-order transport through a single magnetic molecule embedded in a junction, taking into account quantum coherences. In the limit of first-order transport, the master equation, given in Eq. (4.1), can be rewritten as

$$\frac{d\mathcal{P}^{\chi_1}_{\chi_2}}{dt} = 0 = (\varepsilon_{\chi_1} - \varepsilon_{\chi_2})\mathcal{P}^{\chi_1}_{\chi_2} + \sum_{\chi_1^{'}\chi_2^{'}} \Sigma^{\chi_1\chi_1^{'}}_{\chi_2\chi_2^{'}}\Big|_{\varepsilon_{\chi_1}=\varepsilon_{\chi_2}} \mathcal{P}^{\chi_1^{'}}_{\chi_2^{'}}, \tag{4.3}$$

where the self-energies in the second term are now evaluated at $\varepsilon_{\chi_1} = \varepsilon_{\chi_2}$ in order to eliminate the higher orders of the tunnel-coupling strength Γ in the perturbative expansion of the self-energies [67, 70]. This can be justified as follows: For $\varepsilon_{\chi_1} - \varepsilon_{\chi_2} \gg$ the leading-order of Γ, Eq. (4.3) reduces into

$$0 \approx (\varepsilon_{\chi_1} - \varepsilon_{\chi_2})\mathcal{P}^{\chi_1}_{\chi_2}, \tag{4.4}$$

and, hence, the off-diagonal term $\mathcal{P}^{\chi_1}_{\chi_2}$ is now suppressed owning to the large energy difference between the superimposed states, $|\chi_1\rangle$ and $|\chi_2\rangle$. This basically means that *coherent superpositions should not be neglected only if the absolute energy difference between the superimposed states is relatively small compared to the tunnel-coupling strength* Γ. Consequently, in this formalism, the energy difference $|\varepsilon_{\chi_1} - \varepsilon_{\chi_2}|$ must be smaller than or equal to the tunnel-coupling strength Γ [67, 70]. To put the magnitudes of Γ and $|\varepsilon_{\chi_1} - \varepsilon_{\chi_2}|$ into perspective, one should remember that, in the weak coupling regime considered throughout this thesis, the thermal energy $k_\mathrm{B}T$ should be much greater than Γ ($k_\mathrm{B}T \gg \Gamma$). In other words, for the first-order transport discussed here, coherent superpositions can play a role if there are molecular states whose energy difference satisfies the following condition $|\varepsilon_{\chi_1} - \varepsilon_{\chi_2}| \lesssim \Gamma \ll k_\mathrm{B}T$.

With the knowledge of self-energies, Eq. (4.3) can be used to calculate the elements of the reduced density matrix. For first-order transport, there are *eight* irreducible diagrams that describe the possible transitions between the elements of the reduced density matrix of a molecule with two charge states (N and $N+1$). A schematic illustration of these diagrams along with the corresponding self-energies are given in App. B.2. For the sake of illustration, however, one example of these self-energies is discussed here. For instance, the self-energy $\Sigma^{\chi_{N+1}\chi_N}_{\chi_{N+1}^{'}\chi_N^{'}}$ represents the two possible transitions from the density matrix element $\mathcal{P}^{\chi_N}_{\chi_N^{'}}$ to $\mathcal{P}^{\chi_{N+1}}_{\chi_{N+1}^{'}}$, as demonstrated by the two diagrams depicted in Fig. 4.2.

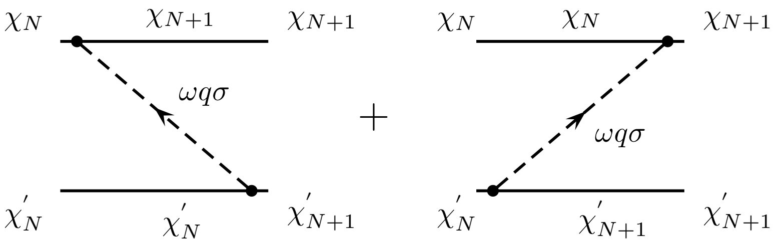

Figure 4.2: Irreducible diagrams for the self-energy $\Sigma^{\chi_{N+1}\chi_N}_{\chi'_{N+1}\chi'_N}$. These diagrams represent the two possibilities for a transition between the reduced density matrix elements $\mathcal{P}^{\chi_N}_{\chi'_N}$ to $\mathcal{P}^{\chi_{N+1}}_{\chi'_{N+1}}$ to take place. The exact expression for each of the diagrams can be found in App. B.2. Importantly, when $|\chi'_N\rangle = |\chi_N\rangle$ and $|\chi'_{N+1}\rangle = |\chi_{N+1}\rangle$, these two diagrams are mirror images. That is, their corresponding self-energies are negative conjugate and, hence, their sum becomes proportional to the imaginary part of either of them. In such a case, it is sufficient to evaluate only one of these two diagrams.

Interestingly, for the case when $|\chi'_N\rangle = |\chi_N\rangle$ and $|\chi'_{N+1}\rangle = |\chi_{N+1}\rangle$, the self-energy $\Sigma_{\chi_{N+1}\chi_N}$[2] stands for the transition rate from a neutral molecular state $|\chi_N\rangle$ to a charged one $|\chi_{N+1}\rangle$ due to the tunneling of an electron with a spin σ into the molecule from the qth electrode. In that case, the two diagrams in Fig. 4.2 become mirror images and, hence, their sum is proportional to the imaginary part of either of them (*cf.* the mirror rule in App. B.1.2). As a result, the expression of the self-energy $\Sigma_{\chi_{N+1}\chi_N}$ collapses to

$$\begin{aligned}\Sigma_{\chi_{N+1}\chi_N} = \imath \sum_{q\sigma} \Gamma^q_\sigma f^q(\varepsilon_{\chi_{N+1}} - \varepsilon_{\chi_N}) &\Bigg(\sum_{M_{N+1},M_N} a_{M_N} b^*_{M_{N+1}} \langle S_N, M_N; 1/2, \sigma | \, S_{N+1}, M_{N+1}\rangle \Bigg) \\ \times &\Bigg(\sum_{M_{N+1},M_N} a^*_{M_N} b_{M_{N+1}} \langle S_N, M_N; 1/2, \sigma | \, S_{N+1}, M_{N+1}\rangle \Bigg).\end{aligned} \tag{4.5}$$

It can be seen that the diagrammatically evaluated self-energy in Eq. (4.5) is identical[3] to the transition rate calculated with Fermi golden rule, given in Eq. (2.21), since it represents a transition between two diagonal elements of the reduced density matrix, namely $\mathcal{P}_{\chi_N}$ and $\mathcal{P}_{\chi_{N+1}}$. Significantly, it should be emphasized that *diagrams that involve transitions between the off-diagonal elements are not captured by Fermi golden rule formalism.* For that reason, the real-time diagrammatic technique is exploited to capture the transitions that involve the coherent superpositions between the states of the molecule.

Using the self-energies in App. B.2, the elements of the reduced density matrix can be acquired. Importantly, depending on the quantum system under consideration, one can immediately see that some of the coherences are either suppressed or irrelevant to first-order transport and, hence, they can be eliminated a priori to simplify the problem. Accordingly, the rest of this section is devoted to answering the fundamental question: which off-diagonal elements need to be taken into consideration when characterizing first-order transport through a magnetic molecule described by the spin Hamiltonian in Eq. (2.3)? On the one hand, in the absence of transverse magnetic anisotropy ($E = 0$), the molecular states are composed of pure spin projections along the z-axis.

---

[2] Note that for the sake of notational brevity, the self-energy $\Sigma^{\chi_{N+1}\chi_N}_{\chi_{N+1}\chi_N}$ is defined as $\Sigma^{\chi_{N+1}\chi_N}_{\chi_{N+1}\chi_N} \equiv \Sigma_{\chi_{N+1}\chi_N}$.

[3] Note that, unlike the transition rate given in Eq. (2.21), the above self-energy is a complex quantity, and that is why the current in Eq. (4.2) is multiplied by $-\imath$.

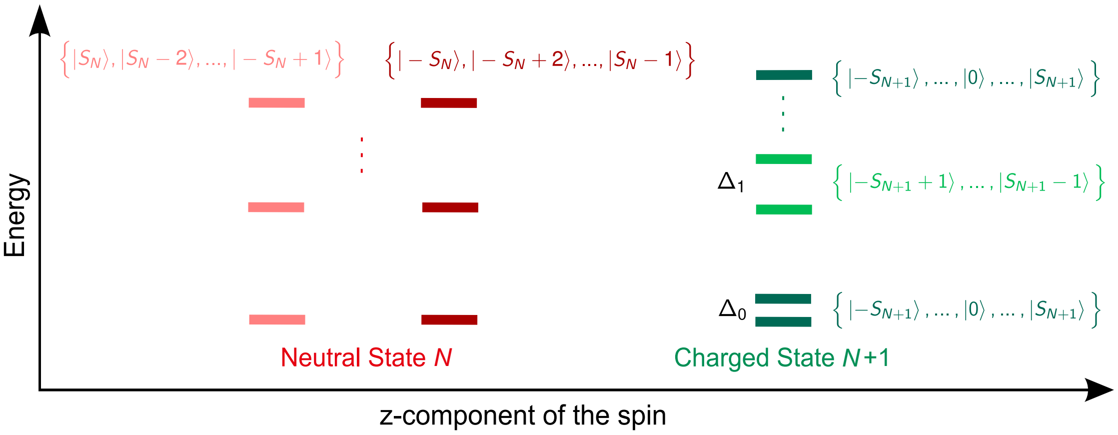

Figure 4.3: Energy spectrum for a magnetic molecule in the neutral and charged states. A molecule with a half-integer spin S_N in the neutral state N and an integer spin S_{N+1} in the charged state $N+1$ is considered. The transverse magnetic anisotropy breaks the rotational symmetry around the z-axis. Thus, the eigenstates of the system split into two uncoupled sets of the S_z spin projections. According to Kramers theorem, the eigenstates of half-integer spin systems are doubly degenerate as evident by the molecular states in the neutral state N. These degenerate molecular states do not belong to the same time-reversed set, as indicated by the different shades of red. Thus, only coherent superpositions between molecular states separated by large energy difference can couple to the diagonal elements. Such coherences, in the limit of first-order transport, are suppressed as seen from Eq. (4.4). On the other hand, for the integer spin S_{N+1}, states belonging to the same set are separated by an energy difference Δ, referred to as the *tunnel-splitting*. For instance, the energy difference between the lowest two energy states in the charged state is denoted by Δ_0. Consequently, for the integer spin case, coherent superpositions should, in general, be taken into consideration, whenever the energy difference Δ is small compared to the tunnel-coupling strength Γ.

Consequently, transitions between the diagonal and off-diagonal elements of the reduced density matrix are forbidden, as such transitions would violate the conservation of spin momentum. In other words, the dynamics of the diagonal and off-diagonal elements decouples and, hence, deriving the diagonal elements using Fermi golden rule formalism, as explained in Sec. 2.3, is sufficient to capture the full dynamics for the reduced density matrix.

On the other hand, as discussed in Chap. 1.3, the presence of transverse magnetic anisotropy splits the molecular states $|\chi_n\rangle$ into two uncoupled sets. Each of these two sets consists of an admixture of the S_z spin projections. Significantly, *the dynamics of the diagonal and off-diagonal elements can only couple for molecular states belonging to the same set of S_z spin projections*. To give an illustration, a generic example is considered for a molecule with a half-integer spin S_N in the neutral state N and an integer spin S_{N+1} in the charged state $N+1$, as depicted in Fig. 4.3. In the case of the half-integer spin S_N, the energy spectrum consists of doubly degenerate molecular states belonging to opposing time-reversed sets[4], as indicated by different shades of red on the left-hand side of Fig. 4.3. Since coherent superpositions can only couple to the diagonal elements for molecular states within the same set, the relevant superpositions in the half-integer spin case are between molecular states separated by a large energy difference. This difference is of the order

---

[4] For a half-integer spin molecule, the degenerate molecular states, even in the presence of transverse magnetic anisotropy, are time-reversed, that is, they only differ by the sign of the magnetic quantum number M.

of the uniaxial anisotropy constant D, which, in the weak coupling regime under consideration, is assumed to be significantly greater than the tunnel-coupling strength Γ. As a result, coherences for the half-integer spin molecule are suppressed.

In contrast, for the integer spin S_{N+1}, according to Kramers theorem, the transverse magnetic anisotropy leads to an energy splitting between states belonging to the same set. For instance, the ground states of the charged molecule in Fig. 4.3 are separated by an energy difference Δ_0, referred to as the tunnel-splitting. For spin $S > 1$, the tunnel splitting Δ_0 is considerably smaller than E (*cf.* $E \leq |D|/3$). Consequently, unlike the half-integer spin, the coherent superpositions between the two ground states of an integer spin molecule are not suppressed and, thus, they should be taken into consideration. Similarly, the two states separated by Δ_1 could also posses off-diagonal interaction. However, since the energy difference between these states Δ_1 is larger than Δ_0, their off-diagonal interaction is expected to be smaller, as seen from Eq. (4.3). Finally, we remark that superpositions between molecular states $|\chi_n\rangle$ with a different charge n are also irrelevant to first-order transport due to the conservation of charge.[5]

So far, we have generically discussed the formalism that can be used to calculate the elements of the reduced density matrix in the sequential tunneling regime. Moreover, depending on the molecule at hand, it was shown that not all of the coherences need to be included. In the next section, an illustrative example is analyzed to explicitly show how the reduced density matrix is constructed and how to determine which off-diagonal elements to take into account.

4.3 Example of transport through a magnetic molecule — impact of coherent dynamics

In this section, an example of transport through a magnetic molecule, taking into consideration the off-diagonal elements of its reduced density matrix, is discussed to illustrate the use of the real-time diagrammatic technique. The molecule under scrutiny is shown in Fig. 4.4 with a spin $S_{N+1} = 1$ in the charged state $N + 1$ and $S_N = 1/2$ in the neutral state N. The neutral molecular states are $|\chi_{-1/2}\rangle = |-1/2\rangle$ and $|\chi_{1/2}\rangle = |1/2\rangle$, whereas the charged molecular states are represented as a linear combination of the S_z projections as follows

$$\begin{aligned} |\chi_0\rangle &= |0\rangle\,, \\ |\chi_+\rangle &= \frac{1}{\sqrt{2}}\,|{-1}\rangle + \frac{1}{\sqrt{2}}\,|1\rangle\,, \\ |\chi_-\rangle &= \frac{1}{\sqrt{2}}\,|{-1}\rangle - \frac{1}{\sqrt{2}}\,|1\rangle\,. \end{aligned} \tag{4.6}$$

As already explained, for the neutral state with spin $S_N = 1/2$, there is no mixing between the spin projections along the z-direction since the transverse magnetic anisotropy only mixes every other state. As a result, the coherent superpositions between the neutral molecular states are completely decoupled form the diagonal occupations and, hence, they play no role in the first-order transport discussed here. By contrast, coherent superpositions between the lowest two energy states in the charged states, namely $|\chi_+\rangle$ and $|\chi_-\rangle$, should be taken into consideration provided that the energy difference $\Delta_0 \lesssim \Gamma$. Consequently, the reduced density matrix of the molecule reads as

---

[5] This includes all off-diagonal elements $\mathcal{P}^{\chi_1}_{\chi_2}$, where the molecular states $|\chi_1\rangle$ and $|\chi_2\rangle$ do not belong to the same charge states.

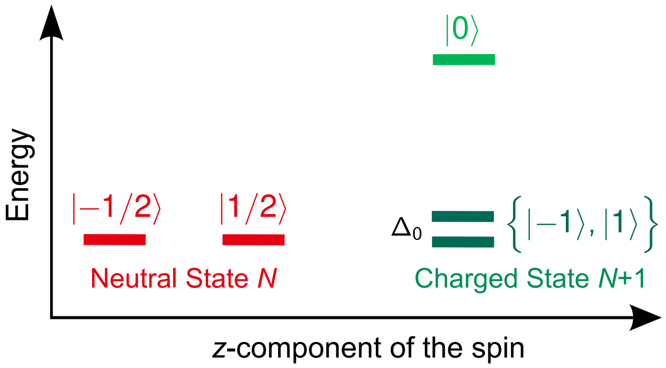

Figure 4.4: Energy spectrum for a magnetic molecule in the neutral and charged states. A molecule with spin $S_N = 1/2$ in the neutral state and $S_{N+1} = 1$ in the charged state is considered. The lowest two energy states, $|\chi_+\rangle$ and $|\chi_-\rangle$, in the charged molecule belong to the same set of S_z spin projections. As a result, transitions between the coherent superpositions of these two states and their diagonal elements are allowed. Thus, the off-diagonal elements $\mathcal{P}_{\chi_-}^{\chi_+}$ and $\mathcal{P}_{\chi_+}^{\chi_-}$ can affect the transport properties. By contrast, the neutral molecular states consist of pure S_z spin projections and, hence, there is coupling between the diagonal and off-diagonal elements of the reduced density matrix.

$$\rho^{\text{red}} = \begin{pmatrix} \mathcal{P}_{\chi_{-1/2}} & 0 & 0 & 0 & 0 \\ 0 & \mathcal{P}_{\chi_{1/2}} & 0 & 0 & 0 \\ 0 & 0 & \mathcal{P}_{\chi_-} & 0 & \mathcal{P}_{\chi_-}^{\chi_+} \\ 0 & 0 & 0 & \mathcal{P}_{\chi_0} & 0 \\ 0 & 0 & \mathcal{P}_{\chi_+}^{\chi_-} & 0 & \mathcal{P}_{\chi_+} \end{pmatrix}, \tag{4.7}$$

where the diagonal elements represent the probabilities of the five molecular states schematically depicted in Fig. 4.4. Moreover, only two off-diagonal elements, $\mathcal{P}_{\chi_-}^{\chi_+}$ and $\mathcal{P}_{\chi_+}^{\chi_-}$, are included in order to account for the coherent superpositions between the two states $|\chi_+\rangle$ and $|\chi_-\rangle$.

Using the formalism explained in Sec. 4.1, the density matrix elements and the tunneling current are calculated through the molecule whose energy spectrum is depicted in Fig. 4.4. Interestingly, *for a molecule inserted between non-polarized electrodes, we found out that the off-diagonal elements are vanishing in the steady state and that the real-time diagrammatic technique collapses into calculating the diagonal probabilities* leading to exactly the same tunneling current as that obtained with Fermi golden rule. In order to understand the reason why coherences vanish, in the next section the master equation will be reformulated in terms of *Bloch-like* equations. This proves useful in tracing the time evolution of coherent superpositions and the conditions under which they play no role in transport. Above all, it should be emphasized that although we discuss a molecule with a specific spin, this conclusion and the explanation that follows hold also for other spin values. However, it is instructive to consider the molecule in Fig. 4.4 for the sake of conceptual simplicity.

4.3.1 Time evolution of coherences using Bloch-like equations

In order to gain a more intuitive understanding of the coherent superpositions between the molecular states introduced in the previous example, here we express the master equation for the elements of the reduced density matrix of the molecule in the form of Bloch equations. For the lowest two energy states of the charged molecule, namely $|\chi_+\rangle$ and $|\chi_-\rangle$, and their coherent superpositions, we define a pseudospin vector $\boldsymbol{\mathcal{S}}$

$$\boldsymbol{\mathcal{S}} = \begin{pmatrix} S_x \\ S_y \\ S_{z,\mathrm{g}} \end{pmatrix} = \frac{1}{2} \begin{pmatrix} \mathcal{P}_{\chi_+}^{\chi_-} + \mathcal{P}_{\chi_-}^{\chi_+} \\ i\big(\mathcal{P}_{\chi_+}^{\chi_-} - \mathcal{P}_{\chi_-}^{\chi_+}\big) \\ \mathcal{P}_{\chi_+} - \mathcal{P}_{\chi_-} \end{pmatrix} . \tag{4.8}$$

Similarly for the neutral state N, we introduce $S_{z,N} = \big(\mathcal{P}_{\chi_{1/2}} - \mathcal{P}_{\chi_{-1/2}}\big)/2$. In addition, we define the probability to find the molecule in the neutral state as $\mathcal{P}_N = \mathcal{P}_{\chi_{1/2}} + \mathcal{P}_{\chi_{-1/2}}$. Likewise, the probability to find the molecule in the charged *ground* states $|\chi_+\rangle$ and $|\chi_-\rangle$ reads $\mathcal{P}_\mathrm{g} = \mathcal{P}_{\chi_+} + \mathcal{P}_{\chi_-}$. As for the charged molecular state $|\chi_0\rangle$, we note that its time evolution is not relevant for investigating the coherent superpositions between the two states $|\chi_+\rangle$ and $|\chi_-\rangle$ since the self-energies between the diagonal element $\mathcal{P}_{\chi_0}$ and the off-diagonal elements $\mathcal{P}_{\chi_-}^{\chi_+}$ and $\mathcal{P}_{\chi_+}^{\chi_-}$ vanish because they belong to a different set of S_z projections (*cf.* Fig. 4.4). However, the state $|\chi_0\rangle$ still appears in the transition rates with the neutral molecular states $|\chi_{1/2}\rangle$ and $|\chi_{-1/2}\rangle$.

Our aim now is to write the master equation in a Bloch-like form to track the various sources and relaxation rates of the coherent superpositions embedded in the pseudospin $\boldsymbol{\mathcal{S}}$. Accordingly, the generalized master equation can be divided into two parts; the first illustrating the time evolution of the occupation probabilities, whereas the other one the time evolution of the pseudospin. Employing the exact master equation, given in Eq. (4.3), the time evolution of the pseudospin $\boldsymbol{\mathcal{S}}$ can be written as

$$\frac{d}{dt}\boldsymbol{\mathcal{S}} = -\begin{pmatrix} \dfrac{1}{\tau_{xy}} S_x \\ \dfrac{1}{\tau_{xy}} S_y \\ \dfrac{1}{\tau_{z,\mathrm{g}}} S_{z,\mathrm{g}} \end{pmatrix} + \frac{1}{2}\begin{pmatrix} \Sigma^+_{\mathrm{coh},N} \\ 0 \\ \Delta^+_{\mathrm{g},N} \end{pmatrix} \mathcal{P}_N + \frac{1}{2}\begin{pmatrix} \Sigma^+_{\mathrm{coh,g}} \\ 0 \\ \Delta_\mathrm{g} \end{pmatrix} \mathcal{P}_\mathrm{g} + \begin{pmatrix} \Sigma^-_{\mathrm{coh},N} \\ 0 \\ \Delta^-_{\mathrm{g},N} \end{pmatrix} S_{z,N} + \boldsymbol{\mathcal{S}} \times \boldsymbol{\mathcal{B}}, \tag{4.9}$$

where the first term represents the relaxation of the x, y and z-components of the pseudospin with the time constants $\tau_{xy} = -2/\big(\Sigma_{\chi_+\chi_+}^{\chi_-\chi_-} + \Sigma_{\chi_-\chi_-}^{\chi_+\chi_+}\big)$ and $\tau_{z,\mathrm{g}} = -2/\big(\Sigma_{\chi_+\chi_+} + \Sigma_{\chi_-\chi_-}\big)$. The three terms involving $\mathcal{P}_N$, $\mathcal{P}_\mathrm{g}$ and $S_{z,N}$ act as sources that can give rise to the pseudospin where $\Sigma^\pm$ and $\Delta^\pm$ are composite self-energies arising from the addition and subtraction of the individual master equations of the elements of the reduced density matrix of the molecule. The expressions of these composite self-energies are given in App. B.3. The final term in Eq. (4.9) signifies the rotation of the pseudospin around an effective magnetic field $\boldsymbol{\mathcal{B}}$ and it takes the following form

$$\boldsymbol{\mathcal{B}} = \begin{pmatrix} B_x \\ B_y \\ B_z \end{pmatrix} = \begin{pmatrix} i\Delta_{\mathrm{g,coh}} \\ 0 \\ i(\varepsilon_+ - \varepsilon_-) + i\Delta_{\mathrm{coh}} \end{pmatrix} . \tag{4.10}$$

Similarly, the time evolution of the pseudospin $S_{z,N}$ reads as

$$\frac{d}{dt} S_{z,N} = -\frac{1}{\tau_{z,N}} S_{z,N} + \frac{\Delta_N}{2}\mathcal{P}_N + \Delta^+_{N,\mathrm{coh}} S_x + \frac{\Delta^+_{N,\mathrm{g}}}{2}\mathcal{P}_\mathrm{g} + \Delta^-_{N,\mathrm{g}} S_{z,\mathrm{g}} + \Sigma^-_{N,\chi_0}\mathcal{P}_{\chi_0}, \tag{4.11}$$

where the relaxation time constant is given by $\tau_{z,N} = -2/\big(\Sigma_{\chi_{1/2}\chi_{1/2}} + \Sigma_{\chi_{-1/2}\chi_{-1/2}}\big)$. Finally, the occupation probabilities of the neutral state and the charged ground states can be written as

$$\begin{aligned} \frac{d}{dt}\begin{pmatrix} \mathcal{P}_N \\ \mathcal{P}_{\mathrm{g}} \end{pmatrix} &= 2\begin{pmatrix} \Sigma^{+}_{N,\mathrm{coh}} & 0 & \Sigma^{-}_{N,\mathrm{g}} \\ \Sigma^{+}_{\mathrm{g},\mathrm{coh}} & 0 & \Delta_{\mathrm{g}} \end{pmatrix}\begin{pmatrix} S_x \\ S_y \\ S_{z,\mathrm{g}} \end{pmatrix} + 2\begin{pmatrix} \Delta_N \\ \Sigma^{-}_{\mathrm{g},N} \end{pmatrix} S_{z,N} \\ &+ \begin{pmatrix} \dfrac{-1}{\tau_{z,N}} & \Sigma^{+}_{N,\mathrm{g}} \\ \Sigma^{+}_{\mathrm{g},N} & \dfrac{-1}{\tau_{z,g}} \end{pmatrix}\begin{pmatrix} \mathcal{P}_N \\ \mathcal{P}_{\mathrm{g}} \end{pmatrix} + 2\begin{pmatrix} \Sigma^{+}_{N,\chi_0} \\ 0 \end{pmatrix}\mathcal{P}_{\chi_0}. \end{aligned} \tag{4.12}$$

So far, Eq.(4.9), (4.11) and (4.12) have been written in the most general form, that is, without making use of any symmetries between the molecular states. However, in order to make progress with these cumbersome expressions, we analyze the case where a molecule is inserted between nonmagnetic electrodes.

As discussed in Sec. 2.4.4, the density of states of spin-up and spin-down electrons near the Fermi level are identical for nonmagnetic electrodes, i.e., spin polarization $P = 0$. Accordingly, transitions that correspond to the tunneling of up and down electrons occur with equal weights (since $\Gamma_\uparrow = \Gamma_\downarrow$). As a result, transport through the molecule can be thought of as two identical channels of spin-up and spin-down electrons. On these grounds, for the molecule under consideration, the transition rates between the charged molecular state $|\chi_+\rangle$ and the two neutral states $|\chi_{1/2}\rangle$ and $|\chi_{-1/2}\rangle$ are equal, i.e., $\Sigma_{\chi_+\chi_{1/2}} = \Sigma_{\chi_+\chi_{-1/2}}$ and $\Sigma_{\chi_{1/2}\chi_+} = \Sigma_{\chi_{-1/2}\chi_+}$. Similarly, for the state $|\chi_-\rangle$, $\Sigma_{\chi_-\chi_{1/2}} = \Sigma_{\chi_-\chi_{-1/2}}$ and $\Sigma_{\chi_{1/2}\chi_-} = \Sigma_{\chi_{-1/2}\chi_-}$. Moreover, the transitions between the off-diagonal elements $\mathcal{P}^{\chi_-}_{\chi_+}$ and $\mathcal{P}^{\chi_+}_{\chi_-}$ and the two states $|\chi_{1/2}\rangle$ and $|\chi_{-1/2}\rangle$ are also symmetric. For instance, the self-energy $\Sigma^{\chi_+\chi_{1/2}}_{\chi_-\chi_{1/2}} = -\Sigma^{\chi_+\chi_{-1/2}}_{\chi_-\chi_{-1/2}}$. Employing these symmetries, the time evolution of the pseudospin $\boldsymbol{\mathcal{S}}$ can be rewritten as

$$\frac{d}{dt}\boldsymbol{\mathcal{S}} = -\begin{pmatrix} \dfrac{1}{\tau_{xy}} S_x \\ \dfrac{1}{\tau_{xy}} S_y \\ \dfrac{1}{\tau_{z,\mathrm{g}}} S_{z,\mathrm{g}} \end{pmatrix} + \begin{pmatrix} \Sigma^{-}_{\mathrm{coh},N} \\ 0 \\ 0 \end{pmatrix} S_{z,N} + \begin{pmatrix} S_x \\ S_y \\ S_{z,\mathrm{g}} \end{pmatrix} \times \begin{pmatrix} 0 \\ 0 \\ B_z \end{pmatrix}, \tag{4.13}$$

where $B_z = i(\varepsilon_+ - \varepsilon_-)$. Likewise, the evolution of the pseudospin $S_{z,N}$ reads

$$\frac{d}{dt} S_{z,N} = -\frac{1}{\tau_{z,N}} S_{z,N}. \tag{4.14}$$

Equation (4.14) indicates that the pseudospin for the neutral state $S_{z,N}$ is completely decoupled from all possible sources, yet it decays with a rate $1/\tau_{z,N}$. Therefore, in the stationary state, $S_{z,N}$ equals zero. That is to say, the probabilities of the states $|\chi_{1/2}\rangle$ and $|\chi_{-1/2}\rangle$ are equal, as calculated before in Sec. 2.4.4 in the case of nonmagnetic electrodes. Furthermore, Eq. (4.13) implies that there are no source terms for the z-component of the charged state pseudospin $S_{z,\mathrm{g}}$, in addition, it couples neither to S_x nor to S_y. Consequently, in the steady state $S_{z,\mathrm{g}}$ decays to zero, i.e., $\mathcal{P}_{\chi_+} = \mathcal{P}_{\chi_-}$, which is justified by the fact that the energy difference between the two states $|\chi_+\rangle$ and $|\chi_-\rangle$ is negligibly small in comparison to the tunnel-coupling strength Γ and, in turn, the thermal energy $k_{\mathrm{B}}T$.[6] Similarly, we can infer that due to the vanishing sources, the x and y-components of the pseudospin also converge to zero in the stationary state. That is to say, the off-diagonal elements of the reduced density matrix of the molecule, given in Eq. (4.7), vanish in the steady state.

Interestingly, from Eq. (4.13) and (4.14) it is clear that the coherences would not vanish if we could force the system to discriminate between the states $|\chi_{1/2}\rangle$ and $|\chi_{-1/2}\rangle$, which, in practice, means that the probabilities $\mathcal{P}_{\chi_{1/2}}$ and $\mathcal{P}_{\chi_{-1/2}}$ would be unequal in the steady state. Based on the discussion of spin-polarized transport in Sec. 2.4.4, we know that the symmetry introduced by the states $|\chi_{1/2}\rangle$ and $|\chi_{-1/2}\rangle$ can be broken by inserting the molecule between two *ferromagnetic* electrodes in the antiparallel magnetic configuration [*cf.* Fig. 2.9(b)]. In that case, the neutral state pseudospin $S_{z,N}$ does not vanish in the steady state (*cf.* Fig. 2.12) which, in turn, can give rise to the x and y-components of the pseudospin $\boldsymbol{\mathcal{S}}$. Consequently, *in the case of ferromagnetic electrodes, coherences do not necessarily vanish.* However, we should emphasize that the results presented in Sec. 2.4.4 in the case of ferromagnetic electrodes are accurate since the tunnel-coupling strength Γ was chosen to be smaller than the energy difference between the two molecular states $|\chi_+\rangle$ and $|\chi_-\rangle$. Thus, it is legitimate to neglect the coherent superpositions without casting any doubts on the obtained results.

To conclude this chapter, we stress that in the absence of the transverse magnetic anisotropy, the dynamics of coherent superpositions is completely decoupled from the diagonal elements owning to the conservation of spin momentum. Thus, coherences do not influence first-order transport. By contrast, the presence of the transverse component of magnetic anisotropy mixes the pure S_z states, which allows for transitions between the diagonal and off-diagonal elements of the reduced density matrix, that is, coherences can impact the transport properties. However, using Bloch-like equations to study the time evolution of the elements of the reduced density matrix, it was shown that for a magnetic molecule embedded between two nonmagnetic electrodes ($P = 0$), coherent superpositions between the molecular states vanish in the steady state. Consequently, *calculating the diagonal elements of the reduced density matrix, using Fermi golden rule, is sufficient to study first-order transport through a magnetic molecule.* On the contrary, the use of *ferromagnetic* electrodes can give rise to non-vanishing coherences in the steady state, provided that the energy difference between the considered states is much smaller than the tunnel-coupling strength Γ, i.e., $\Delta\varepsilon \lesssim \Gamma$, or otherwise coherences are suppressed owning to the energy difference as seen from Eq. (4.4).

---

[6] This is essentially the reason why the transition rates in Eq. (4.3) are evaluated on the assumption that the two states $|\chi_+\rangle$ and $|\chi_-\rangle$ are degenerate, that is $\varepsilon_- = \varepsilon_+$.

5

Conclusion

5.1 Summary

In this thesis, a theoretical model for transport through a single magnetic molecule in the weak coupling regime has been presented. In particular, the subject of analysis is the effect of the interplay between charge, spin and molecular vibrations on the magnetic properties of the molecule and the resulting transport characteristics.

In the opening chapter (Chap. 1), the scientific context of the thesis at hand was motivated. This included a description of the present interest in single-molecule devices along with the importance of transport studies as a spectroscopic tool to examine the properties of individual molecules. In addition, the most commonly employed techniques for fabricating these nanoscopic devices were summarized. Next, the properties of bare magnetic molecules were discussed with the main focus on two degrees of freedom, magnetic and vibrational excitations. Finally, we highlighted recent experimental studies that indicate the significance of molecular vibrations on transport properties of single molecules, in general, and magnetic ones, in particular.

Chapter 2 introduced a theoretical framework for transport through a magnetic molecule inserted in a three-terminal junction. Using Fermi golden rule and classical rate equations, an expression for the transition rate between molecular states was obtained and used to calculate the charge current through single magnetic molecules with uniaxial and transverse magnetic anisotropy. The analysis was taken one step further by examining two additional complexities arising from the presence of electrodes, specifically *asymmetric coupling* and the use of *ferromagnetic electrodes*. First, it was shown that asymmetric coupling modifies the charging and discharging rates of the molecule and, hence, it changes the occupations of molecular states. In practice, this can be a valuable experimental tool for magnifying magnetic transitions that occur at high bias voltages. As for the use of ferromagnetic electrodes, this proves useful to discriminate between the spin-up and spin-down electronic channels, which, in turn, can result in the amplification of certain magnetic transitions. Finally, the *charge-vibron coupling* was incorporated in the transport model, bringing about an additional term in the transition rates, namely the *Franck-Condon factors*. These factors are the main consequence of the coupling between the charge and molecular vibrations and can have drastic effects on transport properties, most notably the Franck-Condon blockade at low bias voltage.

Having laid the theoretical foundation of the present thesis, its main contribution, namely the effect of the *spin-vibron coupling*, was investigated in Chap. 3 in two steps. First, we studied a model for a molecule with uniaxial magnetic anisotropy only. Analogously to the charge-vibron coupling, the interaction between vibrations and the uniaxial component of the spin leads to off-diagonal terms in the molecular Hamiltonian. Thus, in order to diagonalize this Hamiltonian, a canonical transformation was derived, which *eliminates the spin-vibron coupling at the expense of modification of the magnetic anisotropy* of the molecule. Depending on the molecule under consideration and the activated vibrational excitations, the impact of this anisotropy renormalization varies from simply shifting the bias voltage required for magnetic transitions to complete transport blockade. Second, the model was extended to account for molecules with both uniaxial and transverse magnetic anisotropy. It was illustrated that, *owning to the non-vanishing commutators, there is no exact solution for such a model except for two special cases*, either by imposing a restriction on the anisotropy constants of the molecule and the spin-vibron coupling strength or if the total spin of the molecule in both charge states is less than or equal to one. Based on the latter case, it was demonstrated that the spin-vibron coupling also modulates the transverse magnetic anisotropy and can even suppress it.

Chapter 4 was devoted to address the fundamental question whether the formalism of Fermi golden rule with classical rate equations is sufficient for a correct treatment of first-order transport through a single magnetic molecule. For this purpose, the real-time diagrammatic technique was employed to study the effect of coherent superpositions between molecular states on transport properties. For molecules with only *uniaxial* magnetic anisotropy, the molecular states consist of pure S_z spin projections and, hence, the dynamics of coherences and the diagonal elements of the reduced density matrix decouples owning to the conservation of spin. By contrast, in the presence of *transverse* magnetic anisotropy, the molecular states are composed of an admixture of spin projections along the z-axis. Thus, *the time evolution of coherent superpositions between these mixed molecular is expected to be non-trivial.* Nevertheless, by expressing the coherences and occupations in the form of a pseudospin and tracking its time evolution with the help of Block-like equations, it was proved that *coherences in a magnetic molecule embedded between two nonmagnetic electrodes vanish in the stationary state.* Consequently, accounting for the diagonal elements of the reduced density matrix using Fermi golden rule is still appropriate for capturing the quantum mechanical picture. However, for the case of *ferromagnetic* electrodes in the antiparallel magnetic configuration, the effect of coherences does not vanish in the stationary state and, hence, they can impact the transport properties.

5.2 Outlook

Based on the work conducted in the present thesis, there are two potential research directions, which can be summarized as follows:

- As established in Chap. 3, for the interaction between spin and molecular vibrations along both the transverse and uniaxial directions, the molecular Hamiltonian cannot be exactly diagonalized for molecules with a spin greater than one. Accordingly, the goal here would be to find an approximate solution for higher spin values.
- In Chap. 4, it was shown that coherent superpositions vanish for a magnetic molecule embedded between *nonmagnetic* electrodes. However, for spin-valve structures where the ferromagnetic electrodes possess antiparallel magnetization, coherences are non-vanishing. Consequently, it is of particular relevance in this case to investigate the effect of coherences on transport observables, namely current and differential conductance and, in turn, compare these findings with corresponding ones that are obtained by accounting for the diagonal elements of the reduced density matrix using Fermi golden formalism.

Bibliography

[1] Y. Taur, D. A. Buchanan, W. Chen, D. J. Frank, K. E. Ismail, L. O. Shih-Hsien, G. A. Sai-Halasz, R. G. Viswanathan, H. J. C. Wann, S. J. Wind, and H. S. Wong, “CMOS scaling into the nanometer regime”, Proc. IEEE **85**, 486 (1997).

[2] D. J. Frank, R. H. Dennard, E. Nowak, P. M. Solomon, Y. Taur, and H. S. P. Wong, “Device scaling limits of Si MOSFETs and their application dependencies”, Proc. IEEE **89**, 259 (2001).

[3] J. R. Heath, and M. A. Ratner, “Molecular electronics”, Phys. Today **56**, 43 (2003).

[4] W. Lu, and C. M. Lieber, “Nanoelectronics from the bottom up.”, Nat. Mater. **6**, 841 (2007).

[5] N. Weibel, S. Grunder, and M. Mayor, “Functional molecules in electronic circuits.”, Org. Biomol. Chem. **5**, 2343 (2007).

[6] V. Balzani, A. Credi, and M. Venturi, *Molecular devices and machines: a journey into the nano world* (Wiley-VCH Verlag GmbH, 2004).

[7] H. Song, M. A. Reed, and T. Lee, “Single molecule electronic devices”, Adv. Mater. **23**, 1583 (2011).

[8] S. Y. Quek, M. Kamenetska, M. L. Steigerwald, H. J. Choi, S. G. Louie, M. S. Hybertsen, J. B. Neaton, and L. Venkataraman, “Mechanically controlled binary conductance switching of a single-molecule junction.”, Nat. Nanotech. **4**, 230 (2009).

[9] S. Jan van der Molen, and P. Liljeroth, “Charge transport through molecular switches”, J. Phys. Condens. Matter **22**, 133001 (2010).

[10] A. S. Blum, J. G. Kushmerick, D. P. Long, C. H. Patterson, J. C. Yang, J. C. Henderson, Y. Yao, J. M. Tour, R. Shashidhar, and B. R. Ratna, “Molecularly inherent voltage-controlled conductance switching.”, Nat. Mater. **4**, 167 (2005).

[11] B. Y. Choi, S. J. Kahng, S. Kim, H. Kim, H. Kim, Y. J. Song, J. Ihm, and Y. Kuk, “Conformational molecular switch of the azobenzene molecule: A scanning tunneling microscopy study”, Phys. Rev. Lett. **96**, 156106 (2006).

[12] E. Lörtscher, J. W. Ciszek, J. Tour, and H. Riel, “Reversible and controllable switching of a single-molecule junction”, Small **2**, 973 (2006).

[13] H. Park, J. Park, A. K. L. Lim, E. H. Anderson, A. P. Alivisatos, and P. L. McEuen, "Nanomechanical oscillations in a single C_{60} transistor", Nature **407**, 57 (2000).

[14] J. Park, A. N. Pasupathy, J. I. Goldsmith, C. Chang, Y. Yaish, J. R. Petta, M. Rinkoski, J. P. Sethna, H. D. Abruña, P. L. McEuen, and D. C. Ralph, "Coulomb blockade and the Kondo effect in single-atom transistors.", Nature **417**, 722 (2002).

[15] S. Kubatkin, A. Danilov, M. Hjort, J. Cornil, J. Brédas, N. Stuhr-Hansen, P. Hedegård, and T. Bjørnholm, "Single-electron transistor of a single organic molecule with access to several redox states.", Nature **425**, 698 (2003).

[16] J. E. Green, J. W. Choi, A. Boukai, Y. Bunimovich, E. Johnston-Halperin, E. DeIonno, Y. Luo, B. A. Sheriff, K. Xu, Y. S. Shin, H. Tseng, J. F. Stoddart, and J. R. Heath, "A 160-kilobit molecular electronic memory patterned at 10^{11} bits per square centimetre.", Nature **445**, 414 (2007).

[17] J. Lee, H. Chang, S. Kim, G. S. Bang, and H. Lee, "Molecular monolayer nonvolatile memory with tunable molecules", Angew. Chemie - Int. Ed. **48**, 8501 (2009).

[18] N. J. Tao, "Electron transport in molecular junctions", Nat. Nanotech. **1**, 173 (2006).

[19] S. E. Kubatkin, A. Danilov, A. L. Bogdanov, H. Olin, and T. Claeson, "Coulomb blockade effects at room temperature in thin-film nanoconstrictio ns fabricated by a novel technique", Appl. Phys. Lett. **73**, 3604 (1998).

[20] H. Song, Y. Kim, Y. H. Jang, H. Jeong, M. A. Reed, and T. Lee, "Observation of molecular orbital gating.", Nature **462**, 1039 (2009).

[21] J. M. Thijssen, and H. S. J. van der Zant, "Charge transport and single-electron effects in nanoscale systems", Phys. Status Solidi Basic Res. **245**, 1455 (2008).

[22] J. C. Cuevas, and E. Scheer, *Molecular electronics: an introduction to theory and experiment* (Wolrd Scientific, 2010).

[23] D. Gatteschi, R. Sessoli, and J. Villain, *Molecular nanomagnets* (Oxford Univ. Press, 2006).

[24] J. R. Friedman, and M. P. Sarachik, "Single-molecule nanomagnets", Annu. Rev. Condens. Matter Phys. **1**, 109 (2010).

[25] S. Loth, K. von Bergmann, M. Ternes, A. F. Otte, C. P. Lutz, and A. J. Heinrich, "Controlling the state of quantum spins with electric currents", Nat. Phys. **6**, 340 (2010).

[26] C. F. Hirjibehedin, C.-Y. Lin, A. F. Otte, M. Ternes, C. P. Lutz, B. A. Jones, and A. J. Heinrich, "Large magnetic anisotropy of a single atomic spin embedded in a surface molecular network", Science **317**, 1199 (2007).

[27] A. F. Otte, M. Ternes, K. von Bergmann, S. Loth, H. Brune, C. P. Lutz, C. F. Hirjibehedin, and A. J. Heinrich, “The role of magnetic anisotropy in the Kondo effect”, Nat. Phys. **4**, 847 (2008).

[28] M. N. Leuenberger, and D. Loss, “Quantum computing in molecular magnets.”, Nature **410**, 789 (2001).

[29] M. Mannini, F. Pineider, P. Sainctavit, C. Danieli, E. Otero, C. Sciancalepore, A. M. Talarico, M. Arrio, A. Cornia, D. Gatteschi, and R. Sessoli, “Magnetic memory of a single-molecule quantum magnet wired to a gold surface”, Nat. Mater. **8**, 194 (2009).

[30] E. Burzuri, R. Gaudenzi, and H. S. J. van der Zant, “Observing magnetic anisotropy in electronic transport through individual single-molecule magnets”, J. Phys.: Condens. Matter **27**, 113202 (2015).

[31] M. Misiorny, E. Burzurí, R. Gaudenzi, K. Park, M. Leijnse, M. R. Wegewijs, J. Paaske, A. Cornia, and H. S. J. Van Der Zant, “Probing transverse magnetic anisotropy by electronic transport through a single-molecule magnet”, Phys. Rev. B **91**, 035442 (2015).

[32] G. Christou, D. Gatteschi, D. N. Hendrickson, and R. Sessoli, “Single-molecule magnets”, MRS Bulletin **25**, 66 (2000).

[33] J. R. Friedman, M. P. Sarachik, R. Ziolo, and J. Tejada, “Macroscopic measurement of resonant magnetization tunneling in high-spin molecules”, Phys. Rev. Lett. **76**, 3830 (1996).

[34] L. Thomas, F. Lionti, R. Ballou, D. Gatteschi, R. Sessoli, and B. Barbara, “Macroscopic quantum tunnelling of magnetization in a single crystal of nanomagnets”, **383**, 145 (1996).

[35] A. McCaskey, Y. Yamamoto, M. Warnock, E. Burzurí, H. S. J. van der Zant, and K. Park, “Electron-vibron coupling effects on electron transport via a single-molecule magnet”, Phys. Rev. B **91**, 125419 (2015).

[36] A. Benyamini, A. Hamo, S. V. Kusminskiy, F. von Oppen, and S. Ilani, “Real-space tailoring of the electron-phonon coupling in ultraclean nanotube mechanical resonators”, Nat. Phys. **10**, 151 (2014).

[37] R. Leturcq, C. Stampfer, K. Inderbitzin, L. Durrer, C. Hierold, E. Mariani, M. G. Schultz, F. von Oppen, and K. Ensslin, “Franck-Condon blockade in suspended carbon nanotube quantum dots”, Nat. Phys. **5**, 327 (2009).

[38] S. Sapmaz, P. Jarillo-Herrero, Y. M. Blanter, C. Dekker, and H. S. J. van der Zant, “Tunneling in suspended carbon nanotubes assisted by longitudinal phonons”, Phys. Rev. Lett. **96**, 026801 (2006).

[39] B. J. LeRoy, S. G. Lemay, J. Kong, and C. Dekker, “Electrical generation and absorption of phonons in carbon nanotubes”, Nature **432**, 371 (2004).

[40] N. A. Pradhan, N. Liu, and W. Ho, “Vibronic spectroscopy of single C_{60} molecules and monolayers with the STM”, J. Phys. Chem. B **109**, 8513 (2005).

[41] A. N. Pasupathy, J. Park, C. Chang, A. V. Soldatov, S. Lebedkin, R. C. Bialczak, J. E. Grose, L. A. K. Donev, J. P. Sethna, D. C. Ralph, and P. L. McEuen, “Vibration-assisted electron tunneling in C_{140} transistors.”, Nano Lett. **5**, 203 (2005).

[42] B. C. Stipe, M. A. Rezaei, and W. Ho, “Single-molecule vibrational spectroscopy and microscopy”, Science **280**, 1732–1735 (1998).

[43] L. H. Yu, Z. K. Keane, J. W. Ciszek, L. Cheng, M. P. Stewart, J. M. Tour, and D. Natelson, “Inelastic electron tunneling via molecular vibrations in single-molecule transistors”, Phys. Rev. Lett. **93**, 266802 (2004).

[44] N. P. Leon, W. Liang, Q. Gu, and H. Park, “Vibrational excitation in single-molecule transistors: Deviation from the simple Franck-Condon prediction”, Nano Lett. **8**, 2963 (2008).

[45] E. A. Osorio, M. Ruben, J. S. Seldenthuis, J. M. Lehn, and H. S. J. Van Der Zant, “Conductance switching and vibrational fine structure of a [2 × 2] $\mathrm{Co^{II}}_4$ gridlike single molecule measured in a three-terminal device”, Small **6**, 174 (2010).

[46] J. Koch, F. von Oppen, and A. V. Andreev, “Theory of the Franck-Condon blockade regime”, Phys. Rev. B **74**, 205438 (2006).

[47] E. Burzurí, Y. Yamamoto, M. Warnock, X. Zhong, K. Park, A. Cornia, and H. S. J. van der Zant, “Franck-Condon blockade in a single-molecule transistor”, Nano Lett. **14**, 3191 (2014).

[48] M. Ganzhorn, S. Klyatskaya, M. Ruben, and W. Wernsdorfer, “Strong spin-phonon coupling between a single-molecule magnet and a carbon nanotube nanoelectromechanical system.”, Nat. Nanotech. **8**, 165 (2013).

[49] T. T. Heikkila, *The physics of nanoelectronics: transport and fluctuation phenomena at low temperatures, oxford master series in physics, vol. 21* (Oxford Univ. Press, 2013).

[50] T. Ihn, *Semiconductor nanostructures: quantum states and electronic transport* (Oxford Univ. Press, 2010).

[51] A. Messiah, *Quantum mechanics* (Dover Publications, 1999).

[52] D. Griffiths, *Introduction to quantum mechanics* (Pearson Prentice Hall, 2005).

[53] S. Maekawa, S. Valenzuela, E. Saitoh, and T. Kimura, eds., *Spin current*, Vol. 17, Series on Semiconductor Science and Technology (Oxford Univeristy Press, 2012).

[54] E. Y. Tsymbal, and I. Žutić, eds., *Handbook of spin transport and magnetism* (CRC Press, Boca Raton, 2012).

[55] T. Holstein, “Studies of polaron motion: part I. the molecular-crystal model”, Ann. Phys. **8**, 325 (1959).

[56] P. W. Anderson, “Localized magnetic states in metals”, Phys. Rev. **124**, 41 (1961).

[57] G. D. Mahan, *Many-particle physics* (Springer US, 2000).

[58] J. A. Stroscio, and R. J. Celotta, “Controlling the dynamics of a single atom in lateral atom manipulation”, Science **306**, 242–247 (2004).

[59] D. A. Ruiz–Tijerina, P. S. Cornaglia, C. A. Balseiro, and S. E. Ulloa, “Dynamical magnetic anisotropy and quantum phase transitions in a vibrating spin-1 molecular junction”, Phys. Rev. B **86**, 035437 (2012).

[60] F. May, M. R. Wegewijs, and W. Hofstetter, “Interaction of spin and vibrations in transport through single-molecule magnets”, Beilstein J. Nanotechnol **2**, 693 (2011).

[61] M. Wagner, *Unitary transformations in solid state physics* (North-Holland, 1986).

[62] E. Garlatti, S. Carretta, P. Santini, G. Amoretti, M. Mariani, A. Lascialfari, S. Sanna, K. Mason, J. Chang, P. Tasker, and E. K. Brechin, “Relaxation dynamics in a Fe_7 nanomagnet”, Phys. Rev. B **87**, 054409 (2013).

[63] A. Bianchi, S. Carretta, P. Santini, G. Amoretti, J. Lago, M. Corti, A. Lascialfari, P. Arosio, G. Timco, and R. E. P. Winpenny, “Phonon-induced relaxation in the $\mathrm{Cr}_7\mathrm{Ni}$ magnetic molecule probed by NMR”, Phys. Rev. B **82**, 134403 (2010).

[64] S. Carretta, P. Santini, G. Amoretti, M. Affronte, A. Candini, A. Ghirri, I. S. Tidmarsh, R. H. Laye, R. Shaw, and E. J. L. McInnes, “High-temperature slow relaxation of the magnetization in Ni_{10} magnetic molecules”, Phys. Rev. Lett. **97**, 207201 (2006).

[65] E. Garlatti, S. Bordignon, S. Carretta, G. Allodi, G. Amoretti, R. De Renzi, A. Lascialfari, Y. Furukawa, G. A. Timco, R. Woolfson, R. E. P. Winpenny, and P. Santini, “Relaxation dynamics in the frustrated Cr_9 antiferromagnetic ring probed by NMR”, Phys. Rev. B **93**, 024424 (2016).

[66] H. Schoeller, and G. Schön, “Mesoscopic quantum transport: resonant tunneling in the presence of a strong coulomb interaction”, Phys. Rev. B **50**, 18436 (1994).

[67] J. König, J. Schmid, H. Schoeller, and G. Schön, “Resonant tunneling through ultrasmall quantum dots: zero-bias anomalies, magnetic-field dependence, and boson-assisted transport”, Phys. Rev. B **54**, 16820 (1996).

[68] J. Konig, “Quantum fluctuations in the single-electron transistor”, PhD thesis (Universität Karlsruhe, 1998).

[69] S. Legel, “Coherences and correlation effects in coupled quantum dot systems”, PhD thesis (Universität Karlsruhe, 2008).

[70] B. Sothmann, and J. König, “Transport through quantum-dot spin valves containing magnetic impurities”, Phys. Rev. B **82**, 245319 (2010).

A

Appendix

A.1 Lang-Firsov transformation

The coupling between charge and molecular vibrations leads to off-diagonal interactions in the molecular Hamiltonian in Eq. (2.35). Consequently, in order to diagonalize the molecular Hamiltonian, one applies the *Lang-Firsov* transformation as indicated in Sec. 2.5.2. In this appendix, we discuss the details of this transformation starting by transforming the operators of the molecule, electrodes and molecular vibrations using the Baker-Hausdorff formula given in Eq. (2.37) [57]. However, before attempting to transform the operators into the new basis, it should be remembered that the Lang-Firsov transformation is described by

$$\hat{\mathcal{H}}' = \mathrm{e}^{\hat{\mathcal{S}}}\hat{\mathcal{H}}\mathrm{e}^{-\hat{\mathcal{S}}} \quad \text{with} \quad \hat{\mathcal{S}} = \sum_i \lambda_i \big(\hat{b}_i^\dagger - \hat{b}_i\big)\hat{n}_d. \tag{A.1}$$

Using the transformation generator $\hat{\mathcal{S}}$ and the Baker-Hausdorff formula, the transformed creation operator of the molecule reads

$$\begin{aligned}
\tilde{\hat{d}}^\dagger_{l\sigma} =& \mathrm{e}^{\hat{\mathcal{S}}}\hat{d}^\dagger_{l\sigma}\mathrm{e}^{-\hat{\mathcal{S}}} \\
&= \sum_{n=0}^{\infty}\frac{1}{n!}\Big[\sum_i \lambda_i\big(\hat{b}_i^\dagger - \hat{b}_i\big)\hat{n}_d,\, \hat{d}^\dagger_{l\sigma}\Big]_n \\
&= \sum_{n=0}^{\infty}\frac{1}{n!}\Big(\sum_i \lambda_i\big(\hat{b}_i^\dagger - \hat{b}_i\big)\Big)^n [\hat{n}_d,\, \hat{d}^\dagger_{l\sigma}]_n \\
&= \mathrm{e}^{\sum_i \lambda_i\left(\hat{b}_i^\dagger - \hat{b}_i\right)}\,\hat{d}^\dagger_{l\sigma} \\
&= \mathrm{e}^{-\sum_i \lambda_i\left(\hat{b}_i - \hat{b}_i^\dagger\right)}\,\hat{d}^\dagger_{l\sigma} \\
&= \hat{X}^\dagger\hat{d}^\dagger_{l\sigma}.
\end{aligned} \tag{A.2}$$

where $\hat{X}^\dagger = \exp\Big[-\sum_i \lambda_i\big(\hat{b}_i - \hat{b}_i^\dagger\big)\Big]$[1]. Similarly, the annihilation operator for the molecule yields

$$\tilde{\hat{d}}_{l\sigma} = \mathrm{e}^{\sum_i \lambda_i\left(\hat{b}_i - \hat{b}_i^\dagger\right)}\,\hat{d}_{l\sigma} = \hat{X}\hat{d}_{l\sigma}. \tag{A.3}$$

As for the number operator of the molecule $\hat{n}_d = \hat{d}^\dagger_{l\sigma}\hat{d}_{l\sigma}$, we note that the commutator $[\hat{n}'_d, \hat{n}_d]$ equals zero. Thus, the number operator remains unchanged upon this transformation. Similarly, the electrode operators do not change due to the vanishing commutators with the transformation generator $\hat{\mathcal{S}}$. Thus, the creation and annihilation electrode operators read

---

[1] Commutators with a subscript refer to nested commutators. For instance, the commutator $[\hat{A}, \hat{B}]_2 = \Big[\hat{A}, [\hat{A}, \hat{B}]\Big]$.

$$\hat{\hat{a}}^{\dagger q}_{k\sigma} = \hat{a}^{\dagger q}_{k\sigma} \quad \text{and} \quad \hat{\hat{a}}^{q}_{k\sigma} = \hat{a}^{q}_{k\sigma}. \tag{A.4}$$

For the vibronic operators, we start by evaluating the commutator

$$[\hat{\mathcal{S}}, \hat{b}^{\dagger}_{i'}] = \big[\sum_i \lambda_i \big(\hat{b}^{\dagger}_i - \hat{b}_i\big)\hat{n}_d,\, \hat{b}^{\dagger}_{i'}\big] = -\lambda_{i'}\hat{n}_d. \tag{A.5}$$

By plugging this commutator into the Hausdorff-Baker formula, the transformed creation operator reads

$$\begin{aligned} \hat{\hat{b}}^{\dagger}_{i'} =& \mathrm{e}^{\hat{\mathcal{S}}}\hat{b}^{\dagger}_{i'}\mathrm{e}^{-\hat{\mathcal{S}}} \\ &= \hat{b}^{\dagger}_{i'} + \Big[\sum_i \lambda_i \big(\hat{b}^{\dagger}_i - \hat{b}_i\Big)\hat{n}_d,\, \hat{b}^{\dagger}_{i'}\big] + \frac{1}{2}\,\Big[\sum_i \lambda_i \big(\hat{b}^{\dagger}_i - \hat{b}_i\big)\hat{n}_d,\, \hat{b}^{\dagger}_{i'}\Big]_2 + \;\ldots\; + \;\ldots \\ &= \hat{b}^{\dagger}_{i'} - \lambda_{i'}\hat{n}_d. \end{aligned} \tag{A.6}$$

In a similar manner, the annihilation operator for molecular vibration can be written as

$$\hat{\hat{b}}_{i'} = \mathrm{e}^{\hat{\mathcal{S}}}\hat{b}_{i'}\mathrm{e}^{-\hat{\mathcal{S}}} = \hat{b}_{i'} - \lambda_{i'}\hat{n}_d. \tag{A.7}$$

In turn, the transformed molecular Hamiltonian can be obtained by substituting the aforementioned operators as follows

$$\begin{aligned} \hat{\mathcal{H}}'_{\mathrm{mol}} &= \mathrm{e}^{\hat{\mathcal{S}}}\hat{\mathcal{H}}_{\mathrm{mol}}\mathrm{e}^{-\hat{\mathcal{S}}} \\ &= \sum_n \hat{\mathcal{H}}_{\mathrm{spin},n} + (\varepsilon - eV_{\mathrm{g}})\,\hat{n}_d + \sum_i \hbar\omega_i \big(\hat{b}^{\dagger}_i - \lambda_i\hat{n}_d\big)\big(\hat{b}_i - \lambda_i\hat{n}_d\big) + \sum_i \lambda_i\hbar\omega_i\big(\hat{b}^{\dagger}_i + \hat{b}_i - 2\lambda_i\hat{n}_d\big)\hat{n}_d \\ &= \sum_n \hat{\mathcal{H}}_{\mathrm{spin},n} + \big(\varepsilon - eV_{\mathrm{g}}\big)\,\hat{n}_d - \sum_i \hbar\omega_i\lambda_i^2\hat{n}_d^2 + \sum_i \hbar\omega_i\hat{b}^{\dagger}_i\hat{b}_i \\ &= \sum_n \hat{\mathcal{H}}_{\mathrm{spin},n} + \big(\varepsilon - eV_{\mathrm{g}}\big)\,\hat{n}_d - \sum_i \hbar\omega_i\lambda_i^2\hat{n}_d(\hat{n}_d - 1) + \sum_i \hbar\omega_i\lambda_i^2\hat{n}_d + \sum_i \hbar\omega_i\hat{b}^{\dagger}_i\hat{b}_i, \end{aligned} \tag{A.8}$$

where the term $\sum_i \hbar\omega_i\lambda_i^2\ \hat{n}_d(\hat{n}_d - 1)$ modifies the Coulomb energy which is assumed to be high and, hence, can be ignored. Thus, the *transformed molecular Hamiltonian*, reads

$$\hat{\mathcal{H}}'_{\mathrm{mol}} = \sum_n \hat{\mathcal{H}}_{\mathrm{spin},n} + \big(\varepsilon - eV_{\mathrm{g}} + \sum_i \hbar\omega_i\lambda_i^2\big)\,\hat{n}_d + \sum_i \hbar\omega_i\hat{b}^{\dagger}_i\hat{b}_i. \tag{A.9}$$

Equation (A.9) tells us that the molecular Hamiltonian is now diagonal with respect to the vibronic, charge and spin operators. Thus, the same S_z basis can be used to describe the molecular states are described in Sec. 2.5.2. In a similar manner, the tunneling Hamiltonian $\hat{\mathcal{H}}_{\mathrm{tun}}$ is transformed into

$$\begin{aligned} \hat{\mathcal{H}}'_{\mathrm{tun}} &= \sum_{qlk\sigma} \Big\{t^q_{l\sigma}\,\hat{\hat{d}}^{\dagger}_{l\sigma}\hat{a}^q_{k\sigma} + t^q_{l\sigma}\,\hat{a}^{\dagger q}_{k\sigma}\hat{\hat{d}}_{l\sigma}\Big\} \\ &= \sum_{qlk\sigma} \Big\{t^q_{l\sigma}\hat{X}^{\dagger}\,\hat{d}^{\dagger}_{l\sigma}\hat{a}^q_{k\sigma} + t^q_{l\sigma}\hat{X}\,\hat{a}^{\dagger q}_{k\sigma}\hat{d}_{l\sigma}\Big\}. \end{aligned} \tag{A.10}$$

From Eq. (A.10), it can be seen that *the charge-vibron coupling is transfered into the tunneling Hamiltonian*, as manifest in the factor $\hat{X}$. The implications of this additional factor in the tunneling Hamiltonian are discussed in Sec. 2.5.2.

A.2 Derivation of a canonical transformation to eliminate spin-vibron coupling

The interaction between molecular vibrations and the *uniaxial* component of the spin, discussed in Sec. 3.1, resulted in off-diagonal terms in the molecular Hamiltonian (3.1). Thus, in order to diagonalize the molecular Hamiltonian, we employed a canonical transformation in the form

$$\hat{\mathcal{H}}'_{\text{mol}} = \hat{U}\ \hat{\mathcal{H}}_{\text{mol}}\ \hat{U}^{-1} = \mathrm{e}^{\hat{\mathcal{S}}}\ \hat{\mathcal{H}}_{\text{mol}}\ \mathrm{e}^{-\hat{\mathcal{S}}}, \tag{A.11}$$

where

$$\hat{\mathcal{S}} = -\sum_i \sum_n \Lambda_n^i \big(\hat{S}_n^z\big)^2 \big(\hat{b}_i - \hat{b}_i^\dagger\big). \tag{A.12}$$

In this appendix, our aim is to explain the methodology used to obtain this transformation kernel. For a molecular Hamiltonian $\hat{\mathcal{H}}_{\text{mol}} = \hat{\mathcal{H}}_0 + \hat{\mathcal{H}}_{\text{sp-vib}}$, a transformation generator $\hat{\mathcal{S}}$ can be obtained by projecting the spin-vibron interaction term $\hat{\mathcal{H}}_{\text{sp-vib}}$ on the eigenstates of equilibrium Hamiltonian $\hat{\mathcal{H}}_0$ as follows [61]

$$\hat{\mathcal{S}} = \sum_{\chi_n \neq \chi'_n} \frac{1}{E^0_{\chi_n} - E^0_{\chi'_n}}\ |\chi_n\rangle \langle\chi_n| \hat{\mathcal{H}}_{\text{sp-vib}} |\chi'_n\rangle \langle\chi'_n|, \tag{A.13}$$

where $E^0_{\chi_n}$ and $E^0_{\chi'_n}$ are the eigenvalues of the equilibrium Hamiltonian $\hat{\mathcal{H}}_0$.

Before attempting to evaluate the matrix element $\langle\chi_n| \hat{\mathcal{H}}_{\text{sp-vib}} |\chi'_n\rangle$, it is instructive to recall that an arbitrary molecular state can be expressed as $|\chi_n\rangle = |S_n, M_n, n_q\rangle$, where S_n is the total spin of the molecule in the charge state n, M_n is the magnetic quantum number and n_q is the number of vibrational energy quanta. For the sake of brevity, in the following derivation we will write the state as $|\chi_n\rangle = |M_n, n_q\rangle$, in addition, we consider only one vibrational mode and, hence, the summation over i is dropped. Moreover, for notational clarity, the transformation generator is derived assuming there is only one charge state for the molecule, that is, the neutral state $n = N$. Thus, the summation over n can also be dropped. Accordingly, the matrix element, given in Eq. (A.13), reads as

$$\begin{aligned}
\langle\chi_N| \hat{\mathcal{H}}_{\text{sp-vib}} |\chi'_N\rangle &= \langle M_N, n_q| \hbar\omega\Lambda_N \big(\hat{S}_N^z\big)^2 \big(\hat{b}^\dagger + \hat{b}\big) |M'_N, n'_q\rangle \\
&= \hbar\omega\Lambda_N \langle n_q| \big(\hat{b}^\dagger + \hat{b}\big) |n'_q\rangle \langle M_N| \big(\hat{S}_N^z\big)^2 |M'_N\rangle \\
&= \hbar\omega\Lambda_N \Big(\sqrt{n'_q + 1}\ \delta_{n'_q+1, n_q} + \sqrt{n'_q}\ \delta_{n'_q-1, n_q}\Big) (M_N)^2 \delta_{M_N, M'_N}
\end{aligned} \tag{A.14}$$

Next, we plug the above matrix element into Eq. (A.13) as follows

$$\begin{aligned}
\hat{\mathcal{S}} &= \sum_{\chi_N \neq \chi'_N} \frac{1}{E^0_{\chi_N} - E^0_{\chi'_N}} \; \left|\chi_N\right\rangle \left\langle\chi_N\right| \hat{\mathcal{H}}_{\text{sp-vib}} \left|\chi'_N\right\rangle \left\langle\chi'_N\right| \\
&= \sum_{n_q, n'_q} \sum_{M_N, M'_N} \frac{\hbar\omega\Lambda_N}{E^0_{\chi_N} - E^0_{\chi'_N}} \left|M_N, n_q\right\rangle \left\langle M'_N, n'_q\right| \times \big(\sqrt{n'_q + 1}\; \delta_{n'_q+1, n_q} + \sqrt{n'_q}\; \delta_{n'_q-1, n_q}\big)(M_N)^2 \delta_{M_N, M'_N} \\
&= \sum_{n_q, n'_q} \sum_{M_N} \frac{\hbar\omega\Lambda_N}{E^0_{\chi_N} - E^0_{\chi'_N}} \left|M_N, n_q\right\rangle \left\langle M_N, n'_q\right| \times \big(\sqrt{n'_q + 1}\; \delta_{n'_q+1, n_q} + \sqrt{n'_q}\; \delta_{n'_q-1, n_q}\big)(M_N)^2 \\
&= \sum_{n'_q} \sum_{M_N} \hbar\omega\Lambda_N (M_N)^2 \left(\sqrt{n'_q + 1}\; \frac{\left|M_N, n'_q + 1\right\rangle \left\langle M_N, n'_q\right|}{E^0_{M_N} + \hbar\omega - E^0_{M_N}} + \sqrt{n'_q}\; \frac{\left|M_N, n'_q - 1\right\rangle \left\langle M_N, n'_q\right|}{E^0_{M_N} - \hbar\omega - E^0_{M_N}} \right) \\
&= \sum_{n'_q} \sum_{M_N} \Lambda_N \big(\hat{S}^z_N\big)^2 \left(\sqrt{n'_q + 1}\; \left|M_N, n'_q + 1\right\rangle \left\langle M_N, n'_q\right| - \sqrt{n'_q}\; \left|M_N, n'_q - 1\right\rangle \left\langle M_N, n'_q\right| \right)
\end{aligned} \tag{A.15}$$

where the energy of the molecular state $E^0_{\chi_N}$ is decomposed into the energy of the spin state $E^0_{M_N}$ and the vibrational energy quanta for the mode under consideration $\hbar\omega$. Using completeness of the $\left|M_N\right\rangle$ basis

$$\begin{aligned}
\hat{\mathcal{S}} &= \sum_{n'_q} \Lambda_N \big(\hat{S}^z_N\big)^2 \Big(\sqrt{n'_q + 1}\; \left|n'_q + 1\right\rangle \left\langle n'_q\right| - \sqrt{n'_q}\; \left|n'_q - 1\right\rangle \left\langle n'_q\right| \Big) \\
&= \sum_{n'_q} \Lambda_N \big(\hat{S}^z_N\big)^2 \Big(\hat{b}^\dagger \left|n'_q\right\rangle \left\langle n'_q\right| - \hat{b} \left|n'_q\right\rangle \left\langle n'_q\right| \Big) \\
&= \Lambda_N \big(\hat{S}^z_N\big)^2 \big(\hat{b}^\dagger - \hat{b}\big)
\end{aligned} \tag{A.16}$$

Now, the resultant formula can be extended to incorporate n charge states, namely the neutral $n = N$ and the charged $n = N + 1$ state, in addition to, the various vibrational modes denoted by the subscript i. Accordingly, Eq. (A.16) can be rewritten in the form

$$\hat{\mathcal{S}} = -\sum_i \sum_n \Lambda^i_n \big(\hat{S}^z_n\big)^2 \big(\hat{b}_i - \hat{b}^\dagger_i\big) \tag{A.17}$$

B

Appendix

B.1 Summary of diagrammatic rules in energy space

B.1.1 Diagrammatic rules for self-energies

Here one finds the energy-space rules used to diagrammatically evaluate the self-energy corresponding to an irreducible diagram of the Keldysh contour [68, 69]. The self-energy Σ can be generically written as

$$\Sigma = \int d\omega \sum_{\sigma} \sum_{q} \langle \chi' | \, B \, | \chi \rangle \, (-1)^{b} \, (-1)^{c} \, \frac{1}{\Delta E + \imath \eta} \, \gamma^{\pm}_{q,\sigma} \tag{B.1}$$

where

- b is the number of *internal* vertices on the *backward* propagator. Internal vertices signify a product of molecule and electrode operators. For instance, for a transition from a neutral molecular state $|\chi_N\rangle$ to a charged one $|\chi_{N+1}\rangle$, an electron is *annihilated* in the electrode and is *created* in the molecule. Whereas, external vertices can refer to individual bosonic or electrode operators.
- c is the number of crossings between tunnel lines
- ΔE is the energy difference between *left* going and *right* going energies, where the tunneling line is assigned an energy ω
- $\gamma^{+}_{q,\sigma}$ is used if the tunneling line is pointing *backward* with respect to the closed time path with $\gamma^{+}_{q,\sigma} = (1/2\pi) \, \Gamma^{\sigma}_{q} f_q(\omega)$
- $\gamma^{-}_{q,\sigma}$ is used if the tunneling line is pointing *forward* with respect to the closed time path with $\gamma^{-}_{q,\sigma} = (1/2\pi) \, \Gamma^{\sigma}_{q}(1 - f_q(\omega))$
- Each vertex gives rise to a matrix element, $\langle \chi' | \, B \, | \chi \rangle$, where $|\chi'\rangle$ is the molecular state *leaving* the vertex, $|\chi\rangle$ is the molecular state *entering* the internal vertex and B is the molecule charge operator at that particular vertex.

B.1.2 Mirror rule

As mentioned in Sec. 4.2, there exist *eight* irreducible diagrams to characterize the sequential transport through the molecule (or, more generically, a quantum dot). For calculating the *diagonal* elements of the reduced density matrix, it is sufficient to evaluate only *four* diagrams. This is due to the fact that each two diagrams are mirror images of each others, which means one diagram equals to negative the complex conjugate of the other. Thus, their summation equals twice the imaginary part of either. Fig. B.1 represents the two mirror images corresponding to a transition

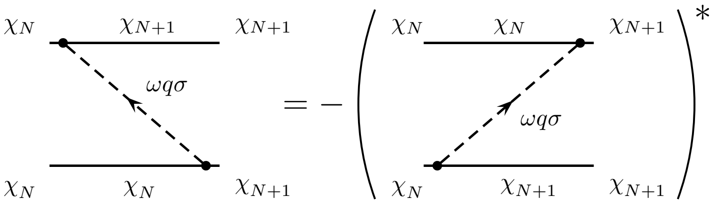

Figure B.1: The mirror rule. Irreducible diagrams for the two possible transitions between the diagonal elements $\mathcal{P}_{\chi_N}$ and $\mathcal{P}_{\chi_{N+1}}$. These two diagrams are mirror images and, hence, the resultant self-energy from their summation $\Sigma_{\chi_{N+1}\chi_N}$ equals to negative twice the imaginary part of the self-energy of either (which can obtained from the rules in App. B.1.1).

from a neutral molecular sate $|\chi_N\rangle$ to a charged molecular state $|\chi_{N+1}\rangle$. The corresponding self-energy $\Sigma_{\chi_N\chi_{N+1}}$ can be obtained by evaluating only one of these two diagrams, taking its imaginary part and then multiplying it by two.

B.1.3 Current self-energies

In order to calculate the *current* self-energies, an additional multiplicative factor is added such that the total current through the molecule reads $I = (I_\mathrm{R} - I_\mathrm{L})/2$. Accordingly, $\pm 1/2$ factors will be multiplied by the original self-energies calculated in App. B.2 to obtain the current self-energies according to the following rules:

- $+1/2$ factor if the *external* vertex lies on the *upper* propagator and the tunneling line goes *out of the left* electrode or if the vertex lies on *lower* propagator and tunneling line goes *into the left* electrode
- $+1/2$ factor if the *external* vertex lies on the *upper* propagator and the tunneling line goes *into the right* electrode or if the vertex lies on the *lower* propagator and the tunneling line goes *out of the right* electrode
- $-1/2$ factor if the *external* vertex lies on the *upper* propagator and the tunneling line goes *into the left* electrode or if the vertex lies on the *lower* propagator and the tunneling line goes *out of the left* electrode
- $-1/2$ factor if the *external* vertex lies on the *upper* propagator and the tunneling line goes *out of the right* electrode or if the vertex lies on the *lower* propagator and the tunneling line goes *into the right* electrode

The effect of this multiplicative factor is twofold. First, it results in vanishing contributions of the circular diagrams to the current (circular diagrams are like the 4 diagrams on the right-hand side of Fig. B.2). Second, the current flowing into the left reservoir, I_L acquires a negative sign such that the total current formula corresponds to $I = \big(I_R - I_L\big)/2$.

B.2 Diagrams and self-energies for first-order transport through a magnetic molecule

In the *first-order tunneling* regime, i.e., sequential tunneling, there exists *eight* irreducible self-energy diagrams for the various tunneling process through the molecule. Figure B.2 shows all the

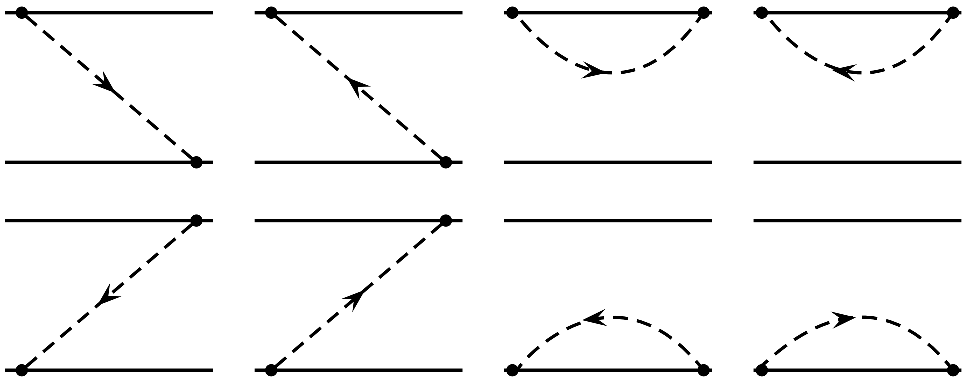

Figure B.2: Irreducible diagrams. Eight irreducible diagrams for first-order transport through a molecule. For calculating only the diagonal elements of the reduced density matrix (probabilities), it is only sufficient to evaluate four diagrams since each two diagrams pair up as mirror images. Thus, their summation equals negative twice the imaginary of either (*cf.* App. B.1.2).

eight diagrams. It should be noted that in the case of transitions between diagonal elements of the density matrix, it is sufficient to evaluate only four diagrams (*cf.* App. B.1.2). The corresponding self-energy expressions are given where each self-energy is the result of summing two diagrams (bottom and top from Fig. B.2). In these expressions, the constants $C_{M_N,\sigma,M_{N+1}}$ are the Clebsch Gordon Coefficients defined as $C_{M_N,\sigma,M_{N+1}} \equiv \langle S_N, M_N; 1/2, \sigma | S_{N+1}, M_{N+1} \rangle$, Ψ refers to the digamma function, β is the thermodynamic beta defined as $1/(k_\mathrm{B}T)$ and E_c is a cut-off energy arising from the Fermi-Dirac integral.

$$\begin{aligned}\Sigma^{\chi_{N+1}\chi_N}_{\chi'_{N+1}\chi'_N} = &-\sum_{q\sigma}\frac{\Gamma^q_\sigma}{2\pi}\Big(\sum_{M_N,M_{N+1}} a_{M_N} b^*_{M_{N+1}} C_{M_N,\sigma,M_{N+1}}\Big)\Big(\sum_{M'_N,M'_{N+1}} a^*_{M'_N} b_{M'_{N+1}} C_{M'_N,\sigma,M'_{N+1}}\Big)\\ &\times\Bigg[\Re\Bigg\{\psi\Bigg(\frac{1}{2}+\frac{\imath\beta\big(\epsilon_{\chi_{N+1}}-\epsilon_{\chi'_N}-\mu_q\big)}{2\pi}\Bigg)\Bigg\}-\psi\Big(\frac{1}{2}+\frac{\beta E_c}{2\pi}\Big)-\imath\pi f^q\big(\epsilon_{\chi_{N+1}}-\epsilon_{\chi'_N}\big)\Bigg]\\ &-\sum_{q\sigma}\frac{\Gamma^q_\sigma}{2\pi}\Big(\sum_{M_N,M_{N+1}} a_{M_N} b^*_{M_{N+1}} C_{M_N,\sigma,M_{N+1}}\Big)\Big(\sum_{M'_N,M'_{N+1}} a^*_{M'_N} b_{M'_{N+1}} C_{M'_N,\sigma,M'_{N+1}}\Big)\\ &\times\Bigg[-\Re\Bigg\{\psi\Bigg(\frac{1}{2}+\frac{\imath\beta\big(\epsilon_{\chi'_{N+1}}-\epsilon_{\chi_N}-\mu_q\big)}{2\pi}\Bigg)\Bigg\}+\psi\Big(\frac{1}{2}+\frac{\beta E_c}{2\pi}\Big)-\imath\pi f^q\big(\epsilon_{\chi'_{N+1}}-\epsilon_{\chi_N}\big)\Bigg]\end{aligned} \tag{B.2}$$

$$\begin{aligned}\Sigma^{\chi_N\chi_{N+1}}_{\chi'_N\chi'_{N+1}} = &-\sum_{q\sigma}\frac{\Gamma^q_\sigma}{2\pi}\Big(\sum_{M_N,M_{N+1}} a^*_{M_N} b_{M_{N+1}} C_{M_N,\sigma,M_{N+1}}\Big)\Big(\sum_{M'_N,M'_{N+1}} a_{M'_N} b^*_{M'_{N+1}} C_{M'_N,\sigma,M'_{N+1}}\Big)\\ &\times\Bigg[\Re\Bigg\{\psi\Bigg(\frac{1}{2}+\frac{\imath\beta\Big[-\big(\epsilon_{\chi'_{N+1}}-\epsilon_{\chi_N}\big)-\mu_q\Big]}{2\pi}\Bigg)\Bigg\}-\psi\Big(\frac{1}{2}+\frac{\beta E_c}{2\pi}\Big)-\imath\pi\Big(1-f^q\big(\epsilon_{\chi'_{N+1}}-\epsilon_{\chi_N}\big)\Big)\Bigg]\\ &-\sum_{q\sigma}\frac{\Gamma^q_\sigma}{2\pi}\Big(\sum_{M_N,M_{N+1}} a^*_{M_N} b_{M_{N+1}} C_{M_N,\sigma,M_{N+1}}\Big)\Big(\sum_{M'_N,M'_{N+1}} a_{M'_N} b^*_{M'_{N+1}} C_{M'_N,\sigma,M'_{N+1}}\Big)\\ &\times\Bigg[-\Re\Bigg\{\psi\Bigg(\frac{1}{2}+\frac{\imath\beta\Big[-\big(\epsilon_{\chi_{N+1}}-\epsilon_{\chi'_N}\big)-\mu_q\Big]}{2\pi}\Bigg)\Bigg\}+\psi\Big(\frac{1}{2}+\frac{\beta E_c}{2\pi}\Big)-\imath\pi\Big(1-f^q\big(\epsilon_{\chi_{N+1}}-\epsilon_{\chi'_N}\big)\Big)\Bigg]\end{aligned} \tag{B.3}$$

$$\begin{aligned}\Sigma^{\chi_N^{'}\chi_N}_{\chi_N^{'''}\chi_N^{''}} = {} & \delta_{\chi_N^{''},\chi_N^{'''}} \sum_{\chi_{N+1}} \sum_{q\sigma} \frac{\Gamma^q_\sigma}{2\pi}\Big(\sum_{M_N,M_{N+1}} a_{M_N} b^*_{M_{N+1}} C_{M_N,\sigma,M_{N+1}}\Big)\Big(\sum_{M_N^{'},M_{N+1}} a^*_{M_N^{'}} b_{M_{N+1}} C_{M_N^{'},\sigma,M_{N+1}}\Big) \\ & \times \left[\Re\left\{\psi\left(\frac{1}{2} + \frac{\imath\beta\big(\epsilon_{\chi_{N+1}} - \epsilon_{\chi_N^{''}} - \mu_q\big)}{2\pi}\right)\right\} - \psi\Big(\frac{1}{2} + \frac{\beta E_c}{2\pi}\Big) - \imath\pi f^q\big(\epsilon_{\chi_{N+1}} - \epsilon_{\chi_N^{''}}\big)\right] \\ & + \delta_{\chi_N,\chi_N^{'}} \sum_{\chi_{N+1}} \sum_{q\sigma} \frac{\Gamma^q_\sigma}{2\pi}\Big(\sum_{M_N^{'''},M_{N+1}} a_{M_N^{'''}} b^*_{M_{N+1}} C_{M_N^{'''},\sigma,M_{N+1}}\Big)\Big(\sum_{M_N^{''},M_{N+1}} a^*_{M_N^{''}} b_{M_{N+1}} C_{M_N^{''},\sigma,M_{N+1}}\Big) \\ & \times \left[-\Re\left\{\psi\left(\frac{1}{2} + \frac{\imath\beta\big(\epsilon_{\chi_{N+1}} - \epsilon_{\chi_N} - \mu_q\big)}{2\pi}\right)\right\} + \psi\Big(\frac{1}{2} + \frac{\beta E_c}{2\pi}\Big) - \imath\pi f^q\big(\epsilon_{\chi_{N+1}} - \epsilon_{\chi_N}\big)\right]\end{aligned} \tag{B.4}$$

$$\begin{aligned}\Sigma^{\chi_{N+1}^{'}\chi_{N+1}}_{\chi_{N+1}^{'''}\chi_{N+1}^{''}} = {} & \delta_{\chi_{N+1}^{''},\chi_{N+1}^{'''}} \sum_{\chi_N} \sum_{q\sigma} \frac{\Gamma^q_\sigma}{2\pi}\Big(\sum_{M_N,M_{N+1}^{'}} a_{M_N} b^*_{M_{N+1}^{'}} C_{M_N,\sigma,M_{N+1}^{'}}\Big)\Big(\sum_{M_N,M_{N+1}} a^*_{M_N} b_{M_{N+1}} C_{M_N,\sigma,M_{N+1}}\Big) \\ & \times \left[\Re\left\{\psi\left(\frac{1}{2} + \frac{\imath\beta\Big[-\big(\epsilon_{\chi_{N+1}^{''}} - \epsilon_{\chi_N}\big) - \mu_q\Big)\Big]}{2\pi}\right)\right\} - \psi\Big(\frac{1}{2} + \frac{\beta E_c}{2\pi}\Big) - \imath\pi\Big(1 - f^q\big(\epsilon_{\chi_{N+1}^{''}} - \epsilon_{\chi_N}\big)\Big)\right] \\ & + \delta_{\chi_{N+1},\chi_{N+1}^{'}} \sum_{\chi_N} \sum_{q\sigma} \frac{\Gamma^q_\sigma}{2\pi}\Big(\sum_{M_N,M_{N+1}^{'''}} a^*_{M_N} b_{M_{N+1}^{'''}} C_{M_N,\sigma,M_{N+1}^{'''}}\Big)\Big(\sum_{M_N,M_{N+1}^{''}} a_{M_N} b^*_{M_{N+1}^{''}} C_{M_N,\sigma,M_{N+1}^{''}}\Big) \\ & \times \left[-\Re\left\{\psi\left(\frac{1}{2} + \frac{\imath\beta\Big[-\big(\epsilon_{\chi_{N+1}} - \epsilon_{\chi_N}\big) - \mu_q\Big)\Big]}{2\pi}\right)\right\} + \psi\Big(\frac{1}{2} + \frac{\beta E_c}{2\pi}\Big) - \imath\pi\Big(1 - f^q\big(\epsilon_{\chi_{N+1}} - \epsilon_{\chi_N}\big)\Big)\right]\end{aligned} \tag{B.5}$$

B.3 Self-energies expressions used in Sec. 4.3.1

The following are the definitions for the self-energies used in Sec. 4.3.1 for a magnetic molecule with $S_{N+1} = 1$ in the charged state and $S_N = 1/2$ in the neutral state.

$$\Delta_N = \frac{\Sigma_{\chi_{1/2}\chi_{1/2}} - \Sigma_{\chi_{-1/2}\chi_{-1/2}}}{2}. \tag{B.6}$$

$$\Delta_{\mathrm{g}} = \frac{\Sigma_{\chi_+\chi_+} - \Sigma_{\chi_-\chi_-}}{2}. \tag{B.7}$$

$$\Delta_{\mathrm{coh}} = \frac{\Sigma^{\chi_+\chi_+}_{\chi_-\chi_-} - \Sigma^{\chi_-\chi_-}_{\chi_+\chi_+}}{2}. \tag{B.8}$$

$$\Sigma^{\pm}_{\mathrm{coh},N} = \frac{\Big(\Sigma^{\chi_-\chi_{1/2}}_{\chi_+\chi_{1/2}} + \Sigma^{\chi_+\chi_{1/2}}_{\chi_-\chi_{1/2}}\Big) \pm \Big(\Sigma^{\chi_-\chi_{-1/2}}_{\chi_+\chi_{-1/2}} + \Sigma^{\chi_+\chi_{-1/2}}_{\chi_-\chi_{-1/2}}\Big)}{2}. \tag{B.9}$$

$$\Sigma^{\pm}_{\mathrm{coh,g}} = \frac{\Big(\Sigma^{\chi_-\chi_+}_{\chi_+\chi_+} + \Sigma^{\chi_+\chi_+}_{\chi_-\chi_+}\Big) \pm \Big(\Sigma^{\chi_-\chi_-}_{\chi_+\chi_-} + \Sigma^{\chi_+\chi_-}_{\chi_-\chi_-}\Big)}{2}. \tag{B.10}$$

$$\Sigma^{\pm}_{N,\mathrm{g}} = \frac{\Big(\Sigma_{\chi_{1/2}\chi_+} + \Sigma_{\chi_{-1/2}\chi_+}\Big) \pm \Big(\Sigma_{\chi_{1/2}\chi_-} + \Sigma_{\chi_{-1/2}\chi_-}\Big)}{2}. \tag{B.11}$$

$$\Sigma^{\pm}_{N,\mathrm{coh}} = \frac{\left(\Sigma^{\chi_{1/2}\chi_-}_{\chi_{1/2}\chi_+} + \Sigma^{\chi_{-1/2}\chi_-}_{\chi_{-1/2}\chi_+}\right) \pm \left(\Sigma^{\chi_{1/2}\chi_+}_{\chi_{1/2}\chi_-} + \Sigma^{\chi_{-1/2}\chi_+}_{\chi_{-1/2}\chi_-}\right)}{2}. \tag{B.12}$$

$$\Sigma^{\pm}_{N,\chi_0} = \frac{\Sigma_{\chi_{1/2}\chi_0} \pm \Sigma_{\chi_{-1/2}\chi_0}}{2}. \tag{B.13}$$

$$\Sigma^{\pm}_{\mathrm{g},N} = \frac{\left(\Sigma_{\chi_+\chi_{1/2}} + \Sigma_{\chi_-\chi_{1/2}}\right) \pm \left(\Sigma_{\chi_+\chi_{-1/2}} + \Sigma_{\chi_-\chi_{-1/2}}\right)}{2}. \tag{B.14}$$

$$\Sigma^{\pm}_{\mathrm{g,coh}} = \frac{\left(\Sigma^{\chi_+\chi_-}_{\chi_+\chi_+} + \Sigma^{\chi_-\chi_-}_{\chi_-\chi_+}\right) \pm \left(\Sigma^{\chi_+\chi_+}_{\chi_+\chi_-} + \Sigma^{\chi_-\chi_+}_{\chi_-\chi_-}\right)}{2}. \tag{B.15}$$

$$\Delta^{\pm}_{\mathrm{g},N} = \frac{\left(\Sigma_{\chi_+\chi_{1/2}} - \Sigma_{\chi_-\chi_{1/2}}\right) \pm \left(\Sigma_{\chi_+\chi_{-1/2}} - \Sigma_{\chi_-\chi_{-1/2}}\right)}{2} \tag{B.16}$$

$$\Delta^{\pm}_{\mathrm{g,coh}} = \frac{\left(\Sigma^{\chi_+\chi_-}_{\chi_+\chi_+} - \Sigma^{\chi_-\chi_-}_{\chi_-\chi_+}\right) \pm \left(\Sigma^{\chi_+\chi_+}_{\chi_+\chi_-} - \Sigma^{\chi_-\chi_+}_{\chi_-\chi_-}\right)}{2}. \tag{B.17}$$

$$\Delta^{\pm}_{N,\mathrm{g}} = \frac{\left(\Sigma_{\chi_{1/2}\chi_+} - \Sigma_{\chi_{-1/2}\chi_+}\right) \pm \left(\Sigma_{\chi_{1/2}\chi_-} - \Sigma_{\chi_{-1/2}\chi_-}\right)}{2}. \tag{B.18}$$

$$\Delta^{\pm}_{N,\mathrm{coh}} = \frac{\left(\Sigma^{\chi_{1/2}\chi_-}_{\chi_{1/2}\chi_+} - \Sigma^{\chi_{-1/2}\chi_-}_{\chi_{-1/2}\chi_+}\right) \pm \left(\Sigma^{\chi_{1/2}\chi_+}_{\chi_{1/2}\chi_-} - \Sigma^{\chi_{-1/2}\chi_+}_{\chi_{-1/2}\chi_-}\right)}{2}. \tag{B.19}$$

C

Appendix

C.1 Additional results for asymmetric tunnel-coupling

In Sec. 2.4.3, the issue of asymmetric coupling was discussed by analyzing an example in which the coupling to the left electrode is stronger than to the right, i.e., $\Gamma_{\mathrm{L}} > \Gamma_{\mathrm{R}}$. Accordingly, for the molecular junction in Fig. 2.6, the rate of charging the molecule was relatively lower than the rate to discharge it and, hence, the molecule dominantly existed in the neutral state N as indicated by the probability plot in Fig. 2.7.

In this appendix, however, we discuss an opposing scenario where the coupling to the right electrode is stronger than to the left one, i.e., $\Gamma_{\mathrm{L}} < \Gamma_{\mathrm{R}}$. Unlike the aforementioned example, the rate of charging the molecule, here, is high comparable to the discharging one. Thus, the molecule is more likely to be in the charged state $N+1$. This can be seen in Fig. C.1 where the probability of the molecule to exist in the charged state is the dominant one even at high bias voltage at which all transitions are allowed.

In order to gain an insight into the effect of the asymmetric coupling, we plot the total tunneling current through the molecule in Fig. C.2. It can be seen that the magnitude of the first transition between the neutral and charged state is amplified, as indicated by the left-most peak in the top

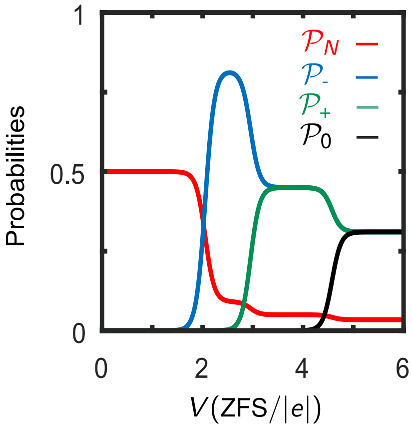

Figure C.1: Probabilities for an asymmetrically coupled molecule. For the calculations performed here, $\Gamma_{\mathrm{R}} = 9\Gamma_{\mathrm{L}}$. The tunnel-coupling strengths are chosen such that the total coupling strength $\Gamma_{\mathrm{L}} + \Gamma_{\mathrm{R}}$ is consistent with the example in Sec. 2.4.2. The probability of the neutral state N is denoted by $\mathcal{P}_N = \mathcal{P}_{1/2} = \mathcal{P}_{-1/2}$. Although the bias voltage V is high enough for all transitions to take place, the molecule prefers to be in the charged state $N+1$. This plot was obtained at a constant gate voltage $V_{\mathrm{g}} = -1$ (ZFS/$|e|$).

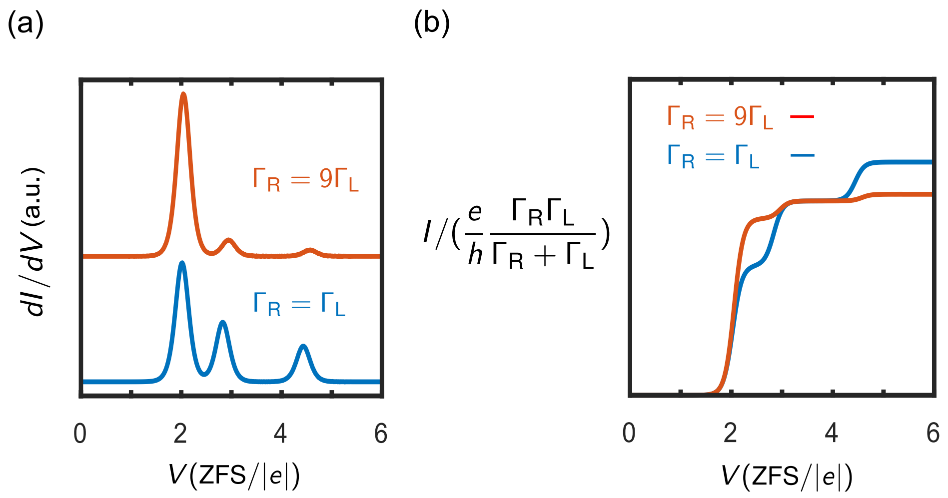

Figure C.2: Differential conductance (a) and current (b) of a molecule in the symmetric and asymmetric coupling cases. The asymmetric coupling magnifies the transition from the neutral molecular states $|\pm 1/2\rangle$ to the charged molecular state $|\chi_-\rangle$ represented by the leftmost peak. Accordingly, the molecule is more likely to exist in the charged state $N+1$. As indicated on the plot, the current, and hence the differential conductance, is normalized by a factor $(e/\hbar)\ \Gamma_L\Gamma_R/(\Gamma_L+\Gamma_R)$ to allow for comparing the two coupling scenarios. This plot was acquired by taking a bias cut at a constant gate voltage $V_g = -1$ (ZFS/$|e|$).

section of Fig. C.2(a). This amplification means that once the molecule is allowed to make a transition from the neutral state N to the charged one $N+1$, it predominantly prefers to be in the charged state, as indicated by the sharp rise in the occupation probability of the state $|\chi_-\rangle$ in Fig. C.1. In turn, transitions from the neutral to the charged state occurring at higher bias voltages are suppressed since the probability of the molecule to exist in the neutral state at high bias is negligible (*cf.* $\mathcal{P}_N$ in Fig. C.1). Consequently, the total current through the molecule primarily comes from the transition $|\pm 1/2\rangle$ to $|\chi_-\rangle$, as manifest in the first high step in the current plot in Fig. C.2(b).

Interestingly, comparing the saturation current through the molecule for $\Gamma_L > \Gamma_R$ and $\Gamma_L < \Gamma_R$, we find that the current in the former is higher even though the total coupling is the same in both cases, i.e., $\Gamma = \Gamma_R + \Gamma_L$. This anomaly can be understood with a back-of-the-envelope calculation as follows: For $\Gamma_L < \Gamma_R$, at high bias the molecule predominantly exists in the charged state $N+1$, each with a probability of approximately 0.3 (*cf.* Fig. C.1). Accordingly, based on Eq. (2.10), the total current can be attributed to the transitions from the *three charged* molecular states $|\chi_-\rangle$, $|\chi_+\rangle$ and $|\chi_0\rangle$ to the *two neutral* ones $|1/2\rangle$ and $|-1/2\rangle$. Thus, the total current can be thought of as $2 \times 3 \times 0.3 = 1.8$ units. By contrast, for $\Gamma_L > \Gamma_R$, the current mainly comes from the transitions from the *two neutral* states to the *three charged* states. Consequently, the total current reads $3 \times 2 \times 0.5 = 3$ units. Accordingly, it can be seen that the total current in the case where $\Gamma_L > \Gamma_R$ is higher, as apparent by comparing Fig. 2.8(b) and Fig. C.2(b). Finally, it should be noted that this is not a general conclusion, but rather depends on the molecular states $|\chi_n\rangle$. For instance, if we assume a molecule with spin $S_N = 1$ in the neutral state and $S_{N+1} = 1/2$ in the charged state, the current will be higher in the case $\Gamma_L < \Gamma_R$ in contrast to the earlier case.